Report No. FHWA-KS-22-05 ▪ FINAL REPORT ▪ June 2022

Utilization of Laser Induced Breakdown Spectroscopy (LIBS) for Real-Time Testing and Quality Control Monitoring of Aggregate Materials used in Highway Construction

Warren H. Chesner
Chris Stein
Arel Weisberg
Matteo Forgione
Henry Justus

Chesner Engineering, P.C.

A Transportation Pooled Fund Study - TPF-5(364)

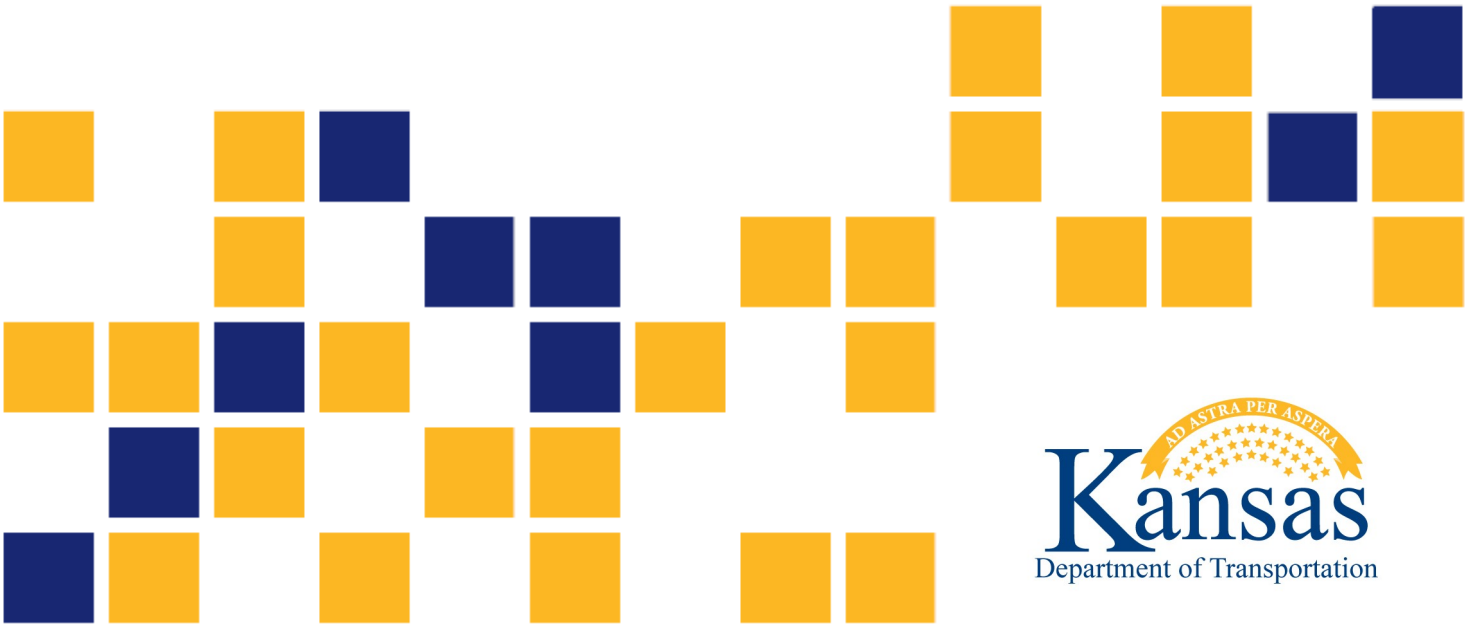

Kansas
Department of Transportation

1 Report No. FHWA-KS-22-05	**2 Government Accession No.**	**3 Recipient Catalog No.**
4 Title and Subtitle Utilization of Laser Induced Breakdown Spectroscopy (LIBS) for Real-Time Testing and Quality Control Monitoring of Aggregate Materials used in Highway Construction		**5 Report Date** June 2022 **6 Performing Organization Code**
7 Author(s) Warren H. Chesner, Chris Stein, Arel Weisberg, Matteo Forgione, Henry Justus		**8 Performing Organization Report No.**
9 Performing Organization Name and Address Chesner Engineering, P.C. 38 W. Park Avenue, Ste 200 Long Beach, New York 11561		**10 Work Unit No. (TRAIS)** **11 Contract or Grant No.** C2115
12 Sponsoring Agency Name and Address Kansas Department of Transportation Bureau of Research 2300 SW Van Buren Topeka, Kansas 66611-1195		**13 Type of Report and Period Covered** Final Report July 2017–June 2022 **14 Sponsoring Agency Code** RE-0738-01 TPF-5(364)

15 Supplementary Notes
For more information write to address in block 9.
Pooled Fund Study TPF-5(364) sponsored by the following DOTs: Kansas, New York, Ohio, and Maryland.

16 Abstract

Laser scanning of transportation aggregate materials provides a means to identify aggregate types, sources, and quality in near real-time. The Transportation Pooled Fund (TPF) effort described in this report began as a sequel to a TRB IDEA Program proof of concept laboratory study in 2012, and culminated in the development of the first commercial laser scanning system for transportation aggregate. This system is currently in operation at the Kansas Department of Transportation materials testing laboratory in Topeka, Kansas.

The results of this TPF effort demonstrate that laser scanning technology can provide new rapid testing quality control and assurance procedures (not possible using classical aggregate testing methods), thereby enhancing the overall quality of the aggregate resources used in products that make up the transportation infrastructure. The technology employed is based on a process referred to as Laser Induced Breakdown Spectroscopy (LIBS). In this process, a high-powered laser pulse is used to excite atoms that make up the minerals of the aggregate. This excitation results in the emission of light over a range of unique wavelengths (spectrum) that can be used to identify or fingerprint the targeted material. Pattern matching and modeling spectral fingerprints provides the means to identify aggregate types and their engineering properties.

The wide applicability of the laser scanning technology was demonstrated by the analyses that were performed for the four state transportation agencies that participated in this TPF study: Kansas, New York, Ohio, and Maryland. The focus of the Kansas effort was to determine whether laser scanning could be used to predict D-cracking aggregate susceptibility, and whether production blends could be evaluated to ensure that the source aggregate materials were all derived from approved sources. The focus of the New York effort was to determine whether laser scanning could be used to predict acid insoluble residue test results. The focus of the Ohio effort was to determine whether laser scanning could be used to predict the percentage of reactive chert and shale in a parent aggregate material. The focus of the Maryland effort was to determine whether laser scanning could be used to identify the quarry source of unknown aggregate materials, and whether laser scanning could be used as a surrogate to predict British Pendulum Number and Dynamic Friction Value test methods used to quantify aggregate friction properties.

17 Key Words Spectroscopic analysis, Aggregate tests, Quality control, Deleterious materials		**18 Distribution Statement** No restrictions. This document is available to the public through the National Technical Information Service www.ntis.gov.	
19 Security Classification (of this report) Unclassified	**20 Security Classification (of this page)** Unclassified	**21 No. of pages** 146	**22 Price**

Form DOT F 1700.7 (8-72)

This page intentionally left blank.

Utilization of Laser Induced Breakdown Spectroscopy (LIBS) for Real-Time Testing and Quality Control Monitoring of Aggregate Materials used in Highway Construction

Final Report

Prepared by

Warren H. Chesner
Chris Stein
Arel Weisberg
Matteo Forgione
Henry Justus

Chesner Engineering, P.C.

A Report on Research Sponsored by

THE KANSAS DEPARTMENT OF TRANSPORTATION
TOPEKA, KANSAS

June 2022

NOTICE

The authors and the state of Kansas do not endorse products or manufacturers. Trade and manufacturers names appear herein solely because they are considered essential to the object of this report.

This information is available in alternative accessible formats. To obtain an alternative format, contact the Office of Public Affairs, Kansas Department of Transportation, 700 SW Harrison, 2nd Floor – West Wing, Topeka, Kansas 66603-3745 or phone (785) 296-3585 (Voice) (TDD).

DISCLAIMER

The contents of this report reflect the views of the authors who are responsible for the facts and accuracy of the data presented herein. The contents do not necessarily reflect the views or the policies of the state of Kansas. This report does not constitute a standard, specification or regulation.

Abstract

Laser scanning of transportation aggregate materials provides a means to identify aggregate types, sources, and quality in near real-time. The Transportation Pooled Fund (TPF) effort described in this report began as a sequel to a TRB IDEA Program proof of concept laboratory study in 2012, and culminated in the development of the first commercial laser scanning system for transportation aggregate. This system is currently in operation at the Kansas Department of Transportation materials testing laboratory in Topeka, Kansas.

The results of this TPF effort demonstrate that laser scanning technology can provide new rapid testing quality control and assurance procedures (not possible using classical aggregate testing methods), thereby enhancing the overall quality of the aggregate resources used in products that make up the transportation infrastructure. The technology employed is based on a process referred to as Laser Induced Breakdown Spectroscopy (LIBS). In this process, a high-powered laser pulse is used to excite atoms that make up the minerals of the aggregate. This excitation results in the emission of light over a range of unique wavelengths (spectrum) that can be used to identify or fingerprint the targeted material. Pattern matching and modeling spectral fingerprints provides the means to identify aggregate types and their engineering properties.

The wide applicability of the laser scanning technology was demonstrated by the analyses that were performed for the four state transportation agencies that participated in this TPF study: Kansas, New York, Ohio, and Maryland. The focus of the Kansas effort was to determine whether laser scanning could be used to predict D-cracking aggregate susceptibility, and whether production blends could be evaluated to ensure that the source aggregate materials were all derived from approved sources. The focus of the New York effort was to determine whether laser scanning could be used to predict acid insoluble residue test results. The focus of the Ohio effort was to determine whether laser scanning could be used to predict the percentage of reactive chert and shale in a parent aggregate material. The focus of the Maryland effort was to determine whether laser scanning could be used to identify the quarry source of unknown aggregate materials, and whether laser scanning could be used as a surrogate to predict British Pendulum Number and Dynamic Friction Value test methods used to quantify aggregate friction properties.

Acknowledgements

Primary support for the work presented in this report was provided by six state transportation agencies:

- Kansas Department of Transportation (KDOT) (the Lead State Agency)
- New York State Department of Transportation (NYSDOT)
- Ohio Department of Transportation (ODOT)
- Maryland State Highway Administration (MDSHA)
- New Mexico Department of Transportation (NMDOT)
- Oklahoma Department of Transportation (ODOT)

The authors gratefully acknowledge the technical input and project guidance provided by Randy Billinger and Kate Andrzejewski (KDOT), Thomas Festa and Bryce Nelson (NYSDOT), Mickey Cronin (ODOT), and Dan Sajedi, Amanuel Welderufael, Intikhab Haider and Darren Swift (MDSHA).

Special thanks are extended to the TPF project coordination staff at Fort Hays State University, and in particular the guidance and support of Dr. Kenneth Neuhauser and Rachel Depenbusch for their efforts in ensuring an efficient administrative process.

This report is dedicated to the memories of William Skerritt (NYSDOT) and Rod Montney (KDOT), two individuals who had the foresight to recognize the importance of researching new, efficient, and innovative approaches for aggregate quality monitoring to replace obsolete older practices. Both Bill and Rod were instrumental in moving the initial laser developmental and demonstration projects forward. It is unlikely that development would have proceeded without their help.

Finally, thanks are extended to Research Team participants including Dr. Nancy McMillan from New Mexico State University (NMSU) who provided guidance and support in earlier model development and proof of concept testing efforts and Eileen O'Neill, who performed laser scanning for this TPF effort.

Table of Contents

List of Tables

List of Figures

Executive Summary

Laser scanning is a spectroscopic analytical tool that offers the potential for rapid cost-effective characterization of aggregate types and their engineering properties. The technology is based on a process that couples a high-powered laser pulse with a target aggregate material. This coupling induces a light emission that contains information that defines the micro-geochemical structure of the target material. The micro-geochemical information is encoded in the spectrum of the light emission, which can be captured and analyzed. The captured spectra in turn can be used to generate predictive models that can be employed as a means to monitor the quality of aggregate materials used in roadway and building construction.

This report presents a description of this technology and the findings and conclusions of Transportation Pooled Fund Study TPF-5(364). As part of this study, aggregate from four participating State transportation agencies were supplied to the Chesner Engineering PC laser scanning laboratory, located in Coeymans, New York, for analysis. The four participating State agencies included the Kansas Department of Transportation (KDOT), the New York State Department of Transportation (NYSDOT), the Ohio Department of Transportation (ODOT), and the Maryland State Highway Administration (MDSHA).

The objectives of the study were to examine the efficacy of models generated by scanning State DOT supplied aggregate materials and evaluating the results in relation to practical quality control issues facing each participating state. Each participating agency defined the specific objectives for the investigation. For example, KDOT focused on the use of scanning to differentiate D-cracking susceptible aggregate from non-susceptible aggregate; and to characterize the identity of aggregates in a blended production mixture. NYSDOT focused on the use of the technology as a surrogate for acid insoluble residue testing. ODOT focused on the use of laser scanning to identify the presence and content of chert and shale materials in ODOT aggregate; and MDSHA focused on the potential for laser scanning to identify the specific quarry source(s) of an unknown aggregate sample; and whether scanning could be used as a surrogate for British Pendulum and Dynamic Friction Value testing.

In addition to a description of the findings and conclusions of each State study, the report reviews the almost decade-long hardware and software developmental history of the laser scanning system, which began with a Transportation Research Board (TRB) IDEA Program proof of

concept study in 2012. This was followed by several intermediate prototype development and demonstration efforts culminating with this TPF effort report. It includes a description of the physical hardware and integrated software developed to enable the targeting of aggregate samples, and the real-time processing and analysis of the spectral data generated. A conceptual discussion is provided of the types of models used to transform the spectral data into formats that could be used to predict aggregate quality. This is to provide DOT engineers and geologists with basic information on the nature of such models and how they process the spectral data.

To facilitate the review of each State's laser scanning and analytical effort, the laser aggregate scanning and evaluation efforts for each participating State are presented in four separate chapters within the report:

- Chapter 3: Kansas Laser Scanning Analysis,
- Chapter 4: New York Laser Scanning Analysis,
- Chapter 5: Ohio Laser Scanning Analysis, and
- Chapter 6: Maryland Laser Scanning Analysis.

The KDOT studies revealed that

- Laser scanning may be used as a quality control tool to identify D-cracking susceptible aggregate.
- To achieve this objective local quarry and/or geologic member models will need to be calibrated for local KDOT aggregate sources.
- Laser scanning can be used to screen production sample mixtures to ensure that only approved materials are introduced into production sample blends.

The NYSDOT studies revealed that

- When proper samples are selected for calibration AIR models are highly predictive and can be used as a surrogate for New York's Acid Insoluble Residue Testing Procedure.
- Development of such models requires that close attention be given to sample selection during model calibration to ensure that the calibrated sample data will represent the test sample population.

The ODOT studies revealed that

- Laser scanning can be used as a quality control tool to identify chert and/or shale in ODOT aggregate at low concentration levels defined in ODOT specifications.
- Statewide Chert and Shale Models can effectively predict chert or shale content.

The MDSHA studies revealed that

- Laser scanning can be used to identify the quarry source of unknown aggregate samples used in Maryland highway applications.
- Laser scanning models can be used as a surrogate to predict DFV values of carbonate and noncarbonate aggregate.

The findings and conclusions presented in this report illustrate the untapped potential of the laser scanning process. In addition to the properties focused on in this report, there seems to be little reason why other material properties could not be simulated. Employing and operating the Sample Laser Targeting (SLT) System does not require any special knowledge of spectroscopy or lasers to operate. The embedded operational and modeling software is run via a Graphical User Interface (GUI) that requires no special knowledge of software or the mechanical operation of the system.

The realization of laser scanning as a transportation agency quality control tool, however, will require a major effort in the development of a spectral database to classify and associate the geochemical properties of a state's aggregate resources with known engineering properties. This is a substantial undertaking that could potentially require years of sample collection, scanning, and traditional testing to characterize aggregate quality from its quarry resources. Those agencies with the resources to pursue the development will be at the forefront of aggregate QC/QA programs in the 21st century.

In December 2021, the Kansas Department of Transportation (KDOT) became the first State Agency in the nation to install a scanning system in its State-run materials laboratory. By installing such a system in its own laboratory KDOT presently has the means to expand the potential for characterizing its own aggregate resources, and to uniquely address the issues that are most pressing to KDOT.

Chapter 1: Introduction

1.1 Background

In April 2012, the Transportation Research Board (TRB) published the results of the first documented study in the US that examined and demonstrated the feasibility of using laser scanning to identify and characterize aggregate materials used in highway construction (Chesner & McMillan, 2012). This study was conducted using a bench scale laser system located in the Department of Geology at New Mexico State University (NMSU). A photograph of the system used in the 2012 study is shown in Figure 1.1.

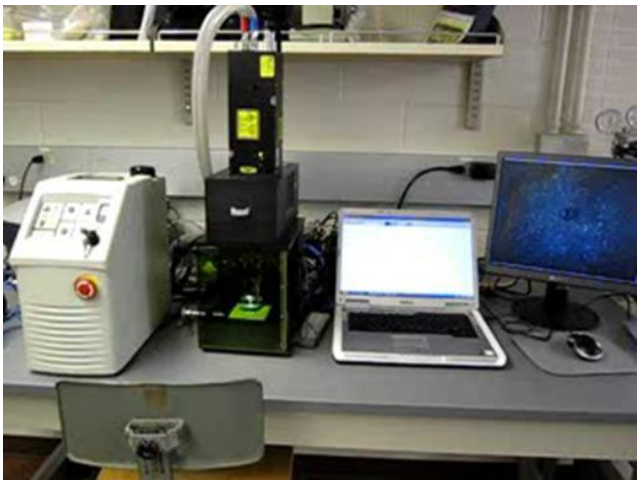

Figure 1.1: NMSU Bench Laser Scanning System

The process used is referred to in the scientific literature as Laser-Induced Breakdown Spectroscopy (LIBS). The LIBS process uses a highly energetic laser pulse to heat and excite the atoms in a localized, high-energy, plasma plume. In such a plasma state, electrons in the target material (aggregate-rock microstructure) will transition from lower to higher energy levels and emit light at intensities and wavelengths characteristic of the atoms and ions present in the plasma. The wavelengths and intensities associated with the light emission generate a spectrum that can be recorded and analyzed. A spectrum is a graphical representation of the relative intensities of the detected radiation, plotted from the shortest wavelength to the highest wavelengths. The magnitude of the detected intensities reflects the elemental and underlying mineralogical composition of the aggregate target material. A spectrum of a Kansas limestone is shown in Figure 1.2.

Since the microstructure of even one aggregate particle can be expected to exhibit a great deal of chemical heterogeneity, each laser shot will generate a unique spectral pattern. A composite of many laser shots will generate a pattern that captures a distribution of the individual spectrum for a given sample, and an average or composite spectrum. This composite spectrum can be described as a "spectral-pattern or fingerprint" of the analyzed aggregate.[1]

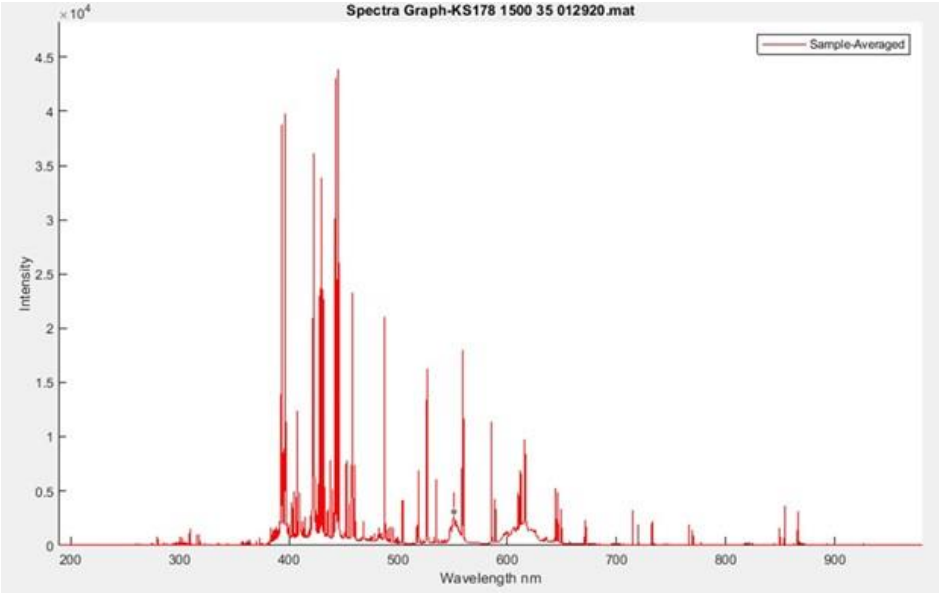

Figure 1.2: Kansas Limestone Spectrum

The idea of fingerprinting aggregate materials using laser scanning conceptually opens the possibility of comparing the underlying chemical makeup of these aggregates. By pattern matching the various spectra generated, each aggregate can be classified into groupings. Aggregates with similar spectral output can be expected to group into categories that exhibit similar engineering properties. Conversely, dissimilar spectra suggest dissimilar properties. The spectral patterns can be effectively employed to determine whether an unknown aggregate is derived from a known source. For example, if an unknown aggregate exhibits a spectral fingerprint that differs from a known aggregate source, it is highly unlikely that the unknown aggregate was derived from that source. Conversely, similar spectra would suggest that the aggregate came from the same source.

[1] The overall heterogeneity encountered is actually a function of both the chemical heterogeneity of the rock structure and the statistical heterogeneity inherent in the plasma morphology, which varies with each laser shot.

The engineering properties of transportation aggregate are dependent on the physical, chemical, and mechanical properties of the manufactured product. Many deleterious properties of aggregate are also dependent on the transportation environment into which they are placed. As a result, there is no guarantee that spectral emissions, which mostly capture the underlying chemical composition of the aggregate, will directly correlate with all engineering properties. Validation studies are necessary to determine the effectiveness of this approach. Nonetheless as will be shown in this report, in most cases, validation testing yields extremely positive results.[2]

Multivariate numerical methods are needed to process the quantity of information embedded in a typical spectral pattern, and to group and classify aggregate types and correlate spectral patterns with engineering properties. These methods are used to calibrate multivariate models that provide the means to predict the quality of an unknown target aggregate. The technology does not require any special sample pre-processing. Once a sample is collected it can be scanned almost immediately and the property of interest predicted by the calibrated models.

Given the above, the successful deployment of laser scanning technology could have far-reaching quality control ramifications. It could provide the means for State transportation agencies to rapidly screen (in near real-time) materials to:

- Identify the quarry source or localized bed source
- Determine whether the material meets existing specifications
- Validate whether a production sample contains pre-approved mixtures
- Permit rapid and ongoing classification of quarry sources
- Identify and quantify the content of deleterious material in an aggregate source

Further interest in the 2012 effort led to a follow-on TRB funded study designed to support the development of a field prototype. In the NMSU bench scale system, shown in Figure 1.1, each aggregate particle in a small sample was independently analyzed one laser shot at a time. An upscaled prototype was deemed necessary to provide the means to rapidly scan large aggregate sample sets to address the heterogeneity inherent in aggregate samples; and to develop software

[2] A spectral emission can be expected to capture both chemical and, in part at least, the physical characteristics since the emission represents a signal of the solid and gaseous (e.g., pore space) composition of the aggregate.

capable of processing the scanned data and convert the data into outputs that apply to transportation applications. This effort was described in Chesner and McMillan (2015).

A photograph of the first commercial prototype, referred to as the Sample Laser Targeting (SLT) system, is shown in Figure 1.3.[3] To process the thousands of spectra generated during a laser scanning process, development of specialized software for use with the SLT was also deemed necessary. This software is referred to by the acronym SAM, which is short for Sample Analytical Module. SAM was developed to collect spectral data from every laser shot on the fly and input these data to pre-calibrated models to predict the quality of the aggregate immediately after scanning is completed.

Figure 1.3: First SLT Prototype (2015)

The successful completion of the aforementioned proof of concept and prototype development efforts provided sufficient incentive to pursue the planning and implementation of two Transportation Pooled Fund (TPF) studies. These pooled funded efforts were designed to explore in greater detail the practical aspects of employing laser scanning as a quality control tool in the transportation industry. At the completion of the first TPF, major modifications were made to the SLT to correct hardware deficiencies observed in the first TPF study. The upgraded SLT was used in the second study. The results of the first TPF study is described in Chesner and

[3] This prototype was installed and operated at the Callanan Quarry site in South Bethlehem, New York.

McMillan (2016). The results of the second TPF study, which was executed over the period of 2018 to 2020, are the subject of this report.

At the present time, the Kansas Department of Transportation (KDOT) has become the first agency in the nation to employ laser scanning in a state transportation laboratory. An SLT system is currently in operation at KDOT's materials laboratory in Topeka, Kansas.

1.2 Objectives and Scope

Transportation Pooled Fund Project TPF-5(364) was initiated in early 2018 with four actively participating agencies. These included Kansas, New York, Ohio, and Maryland.[4]. The primary objective of the effort was to determine how effectively the second-generation SLT could predict the quality of respective state aggregates and to advance modeling and evaluation efforts. Each State agency had uniquely defined objectives:

- Kansas Department of Transportation (KDOT):
  Determine whether laser scanning could be used to predict D-cracking aggregate susceptibility and whether production blends could be used to validate source materials used in aggregate production.
- New York State Department of Transportation (NYSDOT):
  Determine whether laser scanning could be used to predict acid insoluble residue test results.
- Ohio Department of Transportation (ODOT):
  Determine whether laser scanning could be used to predict the percentage of reactive chert and shale in a parent aggregate material.
- Maryland Department of Transportation State Highway Administration (MDSHA):
  Determine whether laser scanning could be used to predict the source of unknown aggregate materials; also, to predict friction properties of MD aggregates.

The scope of work involved the collection of aggregate samples by each participating State agency and the transport or shipment of the samples to the Chesner Engineering Laser Research lab, located at the Port of Coeymans Marine Terminal in Coeymans, New York. Samples were

[4] New Mexico and Oklahoma were part of the Pooled Fund Effort, but staffing issues prevented their full participation.

delivered in 6- x 12-inch cylinders, shown in Figure 1.4. Each cylinder was labelled with a Sample ID and contained 15 to 20 lbs of aggregate for scanning. The number of samples received, and the source of the samples was controlled by each State agency. Additional discussions on sample collection are discussed in each respective State chapter.

Figure 1.4: Sample Cylinders from MDSHA

In addition, each State provided information on the sample source, sample lithology, and engineering test data that was used to characterize the sample. These data were compiled into a computerized database that was integrated into the SAM laser scanning software previously described. All samples received were scanned several times. The typical scan involved approximately 1500 laser shots. Each scan generated a spectrum, which was associated with a particular Sample ID. These data were also stored in the database. The integrated database generated over the course of the project provided the means to develop predictive aggregate quality models for each State. A description of the laser system developed to scan the aggregate, the procedures used to develop the calibration models, and the findings and conclusions of the research are all described in this report.

Chapter 2: The Sample Laser Targeting (SLT) System

Chapter 2 includes a description of the equipment and operations of the laser targeting system developed by the Research Team for aggregate scanning. It also includes a description of spectral data processing steps that were employed to translate a laser-induced-spectra into an output that predicts aggregate properties.

2.1 SLT System: Design and Operations

Theoretically, Laser Induced Breakdown Spectroscopy (LIBS) during the early stages of the technology evaluation appeared to be an ideal process for monitoring transportation aggregate. Samples can be scanned as-received with no pre-processing requirements and results can be obtained in near real-time. Practically however, providing a physical system capable of scanning aggregate is another matter. An effective laser-aggregate scanning system must be capable of:

- Coupling laser light with an aggregate sample;
- Scanning as much of an aggregate sample as possible;
- Collecting the emitted light and storing the spectral data; and
- Processing the spectral data to predict the quality of the scanned sample.

In addition, all of this must be accomplished in a manner that:

- Addresses the physical and mineralogical heterogeneity of aggregate samples;
- Simplifies aggregate handling procedures in a materials laboratory environment;
- Mitigates the potential impact of dust on the optical components and laser light;
- Minimizes the duration of the scanning procedure; and
- Generates results in near real-time.

The first-generation SLT prototype lacked the means to adequately accomplish all of the aforementioned objectives.[5] The second-generation SLT, which was designed and fabricated for

[5] In particular this included the inability to adequately control dust; and provide for a controlled interaction between the laser and the target aggregate material.

this TPF effort, required the development of novel hardware and integrated software to control SLT laser scanning operations and to process the data generated in the process.

The defining feature of the second generation SLT is the aggregate sample chamber. The sample chamber, shown in Figure 2.1, houses a sample tray, a rotating turntable and linear drive designed to rotate the tray around its center axis and linearly along its radial axis; and to linearly move the sample tray in and out of the sample chamber.[6]

The chamber is equipped with a dust suppression system that evacuates dust from the chamber on a continual basis during laser operations and prevents dust from entering and interfering with the laser path between the laser and the target material. Transparent safety glass windows enable the SLT operator to observe the sample chamber during operations.[7]

Figure 2.1: SLT Sample Chamber

The sample tray, which can be removed from the sample chamber, is used as the sample container. Prior to scanning, the tray is filled with the target aggregate and inserted onto the turntable. Different sized sample trays can accommodate aggregate samples weighing 1 pound up to 20 pounds. No other sample pre-processing is necessary. The turntable and linear drive are programmed to move the samples under the laser, which can be programmed to fire at the

[6] The sample tray shown in the figure is 20-inches in diameter.

[7] The Nd-YAG Laser used in the SLT is a Class IV 1064 nm laser. The chamber safety glass prevents eye exposure to the 1064 nm radiation.

aggregate at repetition rates from 1 to 10 Hz for any duration necessary to achieve a defined number of laser shots on the target material.

The Figure 2.2 schematic below, shows a conceptual view of an Nd-YAG laser emitting a high-powered laser beam at a wavelength of 1064 nm. The beam is directed through a reflecting mirror and focusing lens at the sample tray that contains the sample aggregate material.[8] The high power associated with the laser generates a plasma that emits light back to a fiber optic cable that transmits the light to a seven-channel spectrometer and charged coupled detector (CCD). The spectrometer resolves the light into its component wavelengths and the CCD transfers the information electronically to a computer for storage and analysis.

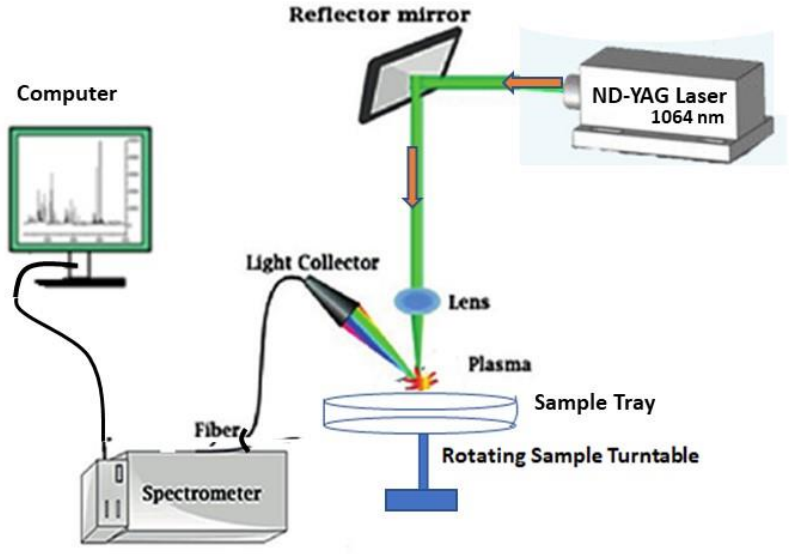

Figure 2.2: SLT Scanning Process

[8] The type of laser used in the SLT is an Nd:YAG laser (neodymium-doped yttrium aluminum garnet) laser; Nd:Y3Al5O12 is a crystal that is used as a lasing medium for select solid-state lasers.

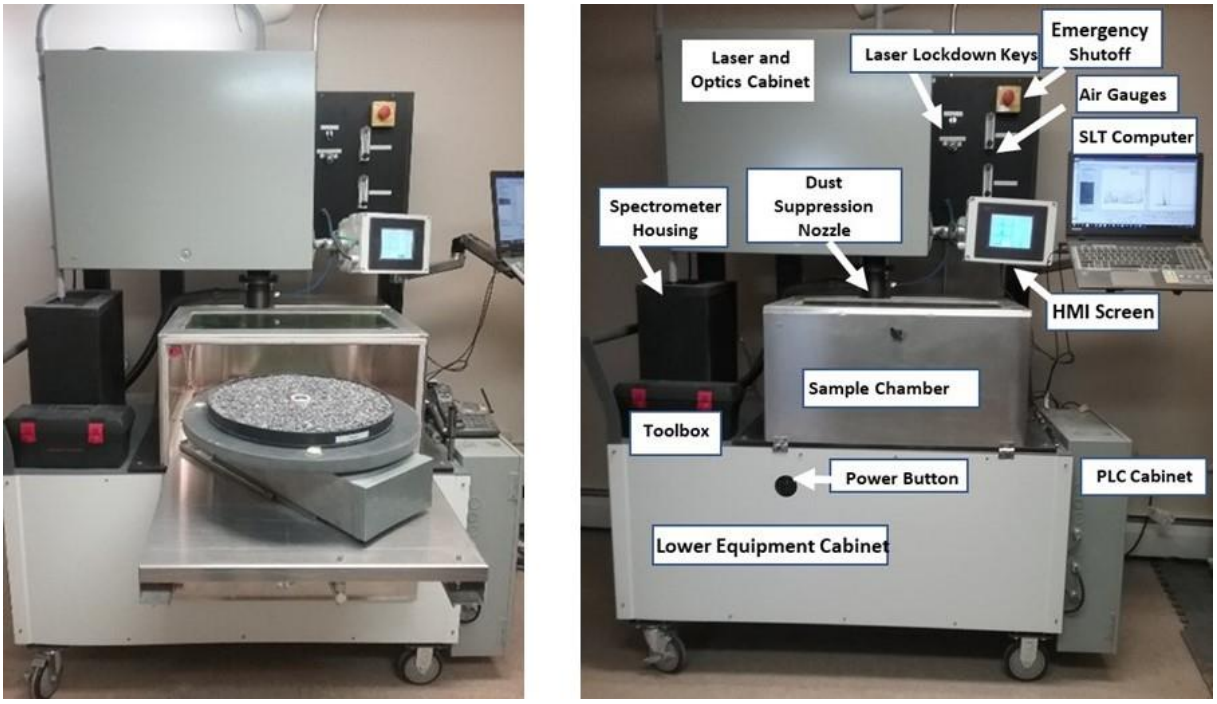

Figure 2.3: SLT Hardware Components

The SLT system components are contained in two cabinets: an upper cabinet and a lower cabinet. The upper cabinet, which is maintained at positive pressure to prevent any ambient dust from entering, houses the laser and the optical train, which consists of mirror and lenses to direct the laser beam to the target aggregate situated in the sample chamber. The lower cabinet houses the power supply, programmable logic controller, compressor, and vacuum system, which collects all dust generated in the sampling chamber.

Figure 2.3 is a photograph of the sample tray table extracted from the sample chamber accompanied by a photograph that shows the SLT with labels to identify the various components making up the system.

2.2 Laser-Aggregate Coupling and Signal to Noise Ratio Screening

Coupling a laser beam with an aggregate sample is not trivial. The focal point of the beam must coincide with the surface of the aggregate. Ideally, this surface should be normal to the beam. In a bench scale laser system, where each particle is individually scanned, focusing and particle orientation can be manually adjusted. In a field system, designed to scan many particles to capture the heterogeneity of the sample, manual adjustment of each sample particle is not realistic. The

SLT sampling tray provides a fixed elevation for the sample, which enables the focal point to be determined for a downward pointing laser beam (see Figure 2.2). However, particle orientation is random and there is no control over interparticle void spaces resulting from the angular configuration of aggregate compacted into a sample tray. Figure 2.4 is an overhead view of an aggregate sample tray; the same view a laser beam has rushing toward the sample.

Figure 2.4: Ohio Coarse Aggregate in SLT Sample Tray

A laser firing at 3 hertz at the tray will couple with the surface of the particles at numerous incident angles relative to the normal. The result is that the light emissions induced by the coupling reaction will deflect in many directions. Optimum light capture can be expected for laser shots that deflect the emitted light along the reverse path of the incoming laser beam. Lower intensities will occur for all other deflection angles. In addition, the interparticle void space between the particles means that a non-significant fraction of laser shots will not couple with the surface of the sample particles. This will also affect the intensity of the emission detected. The combined effect is that a high fraction of laser shots will result in low intensity emissions. These low intensity emissions will adversely affect the accuracy of the detected spectra.

To overcome these limitations, specially developed algorithms were incorporated into the SLT data processing software to analyze each laser shot to determine the suitability of each laser shot for analysis. This algorithm looked at the Signal to Noise Ratio (SNR) of specially selected wavelengths associated with each spectrum. An SNR below a pre-selected threshold value would

filter out the laser shot from subsequent spectral analysis. The SNR was used as a screen to detect and eliminate low intensity emissions from the data collected.[9]

2.3 Spectral Line Analysis

A full spectral signal generated by each laser pulse in the SLT encompasses a range of wavelengths extending from approximately 188 to 980 nanometers (nm). The full spectral signal, however, may not in all cases be the optimal signal for characterizing specific aggregate properties. In these instances, a "Line Analysis" may be more effective.

A Line Analysis is a spectral screen that is designed to reduce the number of wavelengths (lines) in the spectral signal used in the predictive model analysis. Figure 2.5 illustrates the difference between a full spectrum and selected lines embedded in the spectra. The top portion of the figure represents a full spectral signal and the bottom portion, a partial signal, which is a small subset of the wavelengths embedded in the full spectral signal.

Line analysis provides a tool that can isolate wavelengths that yield a spectral pattern that could be more effective in achieving the desired modeled output in a given analysis.[10] Line analysis was employed in several instances in the analyses presented in this report; particularly in the Ohio modeling effort.

Several other spectral normalization and data transformation techniques were also employed to modify or transform the raw spectral data; with the intent of improving model resolution and prediction efficiency. These specific techniques are discussed in the State-specific sections of this report, where they were applied.

[9] For most samples this resulted in approximately 35 to 70 percent of all laser shots being discarded from the analysis.

[10] A reduced number of significant spectral lines, which are most important to the model can, in certain cases, increase model resolution.

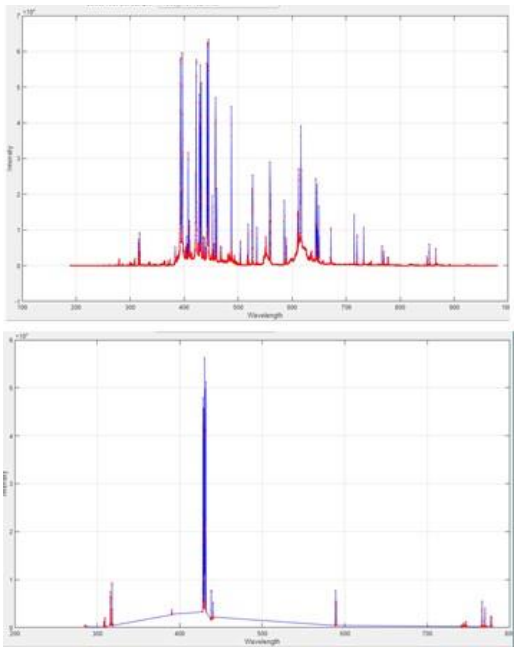

Figure 2.5: Full Spectra vs Line Analysis

2.4 Multivariate Chemometric Models

An aggregate spectral pattern, similar to the Kansas limestone pattern illustrated in Figure 1.2, is the result of recorded emission intensity measurements of approximately 1500 laser shots. Each shot comprises approximately 14,336 different wavelengths, ranging from the near-ultraviolet to the near-infrared range.[11] Many laser shots are required to capture the chemical heterogeneity of a single aggregate sample. It is impractical to manage and analyze the quantity of data generated during laser scans without the assistance of specialized data management software. In addition, to discriminate between and among the spectral patterns generated by the variety of aggregates tested, special mathematical modeling techniques are needed. These techniques fall into a broad category commonly referred to as multivariate analysis. When chemical composition and in particular spectral data are employed as input data, the models are commonly referred to as multivariate chemometric models. A detailed description of multivariate chemometric methods is provided by Geladi (2003) and Geladi et al. (2004). Kramer (1998) provides a general description. Dunn (2022) provides a useful online description.

[11] The 14336 wavelengths span the light spectrum from the near ultraviolet range to the near infrared range: from approximately 188 nm to 980 nm in ~+/- 0.02 nm bins. This represents 14336 separate variables that are included in the analyses.

Two specific modeling methods were employed in this investigation. The first is referred to as Principal Component Analysis (PCA) and the second Partial Least Squares Regression (PLSR). There are numerous sources that describe these methods. Jaadi (2021) and Sartorius AG (2020) provide general descriptions of these methods. Clegg et al. (2009) provide a detailed description of PLSR use in LIBS applications. Numerous software packages also exist that enable analysts to practically employ these methods. Some of these include MATLAB, Unscrambler, SIMCA, SPSS, Smart PLS, and SAS. MATLAB was used to generate the PCA and PLSR models described in this report.[12]

It can be useful to think of chemometric models as techniques to compare the spectral fingerprints of different aggregates. Comparing and classifying spectral fingerprints can then be used to assess the chemical similarities and hence engineering properties of various groupings. The following sections present conceptual representations of PCA and PLSR models.

2.4.1 Principal Components Analysis (PCA)

A PCA model is a classification model. It is used to classify aggregate types (or spectra) by comparing and discriminating between spectra of the aggregates scanned. The model output is typically presented in graphical form where aggregate with similar spectra (chemical microstructure) will cluster in groupings or special fields. This is conceptually identical to a two-dimensional graphical analysis where similar samples will cluster closer to samples that exhibit comparable properties and farther away from samples with dissimilar properties.

An example of such a two-dimensional analysis is presented in Figure 2.6. In Figure 2.6, three aggregate samples—Granite (G), Limestone (L), and Shale (S)—are plotted on a simple two-dimensional graph. There are two variables considered: Hardness and Friability. Values for each variable (Hardness and Friability) have been measured and recorded on a scale ranging from 1 to 10, where 1 in both cases is the lowest rating and 10, the highest. So, a Hardness Value of 10 would be the hardest material and a Friability Value of 10 would be the most friable material. The abscissa (x-axis) on the two-dimensional graph represents the Hardness and the ordinate (y-axis) the

[12] The report's authors employed MATLAB to develop a software package to seamlessly process (in real-time) the laser-generated spectral intensity data for use in both PCA and PLSR models. This software is referred to as SAM, which is short for Sample Analysis Module

Friability. It is easy to observe in the hypothetical representation, that the Limestone (L) and Granite (G) samples plot closer together than the Shale (S). They do so because their respective Hardness and Friability scores are much more similar than those of the shale sample.[13] The soft, friable Shale is in its own group. The Limestone and Granite samples represent harder and less friable aggregate.

Aggregate	Hardness	Friable
Granite (G)	10	1
Limestone (L)	7	3
Shale (S)	3	9

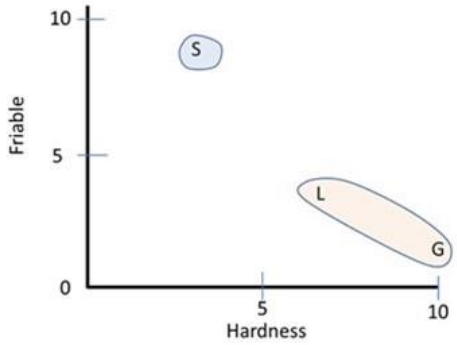

Figure 2.6: Two-Dimensional Hardness vs Friability Plot

A PCA model transforms and projects the multidimensional nature of the spectral data onto a more familiar two-dimensional framework, which can readily be visualized. This transformed coordinate system is referred to as a Principal Components (PC) score plot.

An example of a PC score plot is shown in Figure 2.7. Figure 2.7 shows projections of gravel and shale sample spectra that were generated during this study onto the score plot. The two axes on this new coordinate system are referred to as Principal Component 1 (PC1) and Principal Component 2 (PC2). The samples plot on this two-dimensional diagram can be interpreted like any two-dimensional (x vs y) diagram. Samples that are similar in composition are projected close to each other and those with different compositions are projected in different locations within the new coordinate system, sometimes referred to as PC space. The gravel samples cluster on the left side of the score plot and the shale on the right side. The major difference between the simple two-

[13] Each plotted point in the two-dimensional graph is represented by a two-dimensional vector, defined by two variables: hardness and, friability.

dimensional plot, shown in Figure 2.6, and a PC score plot is that a PC score plot represents samples with multidimensional spectral data.[14]

Throughout this report reference is made to "aggregate fields." Aggregate fields refer to PC score plots that depict aggregate clusters or groupings that identify specific aggregate types. In Figure 2.7 for example two aggregate fields can be clearly identified: gravels and shale. The gravels cluster to the left side of the score plot, primarily distributed along the PC1 axis and in the second and third quadrants. The shales cluster to the right, again along the PC1 axis in the first and fourth quadrants.[15]

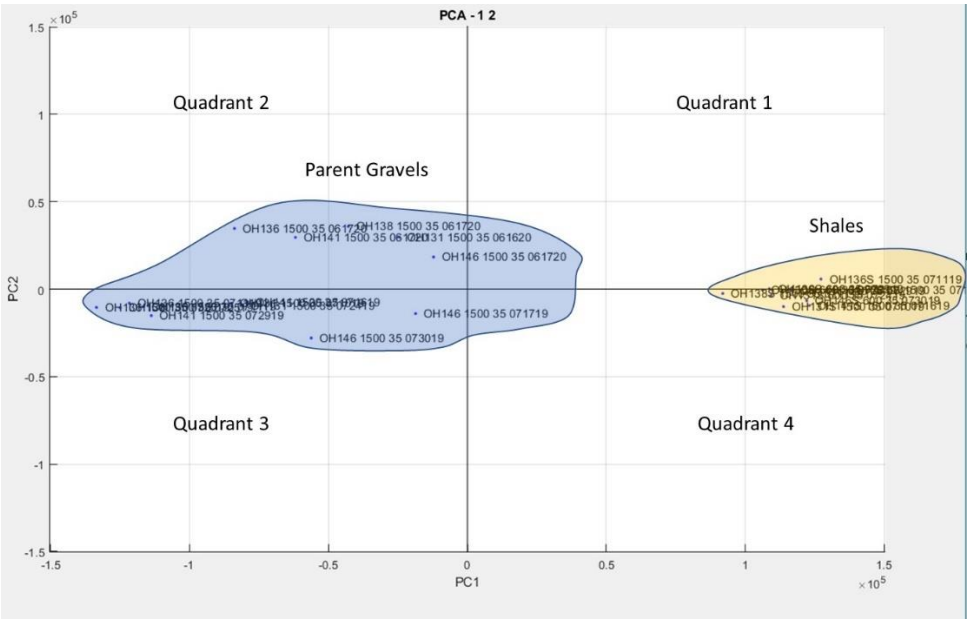

Figure 2.7: PC Score Plot of Gravel and Shale Samples

2.4.2 Partial Least Square Regression (PLSR)

A two-dimensional linear regression model is a line of best fit through a given two-variable data set. Each observation is associated with the two variables: a dependent variable (y) and an independent variable (x). An example is shown in Figure 2.8. Development of such a model requires two steps: a calibration step and a validation or test step. The calibration step establishes

[14] Each plotted point in a score plot is represented by a multidimensional vector, defined by multiple wavelengths (up to 14336) generated during a laser induced emission, which has been transformed to yield a two-dimensional representation of this vector.
[15] The referenced quadrants (1, 2, 3, and 4) are similar to the four quadrants associated with a standard cartesian coordinate plot with the origin at the center.

the relationship between the two variables.[16] Once an effective regression line equation is established (or calibrated), the model can be used to predict the y-values of unknown samples.[17]

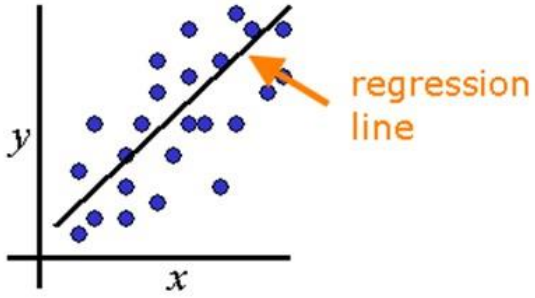

Figure 2.8: Linear Regression Model

A PLSR model is a multidimensional representation of a two-dimensional linear regression model. It analogously establishes, in the calibration step, a relationship between independent variables (X) and a dependent variable (y).[18] Note in this case, a capital X is used to characterize the independent variable, instead of a lower-case x. This is because each X value is not a single variable but represents 14,336 variables. Each individual X is associated with one laser induced spectrum, which is also associated with one variable or one y value.[19] This association is developed by calibrating the model to provide the best linear correlation between the X data and the y-value predictions.

A PLSR model, similar to a PCA model, transforms the multidimensional nature of the analysis, to a two-dimensional framework and coordinate system that can be visualized. A graphical representation of a PLSR model output is shown in Figure 2.9. Figure 2.9 presents the results of an acid insoluble residue (AIR) PLSR model, developed with NY limestone spectral data. The data presented shows the model predictions for a series of unknown samples and compares how effectively the model matched the actual sample values. The model shown in Figure

[16] If the relationship is linear the model will generate the equation of a straight line (y= mx+b).
[17] Effective linear regression calibration implies high correlation and low residual error. Validation requires testing the calibrated model against a second independent set of samples (validation set) to establish how well the model predicts the y-values of the validation set. This also implies good correlation and low residual error.
[18] The dependent variable y is the dependent quantity that the model is predicting.
[19] The x variable is in reality an X matrix containing wavelength and intensity data for each laser shot.

2.9 was calibrated to predict AIR over a wide range of values.[20] To calibrate such a model requires that samples that are part of the calibration set cover the range of AIR values, or more generally y values over which unknown samples will be tested.

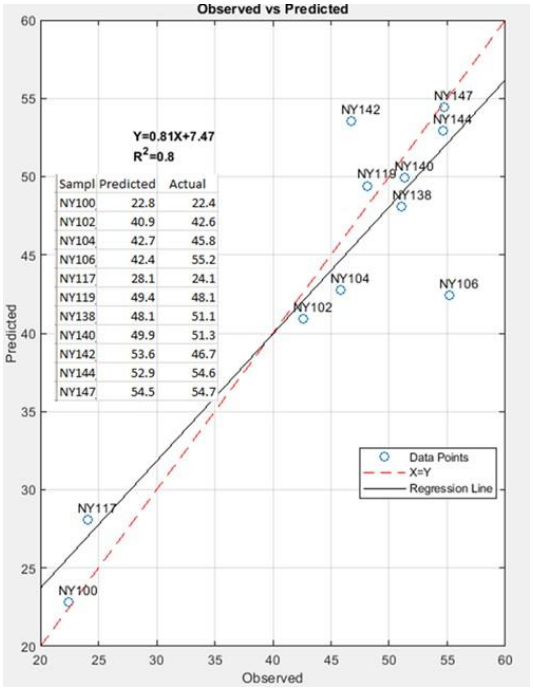

Figure 2.9: PLSR Acid Insoluble Residue Model

There are instances in aggregate analysis where only two outcomes (or y-values) are known. Such a model is referred to as a binary model. A common example is Pass or Fail.[21] This model output considers only one of two dependent variable outputs (y) associated with each independent variable (x). An example is shown in Figure 2.10. The two dependent variables are designated 0 and 1. Such a model is calibrated by assigning a value of 0 to all known failing samples and a value of 1 to all known passing samples. The model is tested by examining whether an independent set of samples will generate y values closer to 1 or closer to 0, for passing and failing samples, respectively. During the calibration, a boundary line between the passing and failing samples can be generated, referred to as the value of apparent distinction (VAD). During

[20] The calibrated AIR range (y value) in this case ranged from 20% to approximately 60%.

[21] An example of a binary model is the Kansas D-Cracking model, which is calibrated on the basis of a training set that contains samples that have passed the KDOT D-cracking test as well as samples that have failed the D-Cracking test. The calibrated model is then used to predict whether unknown samples will pass or fail the test.

model testing those samples exhibiting y values greater than the VAD are judged to be passing while those with values less than the VAD, failing. This type of model is used in several applications described in the report.

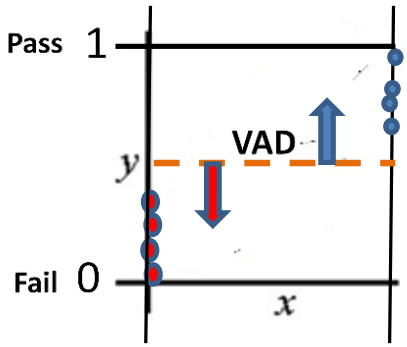

Figure 2.10: Binary Regression Model

2.4.3 Sample Collection Requirements

The collection of samples used to calibrate aggregate models cannot be random. Pre-planning is necessary to ensure that the calibration samples used to develop the model are representative, to the extent possible, of the unknown samples that will be tested. Geologically speaking, this means that the calibration samples (or set) must span the range of conditions expected to be encountered in the unknown samples to be tested. Statistically speaking, this means that the calibration set must be a "representative" of future test samples. From a laser scanning perspective this means that the calibration samples must exhibit spectral patterns that cover the range of spectra that would be expected in future test samples.

The hypothetical PC Score Plot, presented in Figure 2.11, is intended to conceptually illustrate how the sample selection process affects model planning and development. Figure 2.11 depicts a PC Score Plot for scanned samples from a given Geologic Member A. Each scanned sample projects onto the score plot and tends to group with samples that exhibit similar geochemistry. There are three types of samples shown: 1) solid blue, 2) checkered orange, and 3) white samples. Each of the dots represents samples exhibiting specific geochemistry.[22] Geologic

[22] The geochemistry variation could be represented by varieties of limestones, dolostones or other mineralogical species within the geologic member.

Member A is primarily characterized by the solid blue dots (geochemistry a), and Quarry A1 within Member A reflects similar geochemical characteristics. Quarry A2, however, appears to be characterized by an independent geochemistry (geochemistry c), while Quarry A3 appears to be a blend of geochemistry a and geochemistry b.

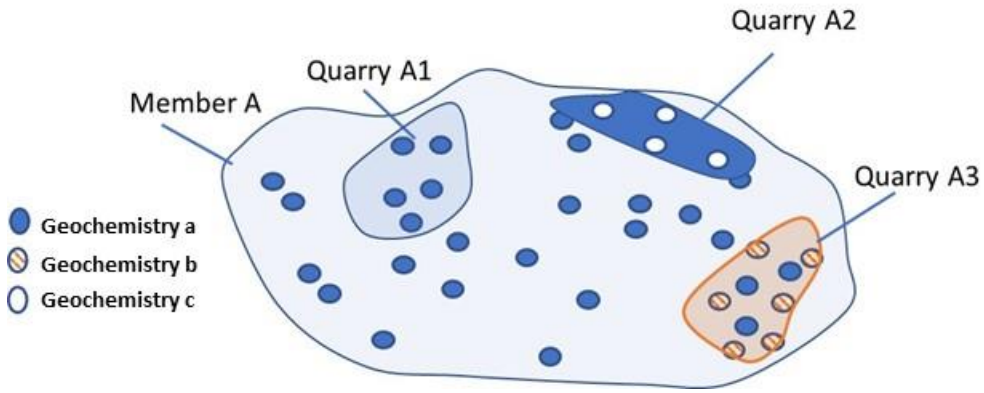

Figure 2.11: Conceptual Representation of the Regional Aggregate Field

Calibrating a model with a distribution of samples present in Member A should effectively model aggregate from Quarry A1 but would not be expected to effectively model aggregate from Quarry A2 or Quarry A3. In the latter cases local aggregate sample scanning would most likely result in an improved model.

2.4.4 Laboratory Data Quality

Both Principal Component Analysis (PCA) and Partial Least Square Regression (PLSR) models utilize the laser induced spectra to predict the model output. There is a notable distinction, however, between the two approaches. PCA classification models are independent of lab data. Scanned sample classification, presented in the form of a score plot, is exclusively dependent on the spectral data. No lab data is required. PLSR models, however, are dependent on lab data to define a specific quantifiable property, used as the dependent variable in the model calibration.

It is known that many aggregate property tests used for quality monitoring lack precision and accuracy. This can be due to sample heterogeneity or inherent deficiencies in the test method. Poor precision and accuracy will impact the accuracy of PLSR model predictions associated with

such properties. When this is the case, additional care must be employed during the lab testing and calibration sample selection process to ensure, to the extent possible, that there is reasonable confidence that the laboratory data associated with the calibration sample dataset are accurate. Laboratory data that exhibit high variance and uncertainty will generate models that reflect this uncertainty.[23]

2.4.5 Super Models and Source Models

Reference is made in subsequent sections of this report to "Super Models" and "Source Models." A Super Model is a model in which many, if not all cluster groups can be included in the calibration set. A Source Model is a model that is calibrated using samples collected from a local cluster. For example, in Figure 2.11, Quarries A2 and A3 would most likely require independent Source Models.

[23] Providing a robust sample database from which uncertain samples can be screened and removed from the calibration set can help to mitigate problems associated with the use of samples with questionable lab data.

Chapter 3: Kansas Laser Scanning Analysis

3.1 Kansas Scanning Objectives

D-cracking is a freeze-thaw related damage in concrete pavements. It has primarily been attributed to the presence of coarse-grained limestone aggregates that do not have sufficient internal resistance to withstand the induced internal pressures associated with the freeze-thaw Kansas environment. Both textural and mineralogical reasons have been reported as possible contributing factors. The exact mechanism involved however is unknown. To mitigate the problem, the Kansas Department of Transportation (KDOT) has developed rigorous testing procedures for limestone aggregate use in concrete. The KDOT practice involves two laboratory tests for qualifying concrete aggregates. The tests include a soundness test KTMR-21 (2012) and a freeze thaw test KTMR-22 (2012). Both tests are time consuming and together can take approximately six months to complete. KDOT manages the approval process by pre-qualifying aggregate sources. Even with prequalified quarries, natural geologic variability has led to continued pavement degradation associated with non-durable concrete aggregates. Laser scanning of KDOT aggregates using the SLT was undertaken to determine whether the LIBS process could provide the means for the rapid identification of D-Cracking susceptible aggregates in near real-time.

Aggregate suppliers commonly blend several materials to produce a finished stockpile before shipping or mixing the blended material in concrete applications. Once blended it is almost impossible to practically check whether the original materials used to make up the blend were derived from approved sources.

The Kansas laser scanning effort included two objectives: Objective 1: Determine whether laser scanning could differentiate between D-Cracking susceptible aggregate sources and non-susceptible sources, and Objective 2: Determine whether laser scanning could verify whether a blended stockpile of two or more aggregate sources were comprised of known original aggregate sources.

3.2 Kansas Aggregate Samples and Sources

During the effort, KDOT supplied for scanning a total of 224 aggregate samples. The aggregates were collected from 23 different geologic members and 21 different quarries. Each geologic member was found to encompass anywhere from one to five quarry locations. A list of all samples collected their respective geologic members and source quarries are tabulated in Table 3.1. All the samples were limestones, except for one granite/diabase sample and four gravel samples. Of the 224 samples collected, 159 samples had associated D-cracking test data, reported as Pass or Fail that could be used in the D-cracking analysis. Fifty-four (54) samples were reported as failing and 105 passing.

3.3 KDOT D-Cracking Model

3.3.1 PLSR Binary Model

Defining whether an aggregate is D-cracking susceptible (or not) lends itself to a PLSR binary model, described in Section 2.4.2 Partial Least Square Regression (PLSR). This type of model generates one of two outputs: Pass or Fail; Yes or No; or for modeling purpose 1 or 0, where the number 1 represents pass, and 0 represents fail.

3.3.2 PLSR Binary Model Calibration

Preliminary calibration models were screened to assess whether all statewide samples could be included in one large Super D-cracking model or whether Source or more localized models were more effective predictors of D-cracking susceptibility. In both cases, D-cracking PLSR models were calibrated by selecting all relevant samples from total or local KDOT D-cracking database, and randomly dividing the samples into two sets: a calibration set and a test set.[24] Each sample in the calibration set was assigned a y-value of 0 or 1, based on the KDOT reported D-cracking lab result (Passing = 1 and Failing = 0).

[24]In the case of a Super Model, the D-cracking samples included all available samples in the KDOT database. In the case of a Source Model, the D-cracking database was limited to specific geologic members from which the aggregate tested was derived.

Table 3.1: KDOT Samples and Sources

Geologic Member	Total Samples	Quarry Name (Samples) [1]	D Cracking Database Samples [2]
Amoore LS Mb	1	Am-A (1)	1
Bennett Reef Limestone Mb	17	Ben-A (17)	11
Bethany Falls Limestone Mb.	10	Bet-A (3) Bet-B (7)	8
Burlington LS Fm.	1	Bu-A (1)	1
Captain Creek Limestone Mb.	7	Cc-A (1) Cc-B (3) Cc-C (3)	5
Copper-Calloway Ls Mb.	2	Co-A (2)	1
Creswell Limestone Mb	24	Cr-A (4) Cr-B (20)	8
Dakota FM	2	Da-A (2)	2
Ervine Creek Limestone Mb.	50	Ec-A (29) Ec-B Ec-C (11) Ec-D (10)	40
Granite/Diabase Gravel Deposit	1 4		
Hartford Limestone Mb.	4	Ha-A (4)	3
Krider Limestone Mb	1	Kr-A (1)	0
Lower Farley LS Mb	1	Lf-A (1)	1
Raytown LS Mb.	8	Ra-A (8)	7
Rock Bluff Limestone Mb.	2	Rb-A (2)	2
South Bend Limestone Mb.	1	Sb-A (1)	1
Spring Hill Limestone Mb.	14	Sp-A (4) Sp-B (7) Sp-C (3)	8
Stoner Limestone Mb.	24	St-A (4) St-B (9) St-C (1) St-C (7) St-D (3)	22
Tarkio Ls Mb	9	Ta-A (2) Ta-B (4) Ta-C (3)	7
Towanda Limestone Mb.	11	To-A (11)	8
Upper Farley LS Mb	11	Uf-A (11)	9
Warsaw LS. FM	3	Wa-A (3)	3
Winterset Limestone Mb.	5	Wi- A (5)	2
Worland Limestone Mb.	11	Wo-A (6) Wo-B (5)	8

3.4 Statewide D-Cracking (Super) Models

Several attempts were made at calibrating a Super D-cracking model with little success. Calibration and validation testing results of one modeling attempt are shown in Figure 3.1. Figure 3.1 is a plot of observed (or known) pass-fail values on the x-axis and predicted values on the y-axis. Recall that the known values can either be 0 or 1. The left side of the figure depicts the calibration results. All the known calibration samples that failed the KDOT D-cracking test (x-axis value = 0), clustered around the predicted y-value of 0; and all the known calibration samples that passed the test (x-axis value = 1), clustered around the y-value of 1. Although the calibration data showed some scatter, the model conformed to the calibration set. Validation testing results, shown on the right side of the figure, however, did not closely cluster around their known respective pass-fail values of 1 and 0. The model output displays a wide variance around the pass-fail values and yielded a prediction of only 71% efficiency. The Super models were not highly predictive. The poor efficiency can be seen by examining the number of failing samples with y-values greater than the VAD value of 0.5, and the number of passing samples with y-values less than 0.5.[25]

[25] A 71% predictive efficiency is calculated by comparing the number of correct D-cracking predictions to the total number of predictions made. A good predicting efficiency would be expected to be 85% or greater.

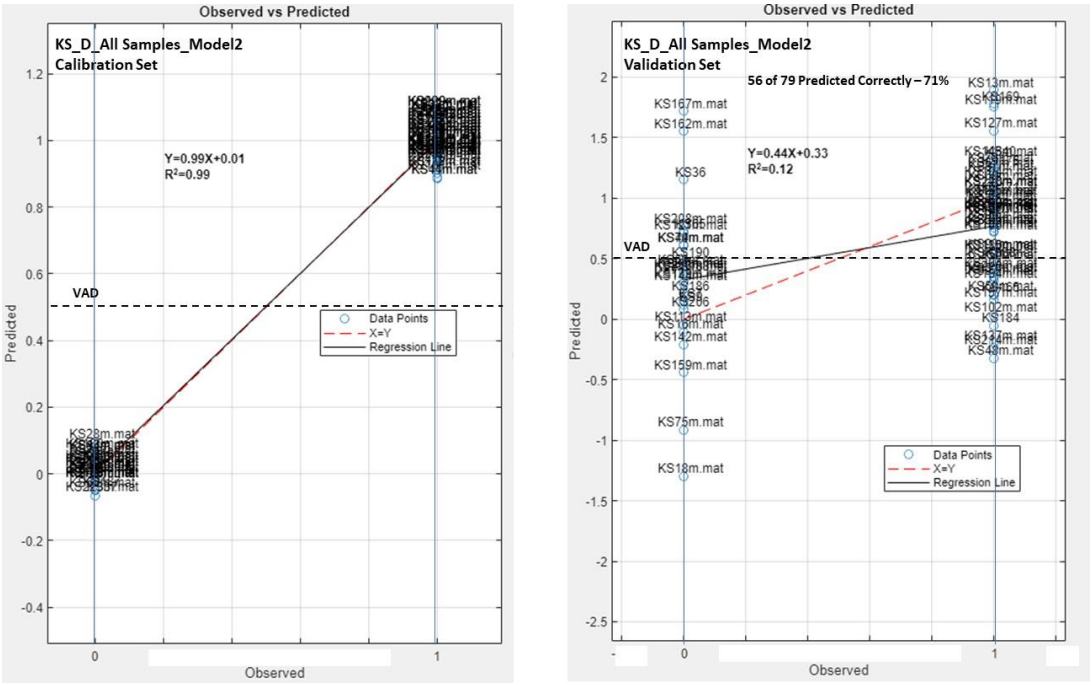

Figure 3.1: Super D-Cracking Model Calibration and Validation: Graphical Results

3.5 Source D-Cracking (Local) Model

KDOT Source Models were defined by geologic member. A listing of the 23 geologic members, and the number of samples available for D-cracking model development per member are listed in Table 3.1. While KDOT provided approximately 159 samples for analysis, only three geologic members contained a sufficient number of samples to attempt model development. These members included: Stoner Limestone, Creswell Limestone, and Ervine Creek.[26]

3.5.1 Stoner Limestone Mb

Twenty-two aggregate samples were available for the Stoner D-cracking modeling effort. Eleven of the 22 were randomly selected for the development of a calibration model and 11 samples were used to validate the model. After development and testing of the first model, a second model was developed by reversing the calibration and validation sets to assess whether sample selection might be introducing a bias in the results of the model.

[26] The Bennett Reef Limestone member had 11 samples available, but only 1 of the 11 (KS113) reportedly failed the KDOT D-cracking test, making model calibration and validation impractical. The number of Creswell Limestone samples available were barely adequate; but Creswell was included for analysis.

The first calibration model and validation test results for the Stoner Model are presented in Figure 3.2. The left side of the figure displays the calibration model and the right side, the validation test. The calibration model exhibited good correlation. The validation test resulted in 11 correct predictions out of 11 samples or prediction 100% efficiency. A list of the samples used in the calibration model and the validation test are respectively included in the figure, along with the numerical y-value predictions. Reversing the calibration and validation sets confirmed the excellent results of the first model. All the D-cracking predictions were correct. The second calibration model and validation test results are presented in Figure 3.3.

3.5.2 Cresswell Limestone Mb

Of the 16 samples available for the development of a Cresswell Limestone D-Cracking model, only eight samples were suitable for use.[27]. This meant that only four samples were available for model calibration and four samples for validation testing.[28]

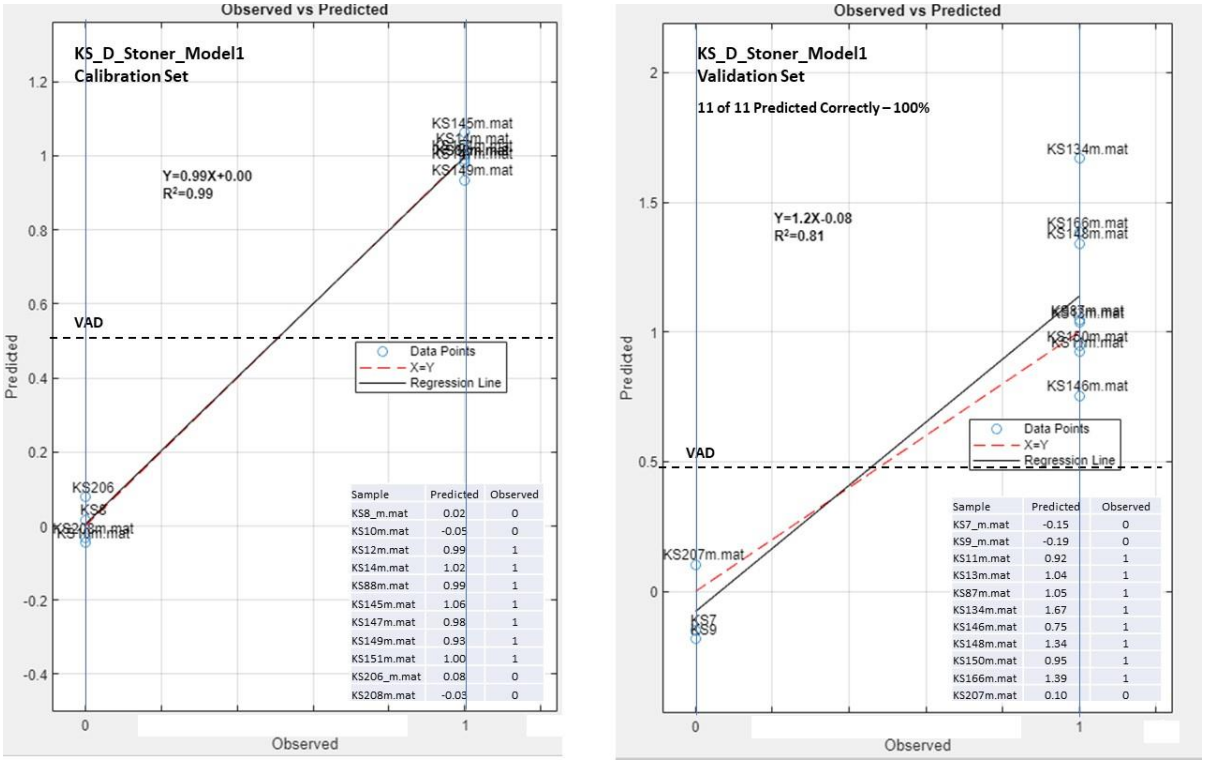

Figure 3.2: Stoner Limestone Model 1 D-Cracking Results

[27] The remaining 8 samples were blends of different beds (production samples) and were judged unsuitable for use in the geologic member model.

[28] So few samples do not provide a sufficient number to develop both a calibration and test set.

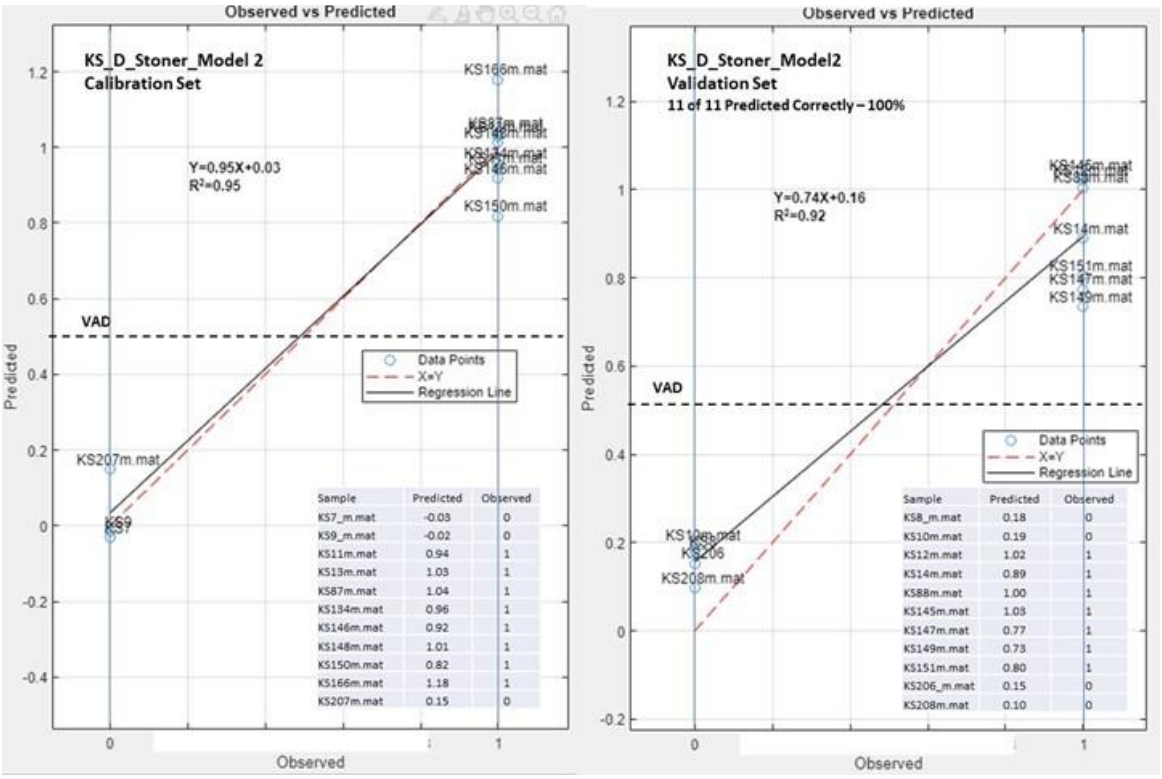

Figure 3.3: Stoner Limestone Model 2 D-Cracking Results

Nonetheless due to the limited number of suitable samples with adequate sample populations a model was generated. After development and testing of the first model, a second model was developed by reversing the calibration and validation sets.

The first calibration model and validation test results for the Cresswell Model are presented in Figure 3.4. The second model results are presented in Figure 3.5. Of the four samples available for validation testing, the first model predicted the results with 100% efficiency. The second model predicted three of the four samples correctly. These data reveal that the potential exists that Creswell Limestone member could serve as a Source or Local D-cracking model. The insufficient number of samples precludes any additional assessment.

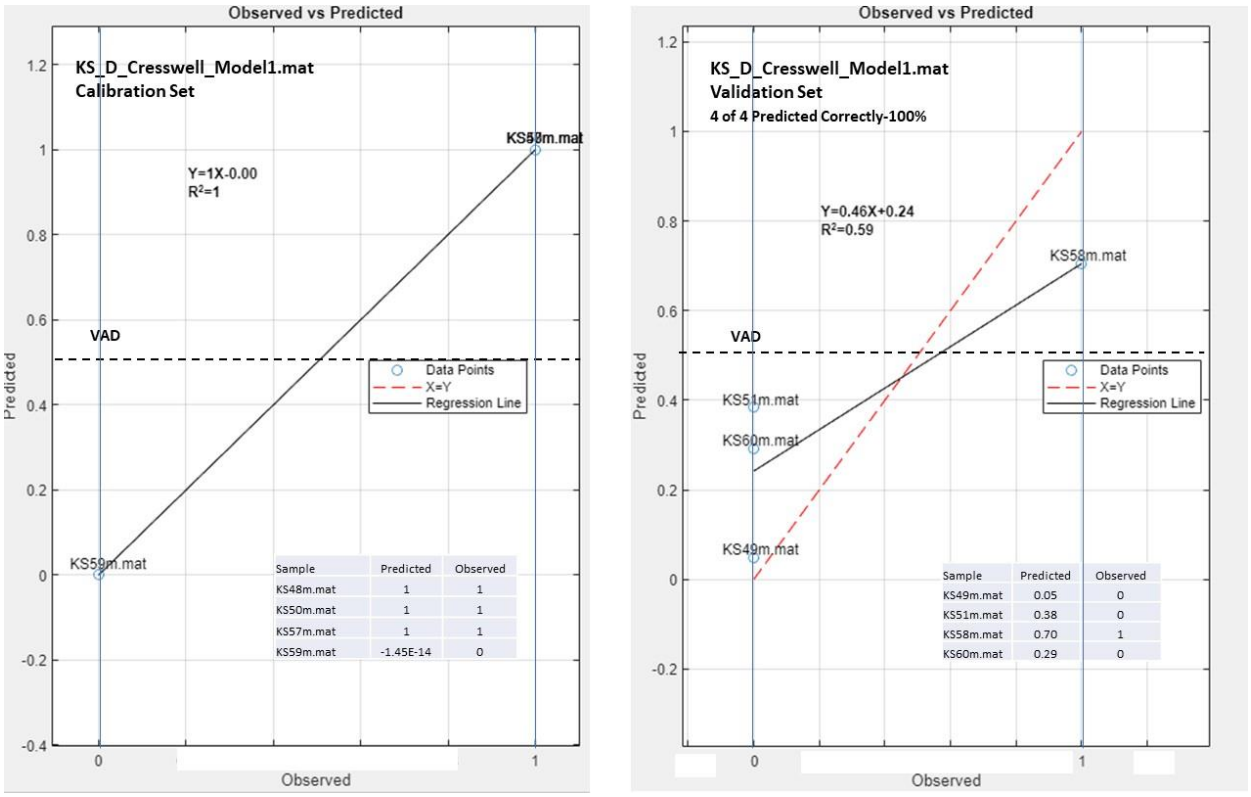

Figure 3.4: Cresswell Limestone Model 1 D-Cracking Results

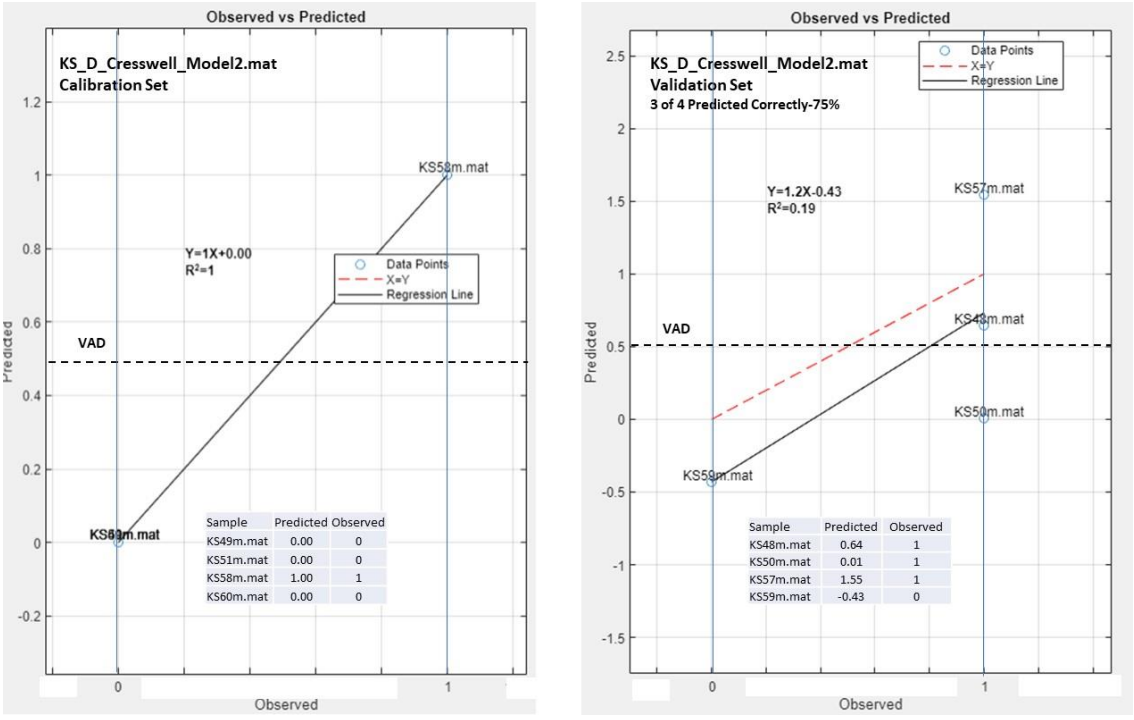

Figure 3.5: Cresswell Limestone Model 2 D-Cracking Results

3.5.3 Ervine Creek Limestone Mb

The Ervine Creek Limestone member provided 40 samples for analysis. In total, this meant that 20 samples could be used for the development of the calibration model and 20 samples for the validation test. It is noteworthy that of the 40 samples collected by KDOT, 20 samples were collected in the year 2018 and 20 samples were collected in the year 2019.

The initial Ervine Creek Modeling effort included all 40 samples. Similar to previously described D-cracking modeling efforts, two models were developed. The first model included the random selection of 20 of the 40 available samples for model calibration and the remaining 20 for model validation. The second model was developed and tested by reversing the calibration and validation sets. The results of the Model 1 and Model 2 efforts are shown in Figure 3.6 and Figure 3.7, respectively. The prediction efficiency of the respective models was 70% and 75%, respectively.

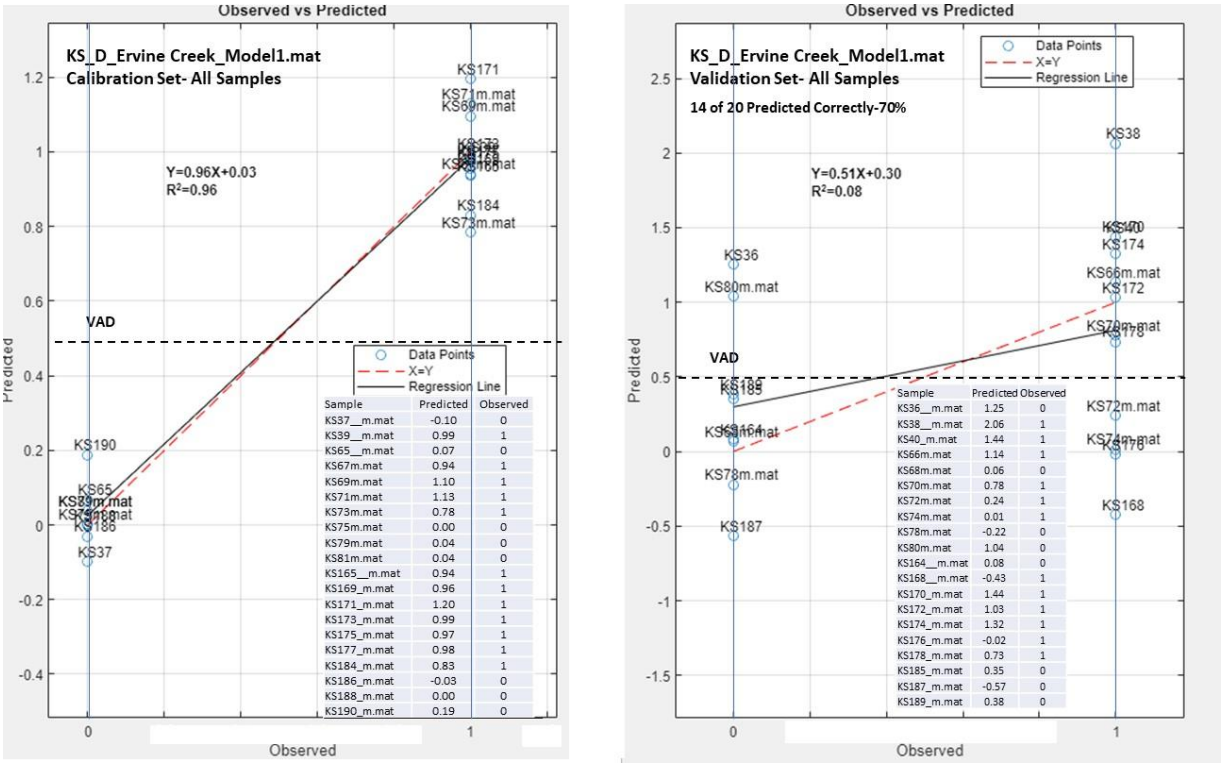

Figure 3.6: Ervine Creek Limestone Model 1 D-Cracking Results (All Samples)

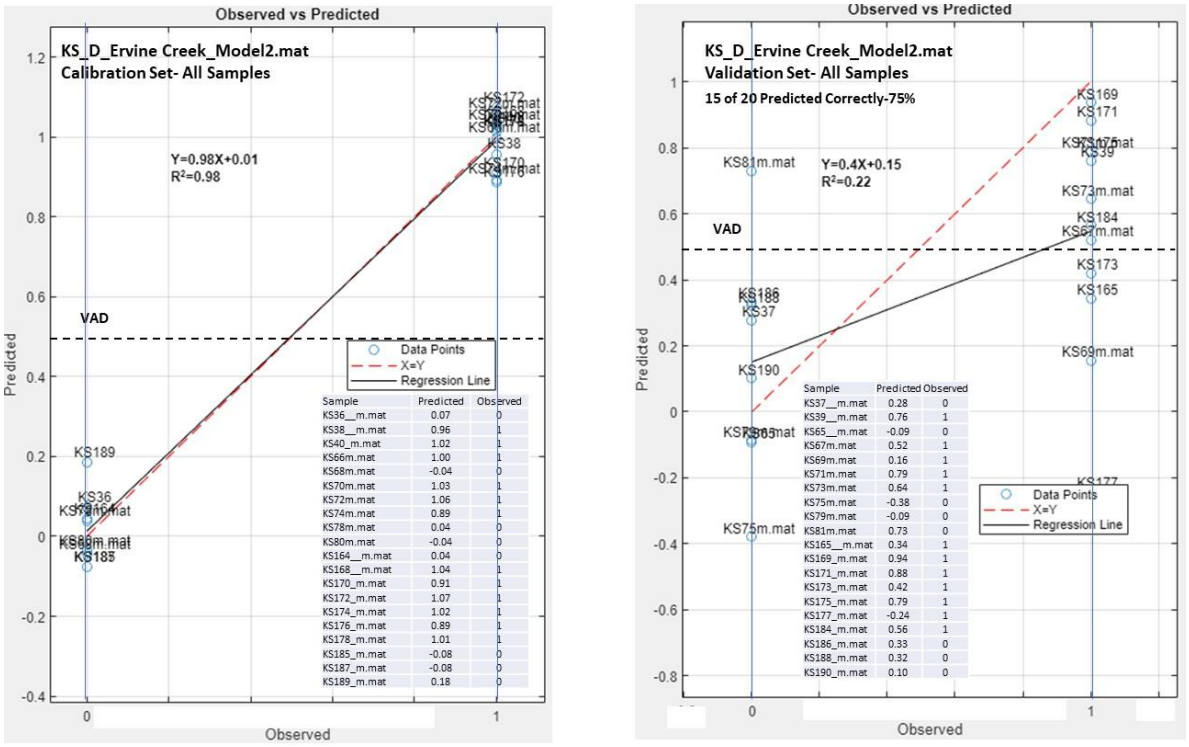

Figure 3.7: Ervine Creek Limestone Model 2 D-Cracking Results (All Samples)

The relatively weak predictive efficiency of the Ervine Creek models that included both the 2018 and 2019 samples suggested a closer look at the spectra associated with the samples collected during each respective year. This was accomplished using a PC Score plot, described in Section 2.4.1 Principal Components Analysis (PCA), to evaluate whether significant spectral differences could be detected between samples collected during the different time periods. The results of this analysis are presented in Figure 3.8. Recalling from Section 2.4.1 Principal Components Analysis (PCA) that in a PC score plot, samples with similar spectra tend to cluster in groupings, the data presented show that almost all of the 2019 samples cluster in the third quadrant of the score plot; and the 2018 sample set almost exclusively span the first and fourth quadrants, extending somewhat into the second. The score plot data suggest that the 2018 samples differ from the 2019 samples. Due to the wide spread of the 2018 grouping, and number of quadrants occupied by this grouping, these data suggest that the 2018 samples exhibit much greater chemical heterogeneity than the 2019 samples.

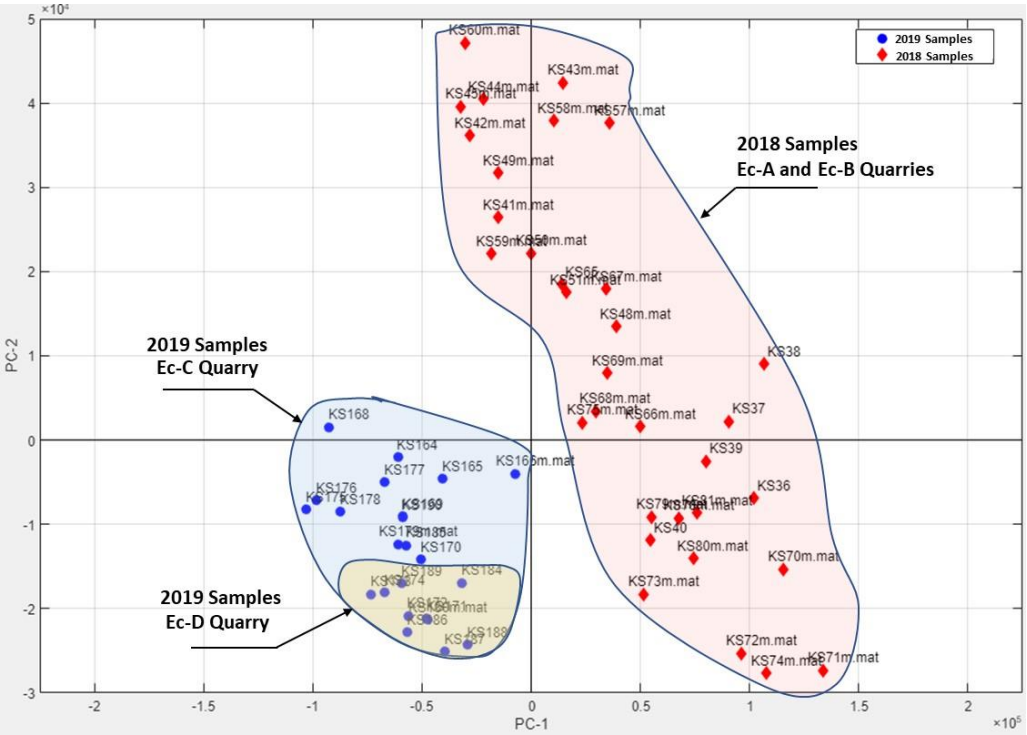

Figure 3.8: PC Score Plot – 2018 and 2019 Samples

All of the 2018 samples were collected from quarries Ec-A and Ec-B. The 2019 samples were collected from quarries Ec-C and Ec-D. In addition, the Ec-C samples cluster separately from the Ec-D quarry samples. The differences between the 2018 and 2019 samples are most likely due to differences in rock chemistry amongst the quarries; and these differences were enough to adversely affect the quality of the total Ervine Creek models, presented in Figure 3.6 and Figure 3.7.

Since an Ervine Creek model that included all Ervine Creek samples was not very effective, two sub-member models were developed. The first sub-member model included samples from the 2018 data set, which consisted of samples from the Ec-A and Ec-B quarries; and the second sub-member included samples from the 2019 data set, which consisted of samples from the Ec-C and Ec-D quarry sites.

The 2018 model results are presented in Figure 3.9 and Figure 3.10. As previously described, two models were developed for this analysis. The first model included the random selection of half of the available samples for model calibration and the remaining half for model validation. The second model was developed and tested by reversing the calibration and validation

sets. Figure 3.9 displays the results of Model 1 and Figure 3.10 the results of Model 2. Model 1 yielded 70% predictive efficiency and Model 2 a 90% efficiency.

The 2019 model results are presented in Figure 3.11 and Figure 3.12. Two models were also developed for the 2019 samples. Figure 3.11 displays the results of Model 1 and Figure 3.12, Model 2. Model 1 yielded a 100% predictive efficiency and Model 2 an 80% efficiency. Separate models for the Ec-C quarry site or the Ec-D site could not be developed because all 11 Ec-C samples passed D-cracking and of the seven Ec-D samples available for analysis, six failed the D-cracking test. Only by combining the two quarries, which is represented in the 2019 models, presented in Figure 3.11 and Figure 3.12, were there sufficient data for model calibration.[29]

A summary table for the Ervine Creek models is presented below. It is notable that the efficiency of the models improves as the calibration set moves from a wider geologic member analysis to a local quarry analysis.[30]

Table 3.2: Ervine Creek Prediction Efficiency Summary

Ervine Creek Geologic Source	Modelled Prediction Efficiency (%) [1]
Total Ervine Creek Member	70-75
Ec-A and Ec-B Quarries Only (2018 Data)	70-90
Ec-C and Ec-D Quarries (2019 Data)	80-100

[1] Prediction efficiency range of the two models developed for each analysis.

[29] Model calibration requires a calibration set that contains distribution of passing and failing samples.

[30] The 2019 data was shown to model better than the 2018 data. In addition to the differences in rock chemistry between the samples collected and scanned during the two periods, a second factor could have influenced the results. Laser scanning operations improved each year. This was due to both hardware upgrades and operator experience. Such improvement could have yielded better spectral resolution in 2019 compared to 2018, thereby generating improved models.

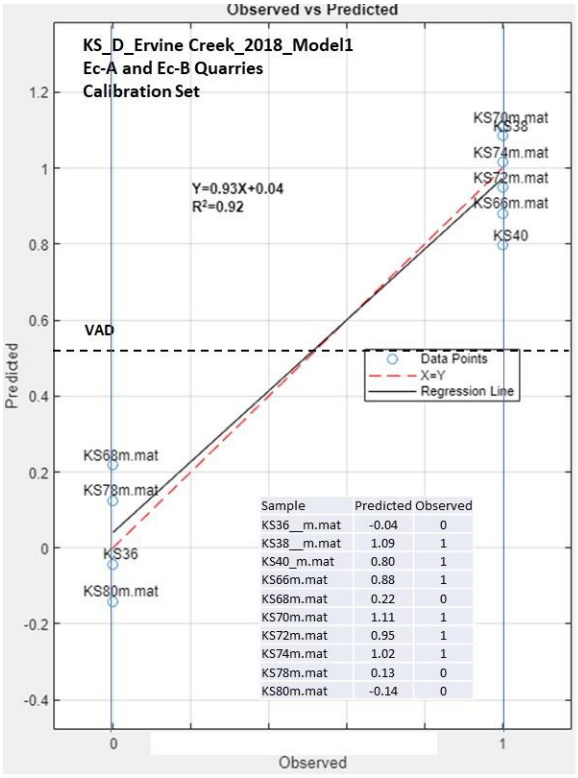

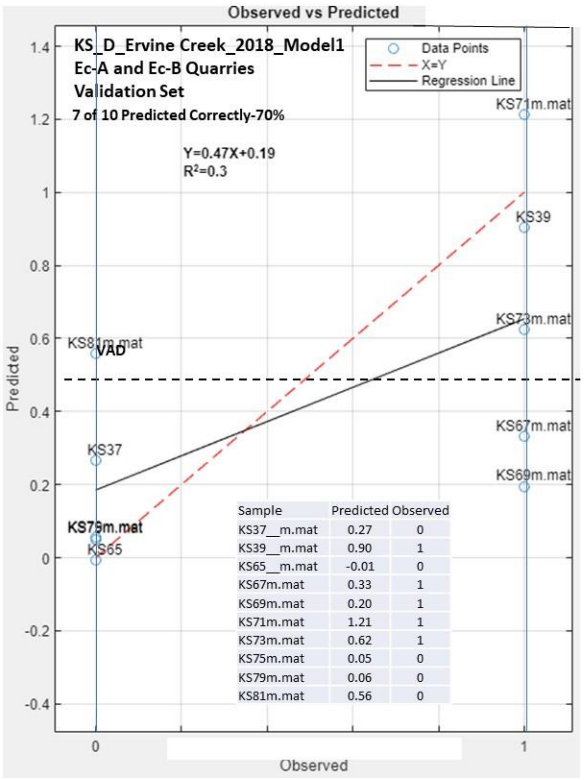

Figure 3.9: Ervine Creek 2018 Model 1 D-Cracking Results

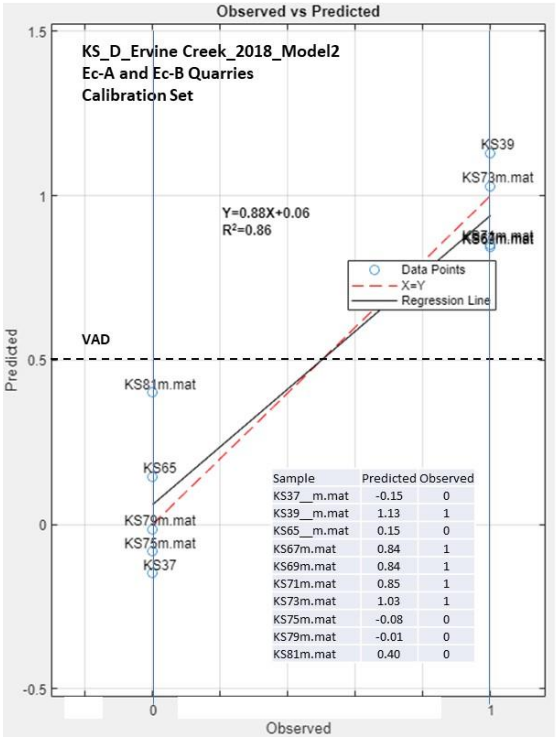

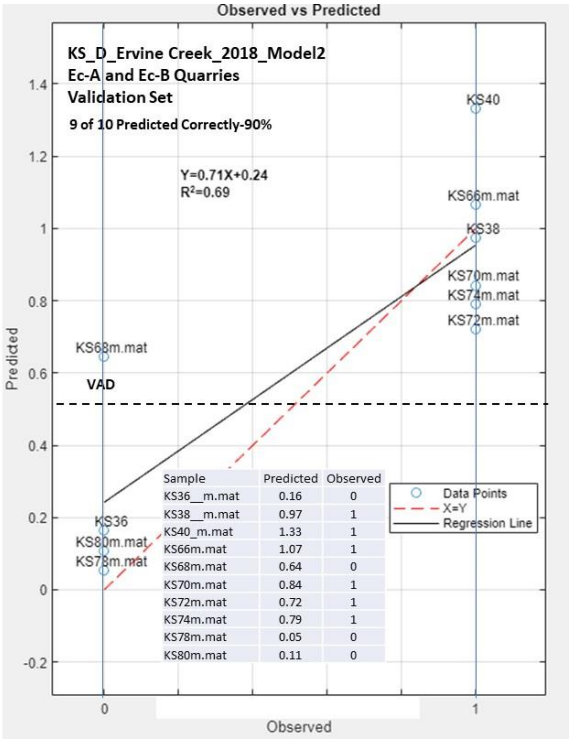

Figure 3.10: Ervine Creek 2018 Model 2 D-Cracking Results

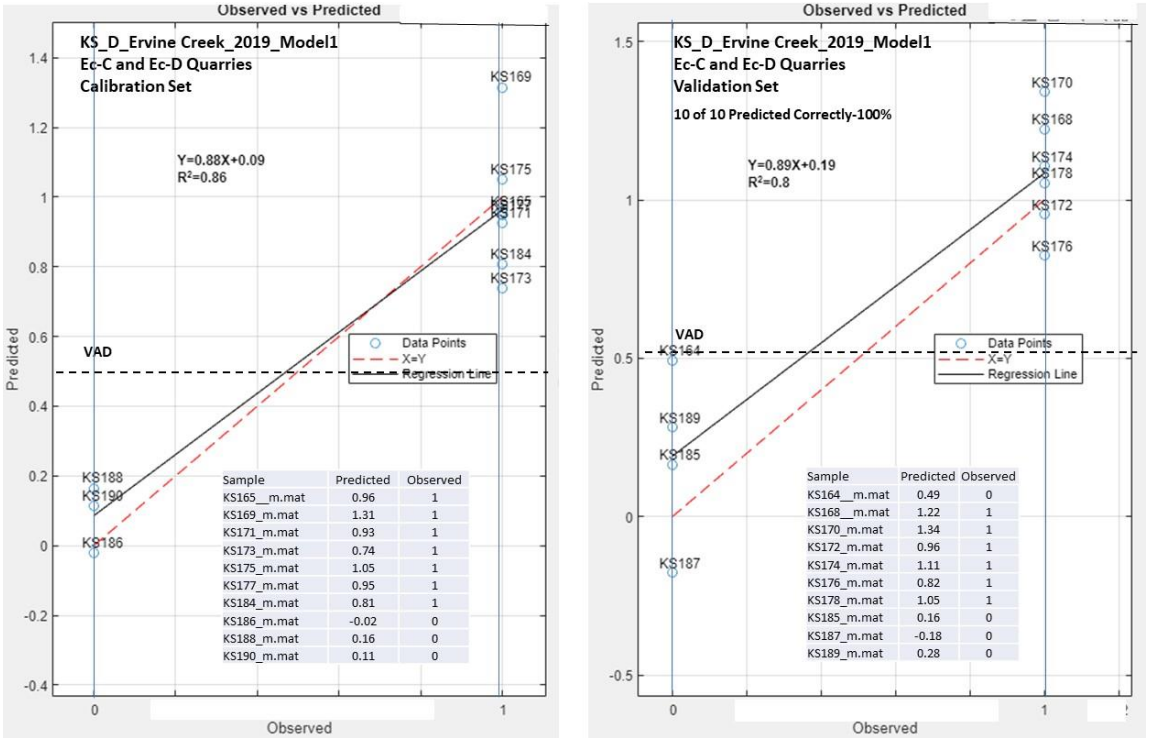

Figure 3.11: Ervine Creek 2019 Model 1 D-Cracking Results

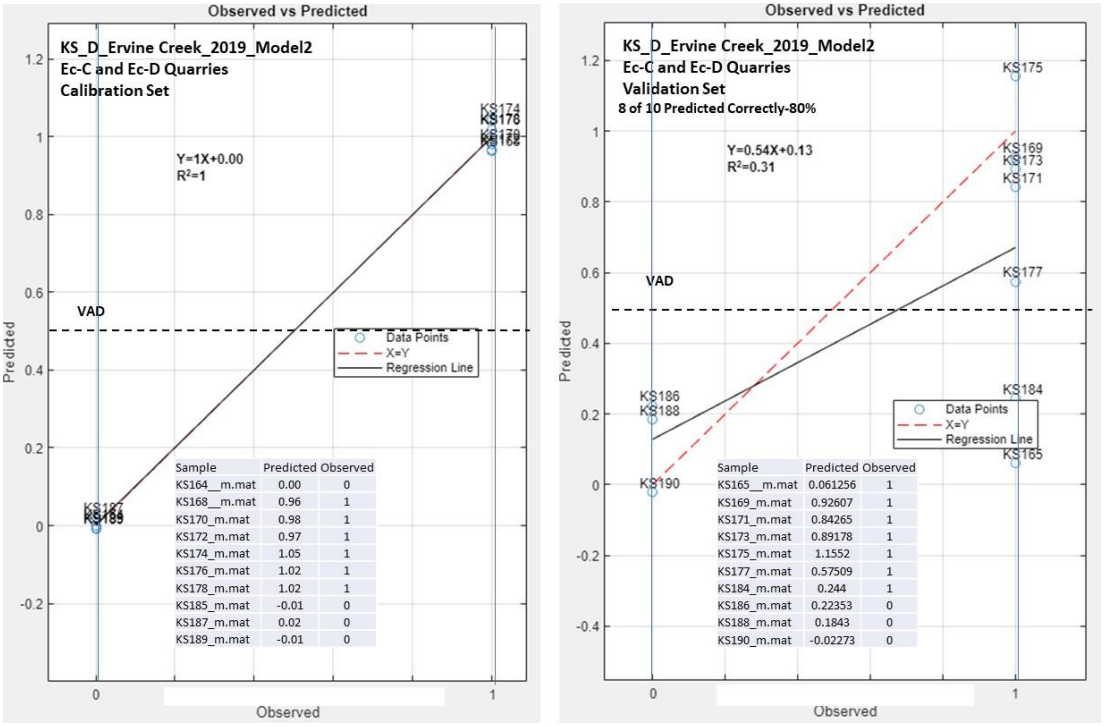

Figure 3.12: Ervine Creek 2019 Model 2 D-Cracking Results

3.6 Unknown KDOT Sample D-Cracking Analysis

In this study phase, KDOT provided 50 unknown samples, identified as sample KSU1–KSU50. The objective was to determine the D-crack susceptibility of each of the unknowns. Table 3.3 lists the unknown samples, grouped by geologic members. The KSU1–KSU50 samples comprise eight different members. Only Ervine Creek had a sufficient number of calibration samples to develop a working model.

The Ervine unknown sample modeling results are presented in Table 3.4. The table lists the y-value results of a PLS model developed for Ervine Creek (KS_D_Ervine Creek_Model1). All y-values above 0.5 suggest passing D-cracking results and those below 0.5, failing results. All of the KSU Ervine Creek samples were projected to pass. These blank samples (KSU12–KSU24) all were reported by KDOT as passing samples after the projections were made.

Table 3.3: Unknown Sample Modeling Summary and Results

Unknown Sample Members	Samples	D-Cracking Model Predictions
Dakota	KSU43-KSU44	Only 2 samples were available for calibration, so could not develop a calibration model
Ervine Creek	KSU12_KSU24	Model was developed with 20 calibration samples 12 passing and 8 failing Reference model = KS_D_Ervine Creek_Model1
Lower Farley	KSU11	Only 1 sample was available for calibration.
Raytown	KSU45_KSU52	7 samples were available for calibration, but all samples passing so could not generate a calibration model.
Rock Bluff	KSU16- KSU20	Only 2 samples were available for calibration, so could not develop a calibration model
Tarkio	KSU25-KSU31	7 samples were available for calibration, but only 1 of the 7 failed the KDOT D-cracking test so could not generate a calibration model.
Towanda	KSU32-KSU42	8 samples were available for calibration, but only 1 of the 8 failed the KDOT D-cracking test so could not generate a calibration model.
Upper Farley Unknowns	KSU1-KSU10	Insufficient calibration samples available

Table 3.4: Ervine Creek Unknown Sample Model Results (y-value predictions)

Sample	Predicted
KSU12	1.46
KSU13	1.30
KSU14	1.03
KSU15	1.47
KSU17	1.65
KSU18	1.38
KSU19	1.52
KSU21	1.52
KSU22	1.53
KSU23	1.65
KSU24	1.28

3.7 Blended Field-Production Sample Analysis

Once production samples that contain a blend of two or more aggregate sources are produced in the field, it is almost impossible, using standard aggregate testing methods, to determine whether the individual sources comprising the blend were all derived from pre-approved materials. The following subsections contain a series of analyses of blended KDOT samples that illustrate how laser scanning analysis can address this issue.

3.7.1 Tarkio Limestone, Ta-A. Quarry, Source Beds 1-5 Validation

According to KDOT, two aggregate samples, labelled KS116 and KS117, were reported to have been collected from the same quarry site (Quarry Label Ta-A) and the same beds within the quarry.

The KDOT question: Were the KS116 and 117 samples collected from the same beds?

Classification of sample spectra can be undertaken by employing a PCA model to determine whether the samples spatially cluster into separate groups or one group. Clustering into separate groups would indicate that the samples are measurably different. Two sample sets clustering together would indicate that the samples are not measurably different. A PCA model was created using 19 individual scans of sample KS116 and 21 scans of sample KS117. The model results are presented in the PC score plot shown in Figure 3.13. The score plot depicts the spatial distribution of individual KS116 and KS117 sample scans. The spatial distribution of the KS116

and KS117 scans appear random and do not cluster into separate groupings. This suggests that their spectra and underlying chemistry are similar. It can therefore be assumed that KS116 and KS117 were derived from the same source.

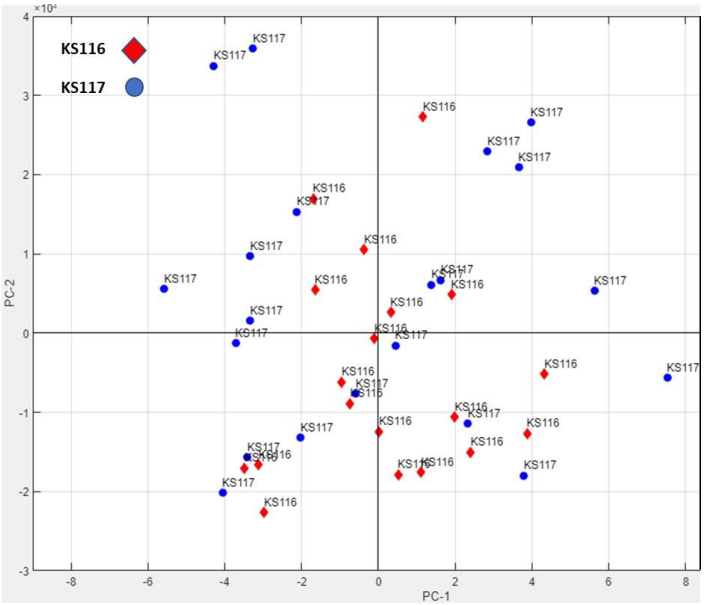

Figure 3.13: KS116-KS117 Source Bed Validation

Samples KS203 and 204 were collected from a different part of the same Ta-A quarry and from designated Beds 1 and 2.

The KDOT Question: Are the KS203 and 204 samples similar to the KS 116 and 117 samples?

When the scanned spectra from both the KS203 and 204 samples are included in the PCA model, with the KS116 and 117 samples, the results show that the 203 and 204 samples cluster in a separate grouping, indicating that the 203 and 204 spectra are measurably different than the 116 and 117 spectra. This is shown in Figure 3.14. The KS203 and 204 also appear to form their own separate subgroupings, suggesting that there are differences between the 203 and 204 samples.

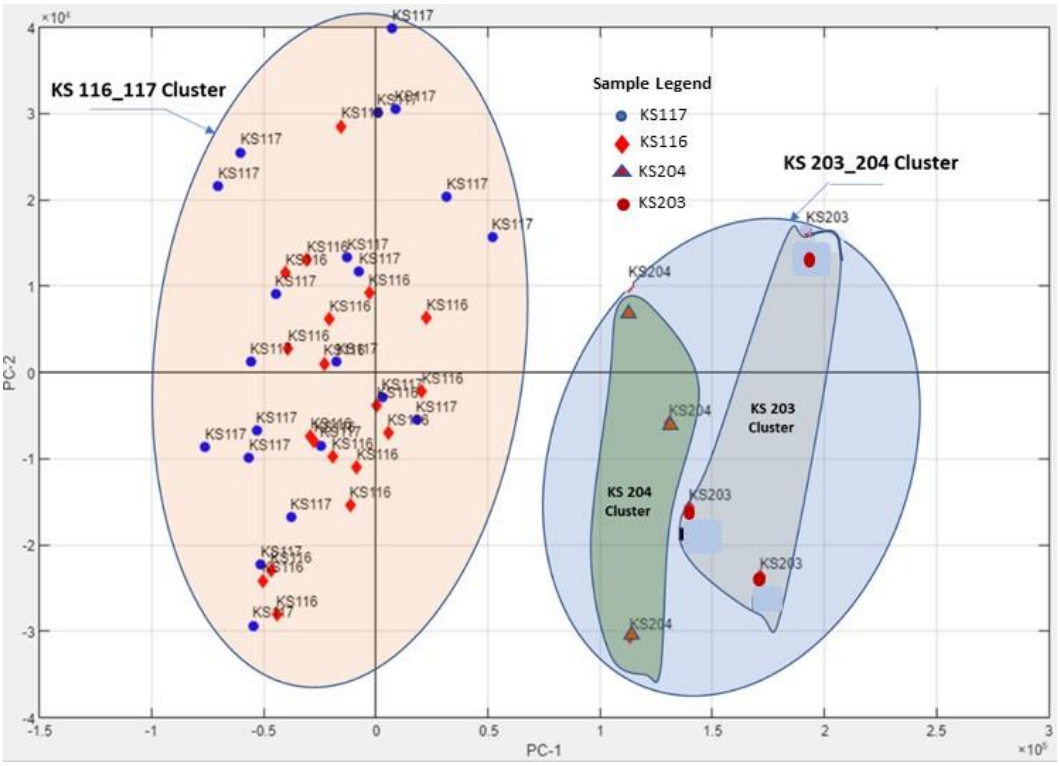

Figure 3.14: KS116-KS117 and KS203-KS204 Comparison

3.7.2 Stoner Limestone Mb, St-B Quarry Production Sample Validation

Four different production samples (KS85, 86, 87, and 88) were reported to be mixtures of four ledge samples from the quarry site, labelled St-B in the Stoner limestone member. Samples collected from these four ledge samples were respectively labelled KS11, 12, 13 and 14.

The KDOT question: Are each of the production samples (KS85, 86, 87, and 88) mixtures of the four ledge samples (KS11, 12, 13, and 14)?

PCA models were developed for each of the four production samples to determine whether the production samples would fall into a PC score field defined by the four ledge samples. The results of the analysis for each of the four production samples (KS85, 86, 87, and 88) are presented in Figure 3.15, Figure 3.16, Figure 3.17, and Figure 3.18, respectively. Each of the PC score plots displays the two-dimensional projections of the multidimensional spectral array associated with each ledge sample and the specific production sample being evaluated. In Figure 3.15, for example, this would include the four ledge samples (KS11, 12, 13, and 14) and the production sample (KS85). The ledge samples together span an area in PC space defined by the ellipse, drawn over

the score plot. The boundary of this ellipse defines what is termed the Ledge Field. In addition, the production sample, KS85, which was scanned three times defines its own smaller KS85 Production Field, highlighted in the figure.

If the Production Sample KS85 is a mixture of KS11, 12, 13, and 14, then the KS85 Production Sample field must fall within the boundary of the KS11, 12, 13, and 14 sample Ledge Field. The KS85 Production Sample field does fall within the Ledge Field boundary and so it is concluded that it is likely that KS85 is a mixture of the KS11, 12, 13, and 14 ledge samples.

The results of the remaining analyses are summarized in Table 3.5. Each of the production samples are likely mixtures of the ledge samples.[31]

Table 3.5: Stoner-St-B Production Sample Validation Results

Production Samples	Mixture of Ledge Samples (KS11, 12, 13, and 14)
KS85	Yes
KS86	Yes
KS87	Yes
KS88	Yes

[31] If the production sample field falls within the ledge field boundary, then one can conclude that it is "likely" that the production sample is a mixture of the ledge samples. This is because the production samples could be a mixture of other samples that also generate a ledge field that encompasses the Production Sample Field. If, however, the Production sample does not fall within a ledge sample field, then it can be concluded that the Production Sample is "not" a mixture of the ledge samples.

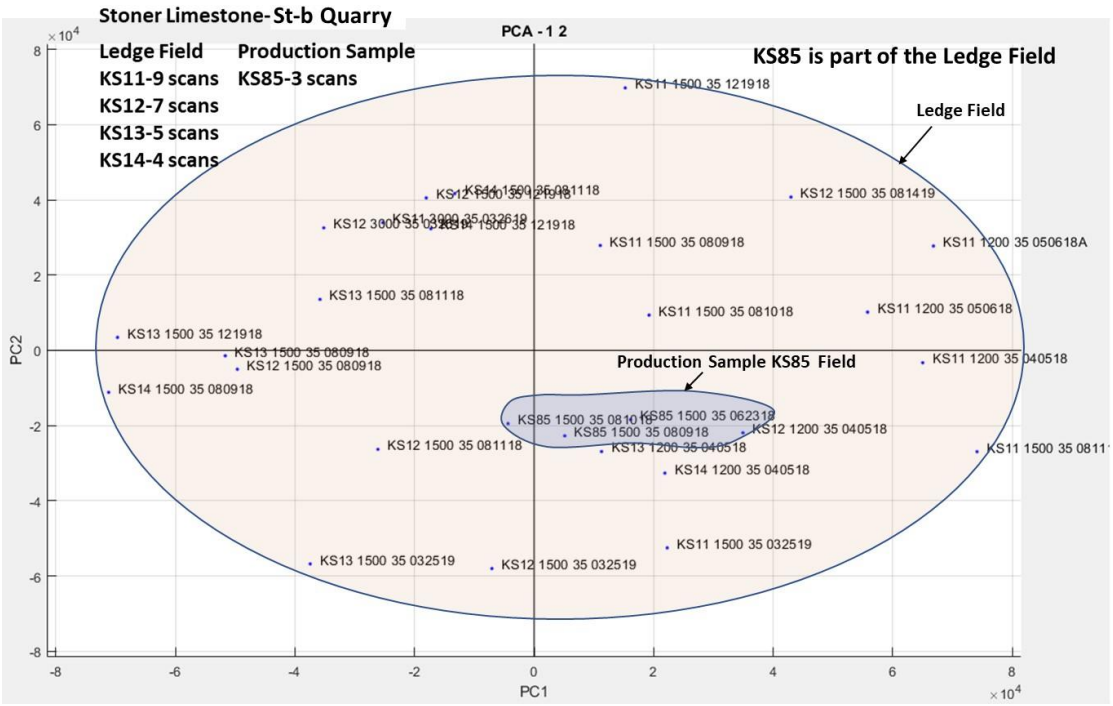

Figure 3.15: KS85 Production Sample Validation

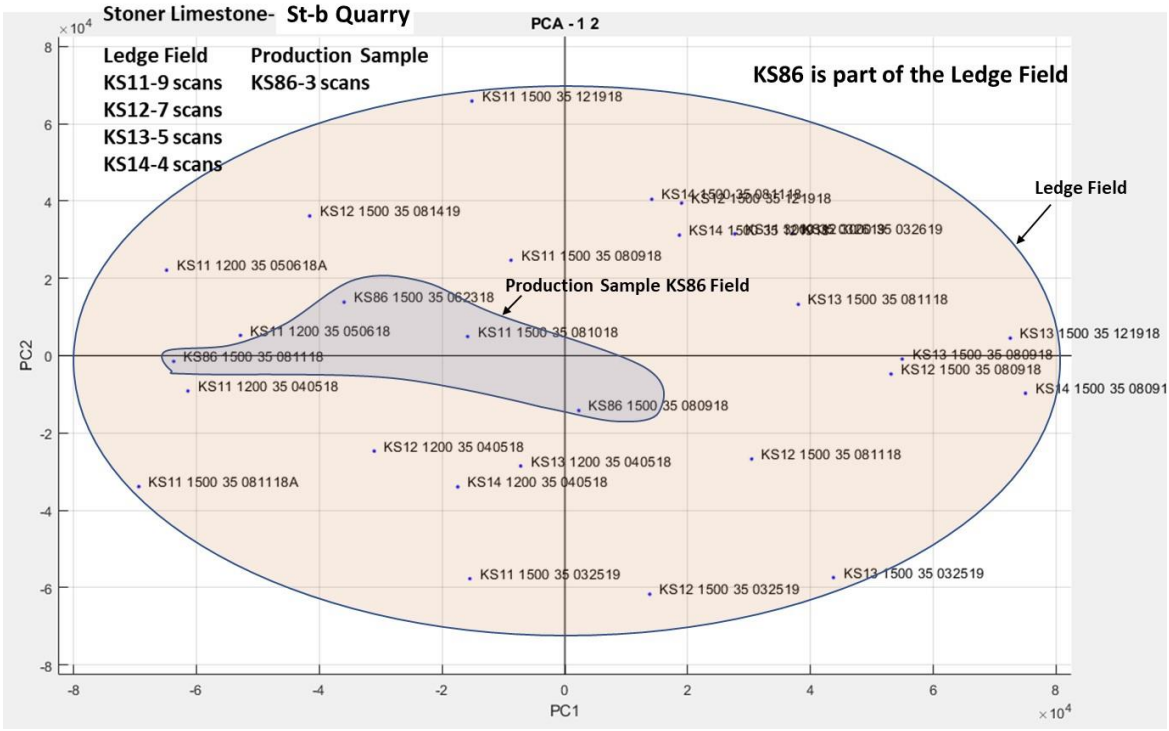

Figure 3.16: KS86 Production Sample Validation

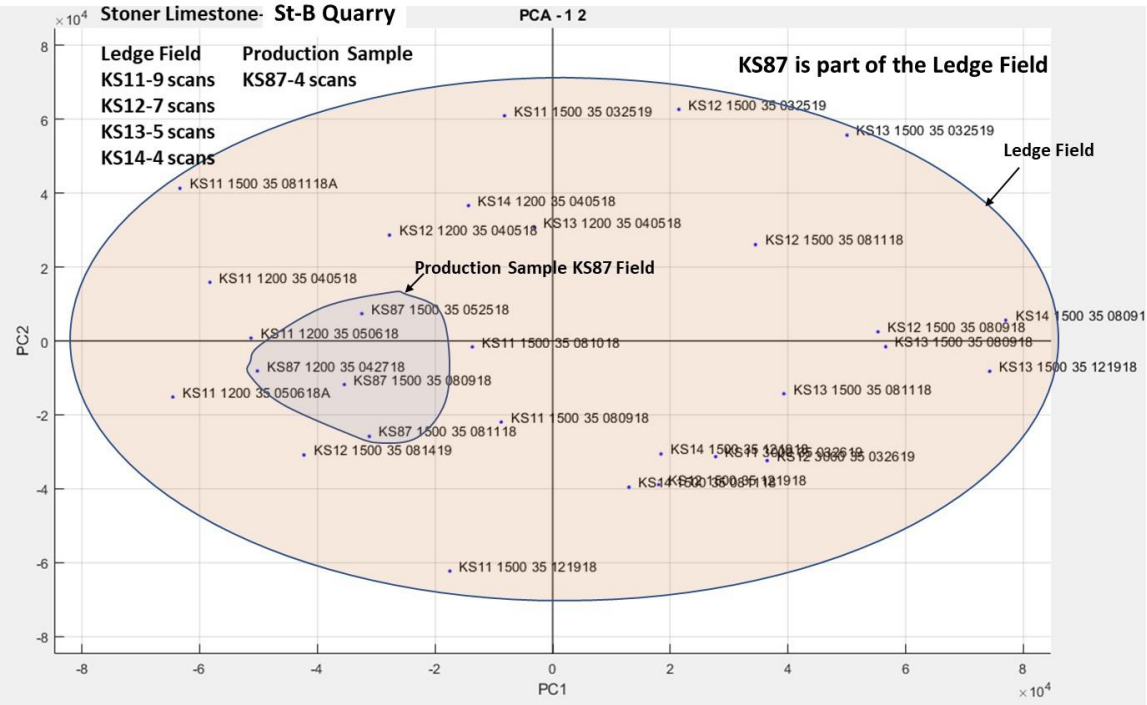

Figure 3.17: KS87 Production Sample Validation

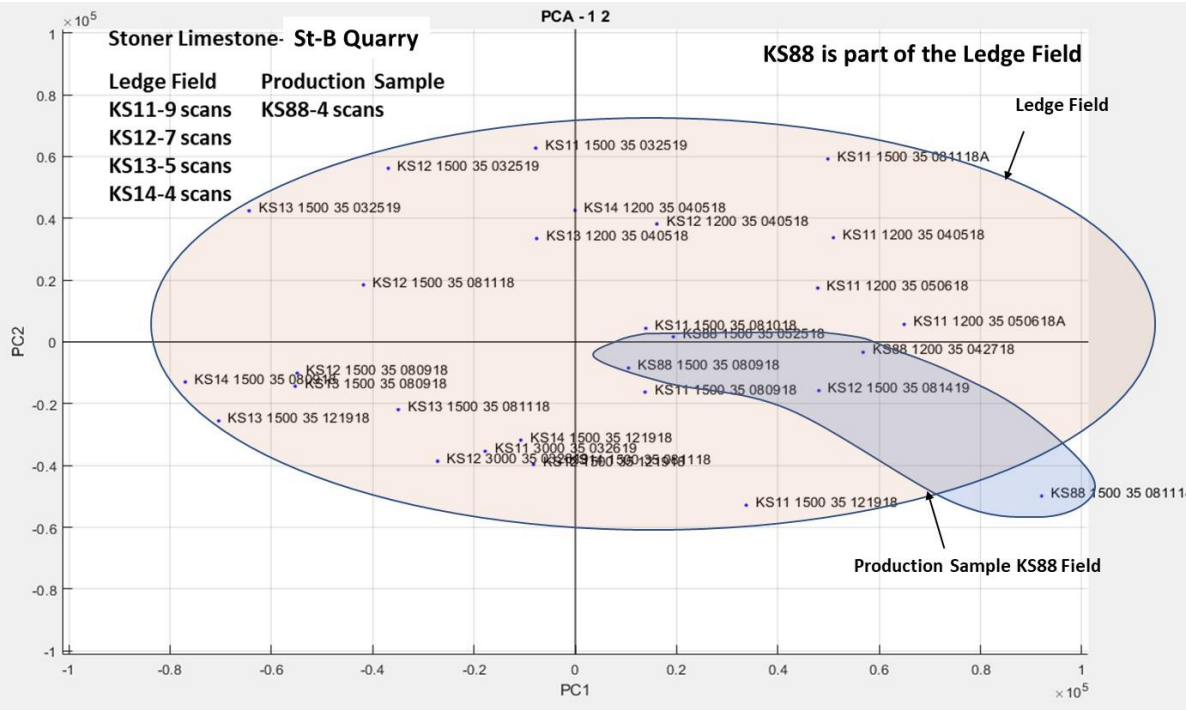

Figure 3.18: KS88 Production Sample Validation

3.7.3 Bethany Falls Mb, Bet-B Quarry Production Sample Validation

Four different production samples (KS91, 92, 93, and 94) were reported to be mixtures of three different ledge samples from the Bethany Falls, Bet-B Quarry. Samples collected from the three ledge samples were respectively labelled KS95, 96, and 97.

The KDOT question: Are each of the production samples (KS91, 92, 93, and 94) mixtures of the three ledge samples (KS95, 96, and 97)?

The Bethany Falls, Bet-B Quarry analysis was undertaken in the same manner as the Stoner Limestone Mb, St-B Quarry, previously described. PCA models were developed for each of the four production samples to determine whether the production samples would fall into a PC score field defined by the three ledge samples. The results of the analysis for each of the four production samples (KS91, 92, 93, and 94) are presented in Figure 3.19, Figure 3.20, Figure 3.21, and Figure 3.22, respectively. The results are summarized in Table 3.6.

Table 3.6: Bethany LS- Bet-B Sample Validation Results

Production Samples	Mixture of Ledge Samples (KS11,12,13 and 14)
KS91	Yes
KS92	Yes
KS93	Yes
KS94	No

All of the production samples, with the exception of KS94 fell within the ledge field boundary. It is concluded that KS94 is not a mixture of the ledge field samples.

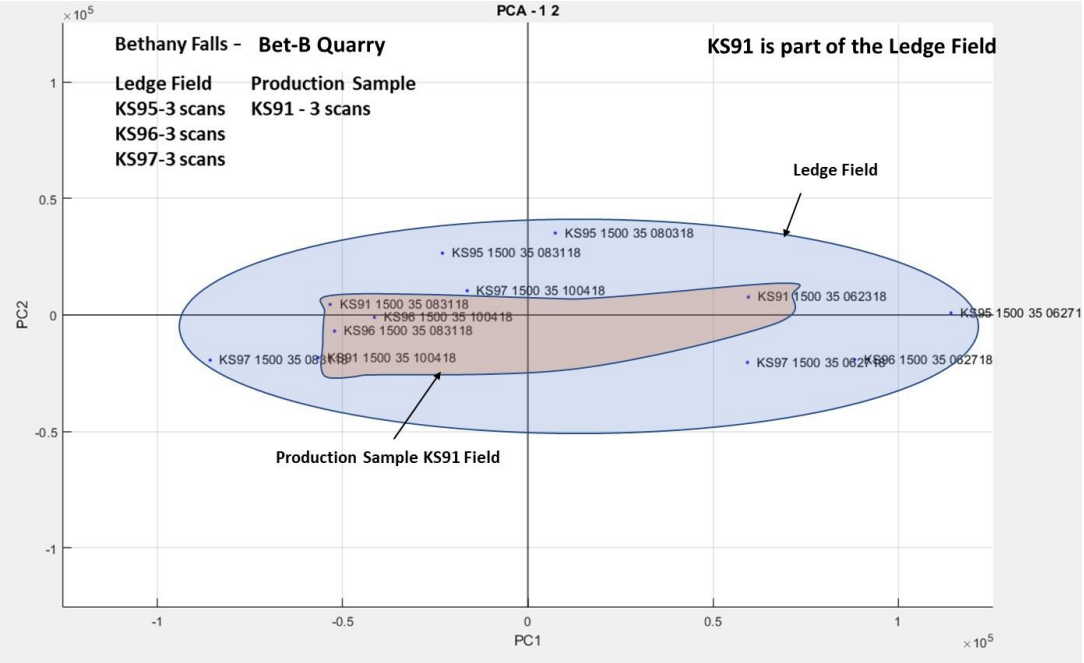

Figure 3.19: KS91 Production Sample Validation

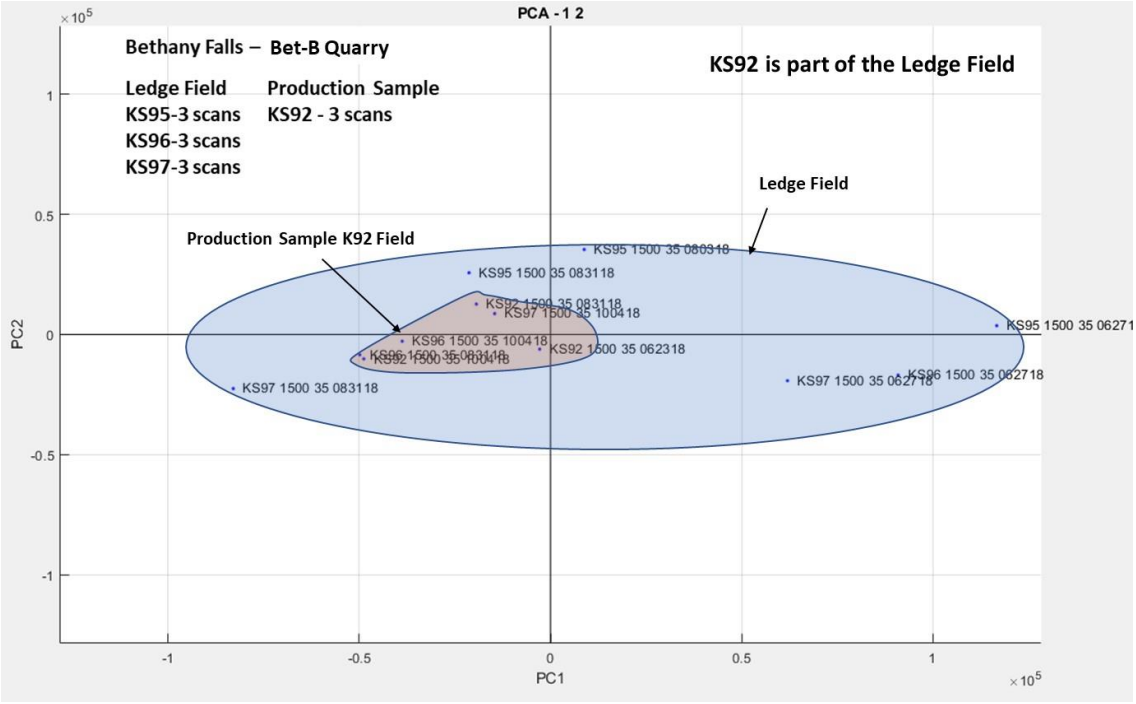

Figure 3.20: KS92 Production Sample Validation

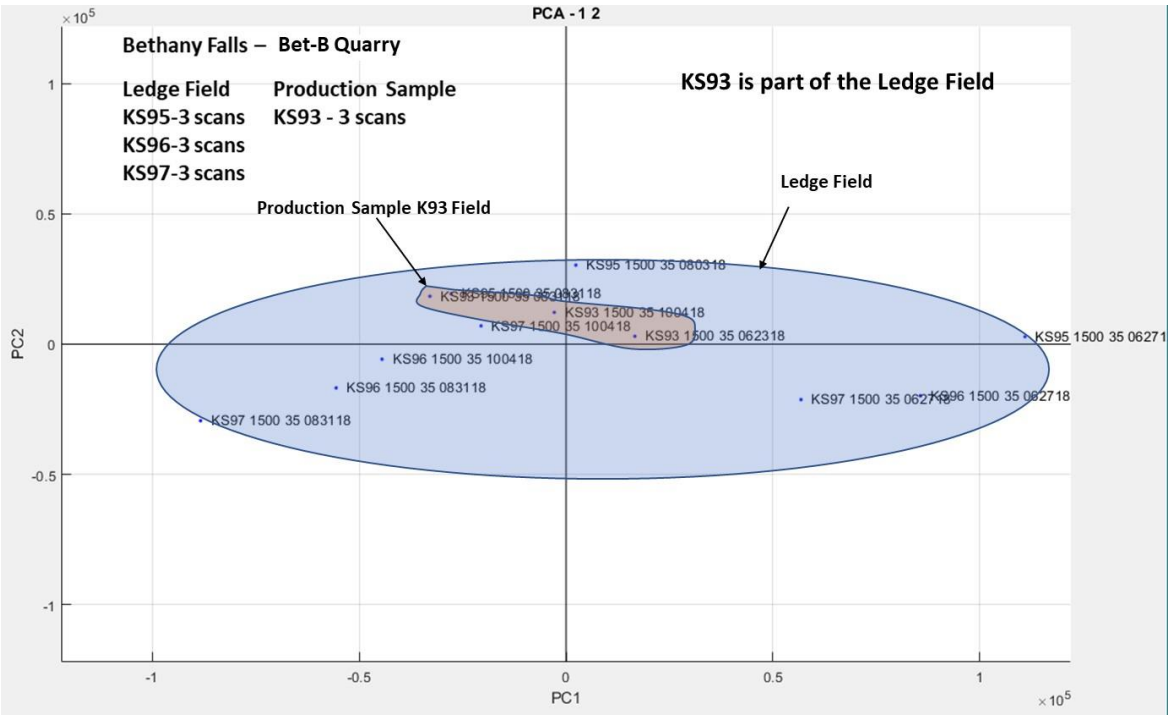

Figure 3.21: KS93 Production Sample Validation

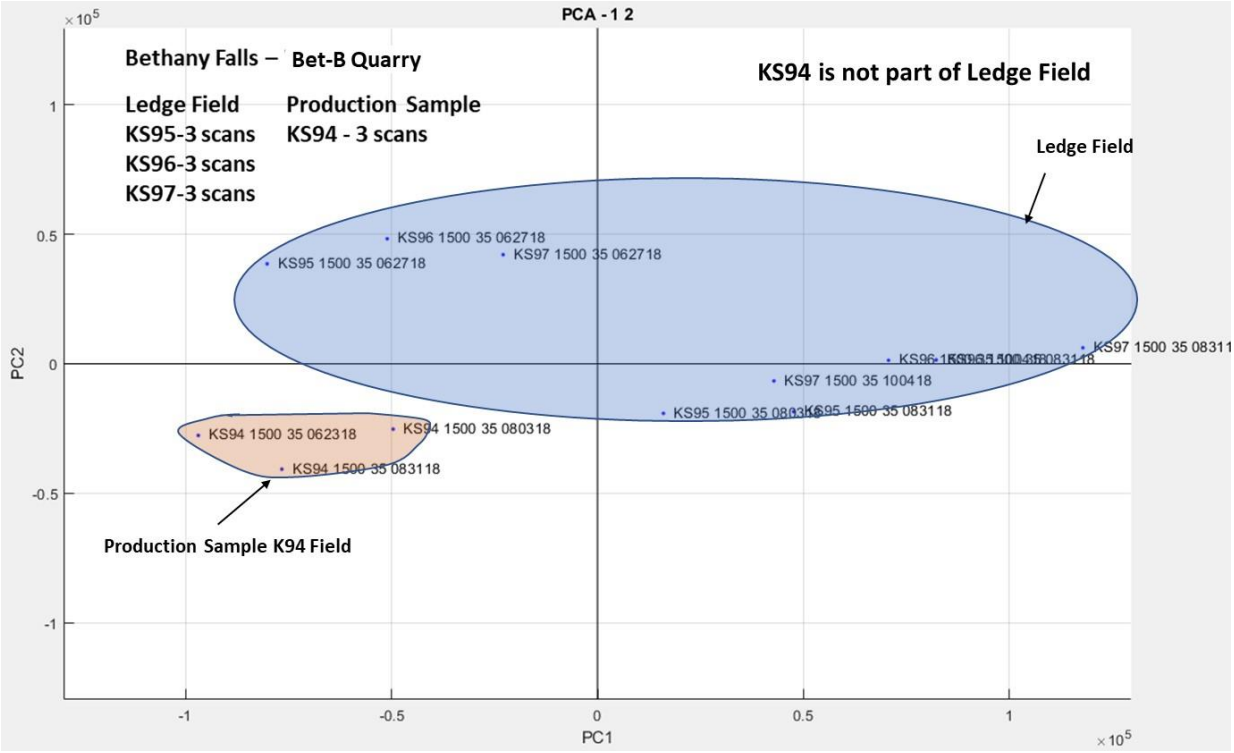

Figure 3.22: KS94 Production Sample Validation

3.7.4 Towanda Mb, To-A. Production Sample Validation

Eight different production samples (KS98, 99, 100, 101, 102, 103, 104, and 105) were reported to be mixtures of two different ledge samples from the Tonawanda Member, To-A Quarry. Samples collected from the two ledge samples were respectively labelled KS106 and 107.

The KDOT question: Are each of the production samples (KS98-KS105) mixtures of the two ledge samples (KS106 and KS107)?

The Towanda Mb, To-A Quarry analysis was undertaken in the same manner as the prior analyses. PCA models were developed for each of the eight production samples to determine whether the production samples would fall into a PC score field defined by the two ledge samples. The results of the analysis for each of the eight production samples (KS98-KS105) are presented in Figure 3.23, Figure 3.24, Figure 3.25, Figure 3.26, Figure 3.27, Figure 3.28, Figure 3.29, and Figure 3.30, respectively. The results are summarized in Table 3.7.

Table 3.7: Towanda Mb, To-A Sample Validation Results

Production Samples	Mixture of Ledge Samples (KS106, 107)
KS98	No
KS99	Yes
KS100	No
KS101	No
KS102	No
KS103	No
KS104	No
KS105	No

With the exception of KS99, none of the production samples fell within the ledge field boundary. It is concluded that KS99 is the only sample that is a likely mixture of the ledge field samples.

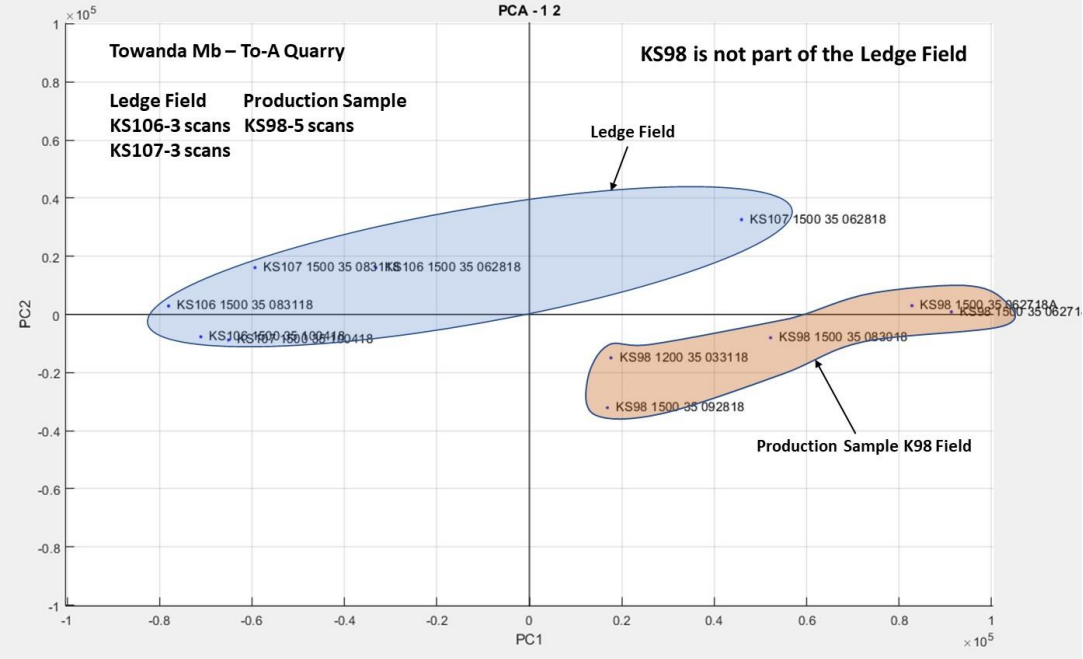

Figure 3.23: KS98 Production Sample Validation

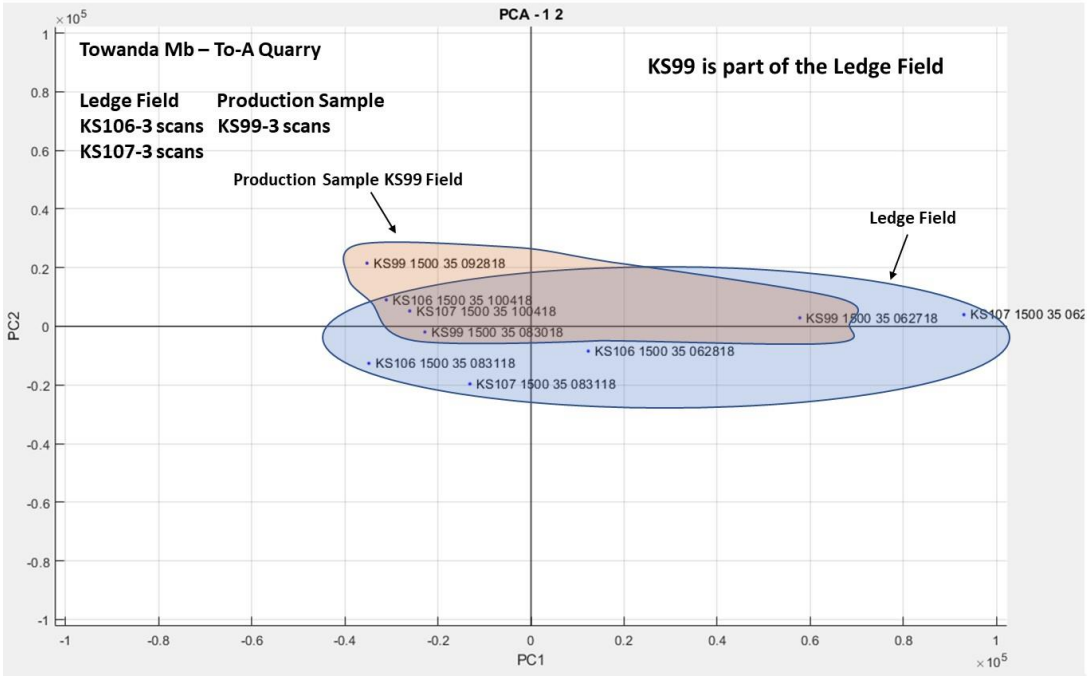

Figure 3.24: KS99 Production Sample Validation

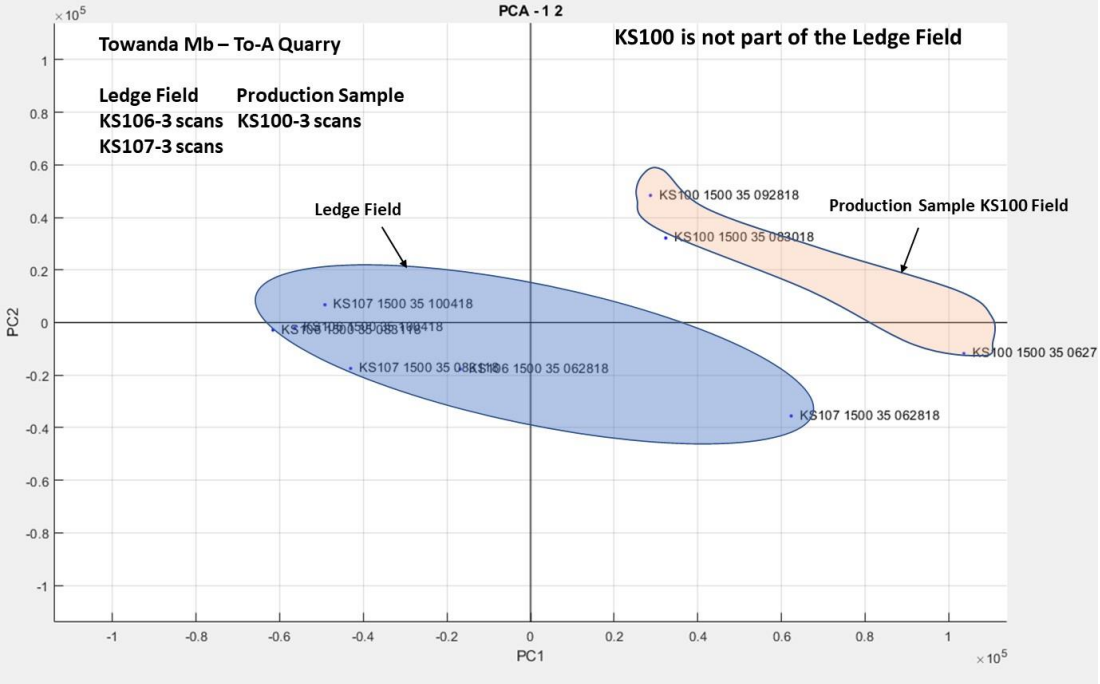

Figure 3.25: KS100 Production Sample Validation

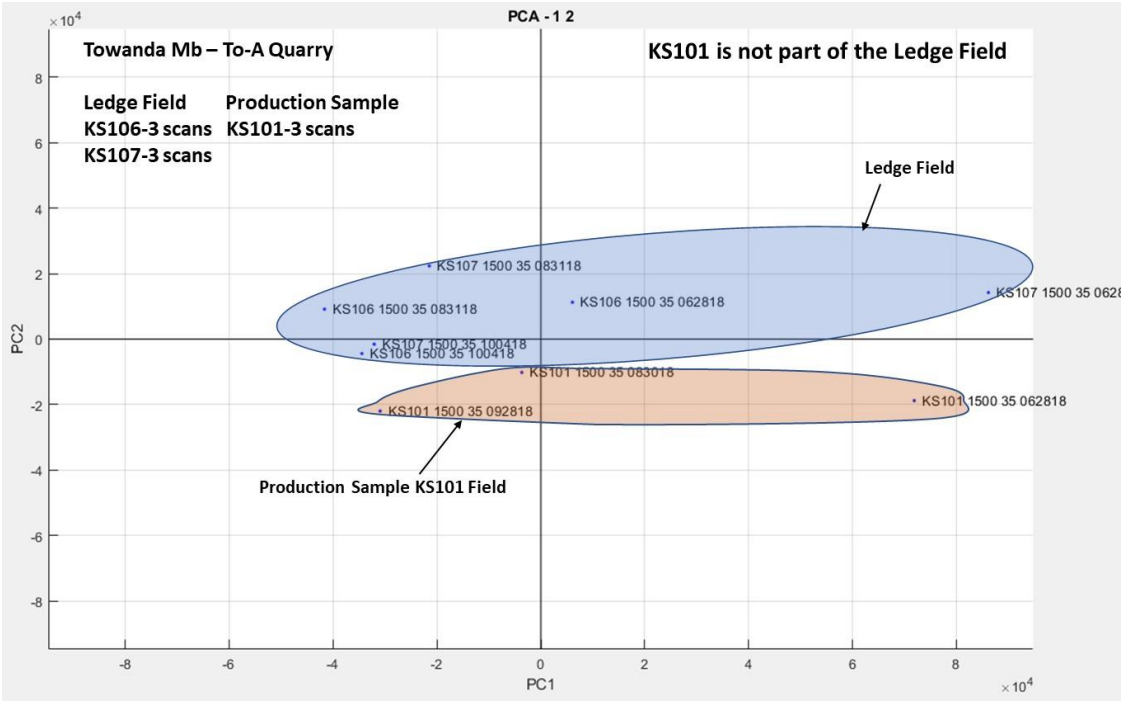

Figure 3.26: KS101 Production Sample Validation

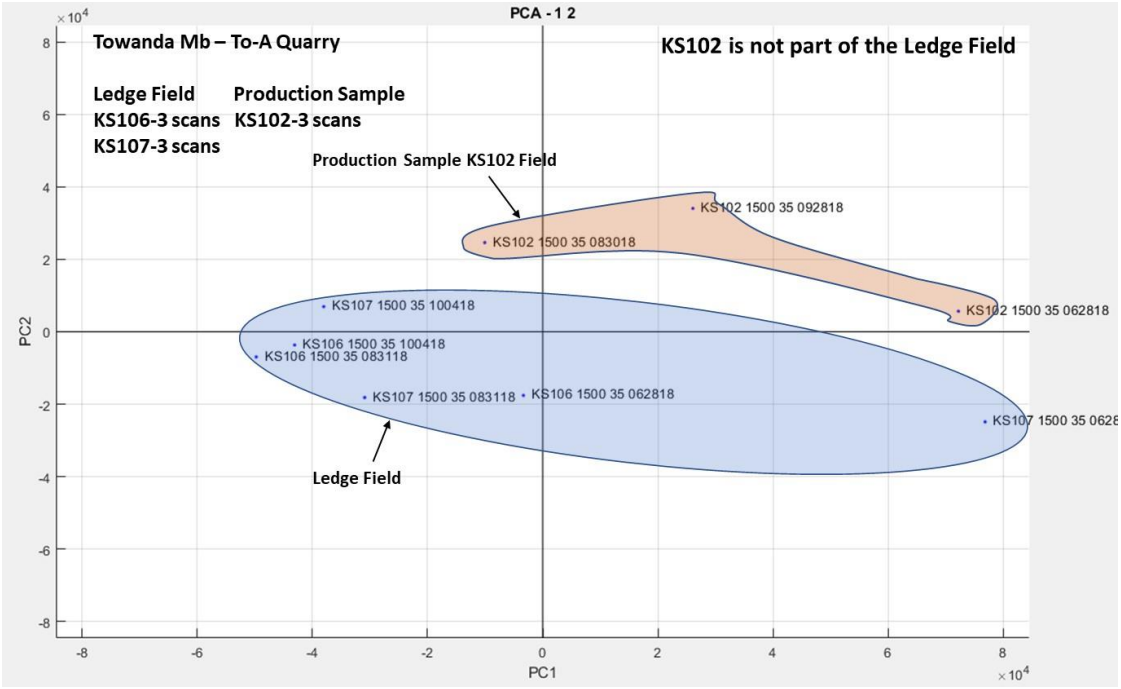

Figure 3.27: KS102 Production Sample Validation

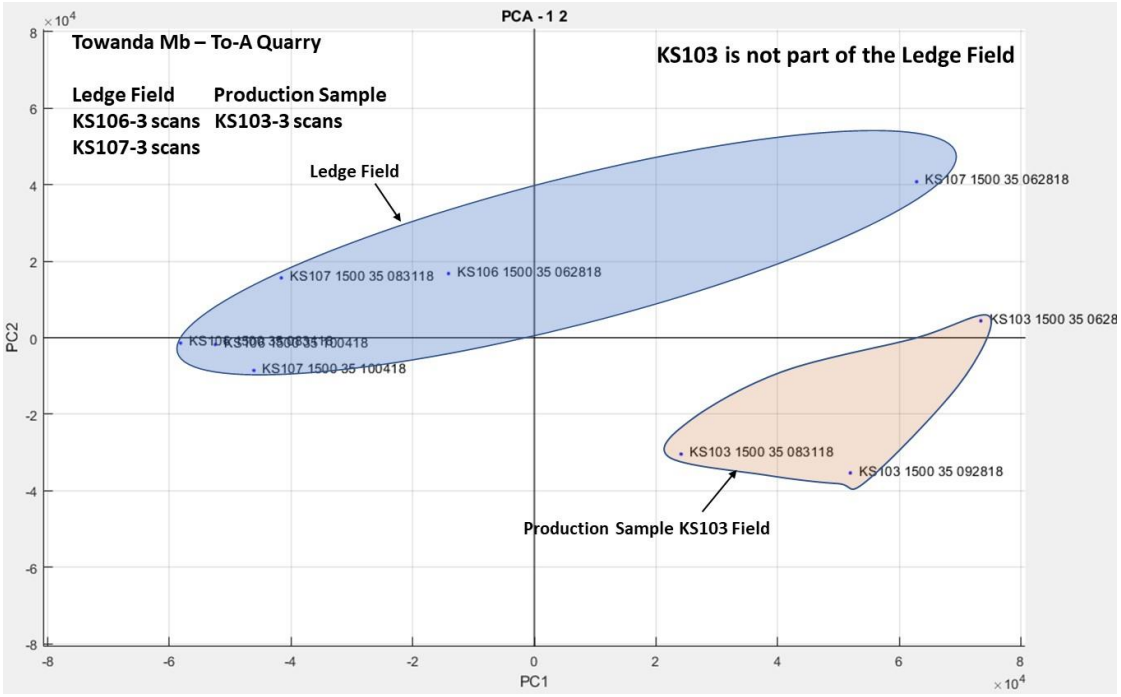

Figure 3.28: KS103 Production Sample Validation

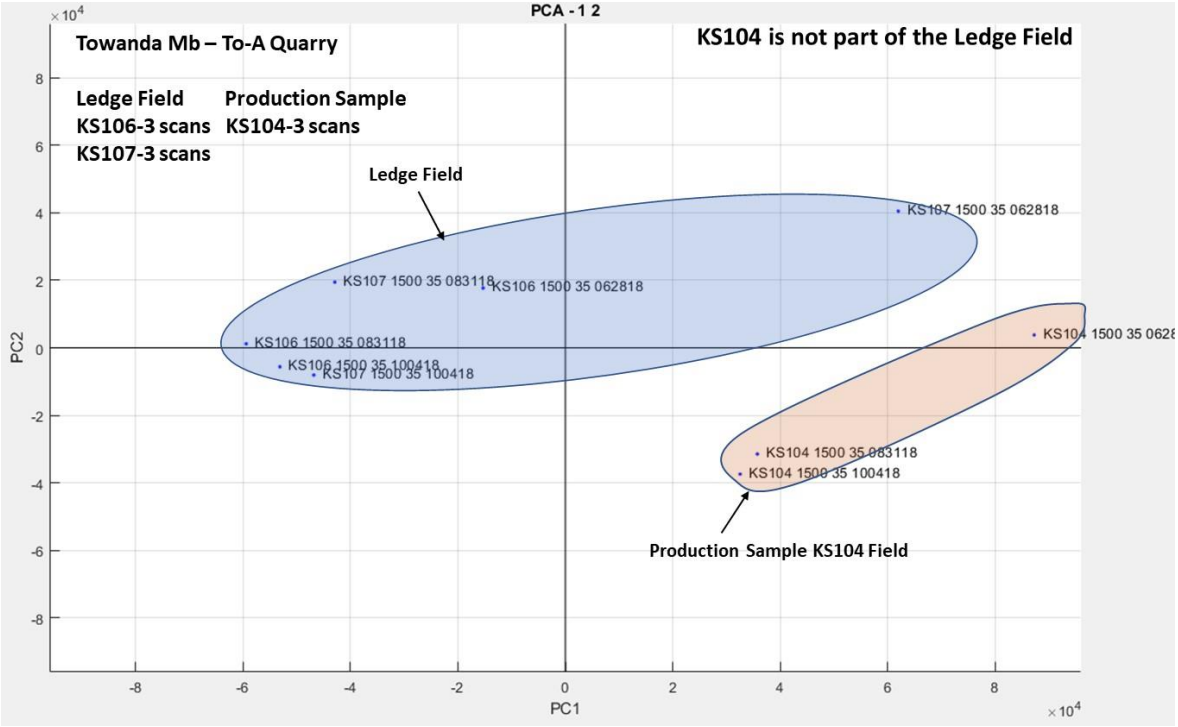

Figure 3.29: KS104 Production Sample Validation

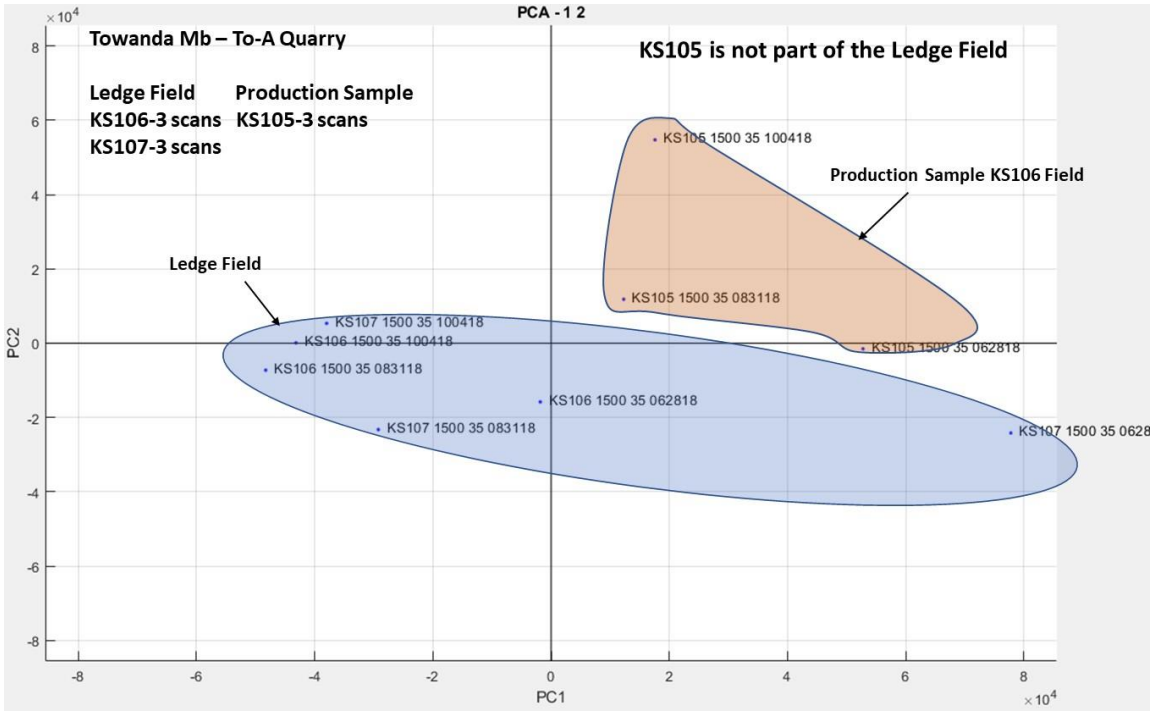

Figure 3.30: KS105 Production Sample Validation

3.8 KDOT Findings and Conclusions

3.8.1 Findings

- Laser scanning PLSR Source models with aggregate samples from common geologic members properly identified D-cracking susceptible aggregate between 80 and 100% of the time.
- Laser scanning PLSR Super Models were less predictive, identifying D-cracking susceptible aggregate approximately 70% of the time.
- Laser scanning PCA models were effective in validating the aggregate identities of production sample mixtures.

3.8.2 Conclusions

- Laser scanning may be used as a quality control tool to identify D-cracking susceptible aggregate – between 70% and 100% of the time, depending on whether PLSR Source Models or Super Models are used.
- To achieve this, it is most likely that the calibration of KDOT Source Models will be required.
- Laser scanning can be used as an effective quality control tool to screen production sample mixtures to ensure that only approved materials are introduced into production blends.

Chapter 4: New York Laser Scanning Analysis

4.1 New York State Scanning Objectives

NYSDOT uses its own acid insoluble residue (AIR) test MM28 (2007), to assess the friction properties of aggregates used in State paving applications. This test method typically takes several days to complete and makes use of corrosive concentrated acid solutions that emit noxious fumes that must be controlled. An alternative method in which many aggregate samples could be rapidly screened within minutes for AIR, thereby reducing or eliminating the need for MM28 testing would be a welcomed option. The New York State effort focused on evaluating how well laser induced spectra could be used as a surrogate for predicting AIR. The modeling effort involved calibrating and testing Partial Least Square Regression (PLSR) models to predict sample aggregate AIR values.

4.2 New York State DOT Aggregate Samples and Sources

NYSDOT provided approximately 124 samples for scanning. Of the 124 samples, 101 contained AIR data and sufficient lithological data to characterize the sample. The Research Team supplemented these samples with an additional 23 samples collected from the R83 quarry, resulting in a total of 124 samples with sufficient lithological data for analysis. Table 4.1 lists the 13 lithological categories that were associated with these samples.

Table 4.1: Lithological Categories for NY Samples (Legend)

L = Limestone
D =Dolomite
D/L = Dolomite & Limestone
DS = Dolostone
G = Granite
SS = Sandstone
L-x% = Mix with x% Limestone
M = Marble
T = Traprock
SS/SH/Q = Mix Sandstone, Shale, and Quartzite
CM = Crushed Marble
MMET = Mixed Metamorphic
SS/SH = Mixed Sandstone and Shale

All samples provided by NYSDOT were collected as part of the Department's annual quality assurance program, and included limestones, dolomites, marble, granite, shale, traprock, sandstones, and various mixtures from 50 different quarry sources across the eight NYSDOT Transportation Regions.[32] Table 4.2 through Table 4.9 provide, by region, the source quarry for each sample collected.[33]

Table 4.2: NYSDOT Region 1 Samples

Quarry	Sample ID	Lithology
R11	NY110 NY333	L
R12	NY111	L
R13	NY506	D
R14	SM18	SS/SH/Q
R15	SM10	SS/SH
R16	NY124	L
R17	NY300	DS
R18	SM3, 4, 5	L
R19	NY342	DS
R110	NY123	D

Table 4.3: NYSDOT Region 2 Samples

Quarry	Sample ID	Lithology
R21	SM14	SS/SH/Q
R22	SM15	SS/SH/Q
R23	NY125	D/L
R24	NY126	D/L
R25	NY325	L
R26	NY324	L

Table 4.4: NYSDOT Region 3 Samples

Quarry	Sample ID	Lithology
R31	NY501	L
R32	NY127	D
R33	NY128	D
R34	NY348	D
R35	NY327	L

[32] These samples were collected over the course of the two TPF studies spanning a period from 2015 through 2019.
[33] Source quarries are unnamed and identified only by a Regional Code.

Table 4.5: NYSDOT Region 4 Samples

Quarry	Sample ID	Lithology
R41	NY313 NY320	L
R42	NY131	L
R43	NY133 NY134	L
R44	SM20	D
R45	SM19	L
R46	NY112 NY312	L
R47	NY129 NY350	D
R48	NY130 NY349	D
R49	SM21	D

Table 4.6: NYSDOT Region 5 Samples

Quarry	Sample ID	Lithology
R51	NY322	L-80%
R52	SM11	MMET
R53	NY315	L
R54	NY303	DS
R55	SM13	SS/SH/Q
R56	NY135 NY323	L
R57	NY136 NY431 SM1 SM2	L

Table 4.7: NYSDOT Region 6 Samples

Quarry	Sample ID	Lithology
R61	SM8	M

Table 4.8: NYSDOT Region 7 Samples

Quarry	Sample ID	Lithology
R71	SM7	M
R72	NY120	D
R73	NY502	L
R74	NY503	L
R75	NY121	D
R76	NY122	D

Table 4.9: NYSDOT Region 8 Samples

Quarry	Sample ID	Lithology
R81	SM17	D
R82	NY118	L
R83	NY100-107 NY117 NY119 NY137-145 NY147	L
R84	NY108	L
R85	NY109 NY337 NY444	L
R86	NY304	G
R87	NY355	M
R88	NY306	DS
R89	NY451	T
R810	SM16	CM
R811	NY486	M
R812	SM9	MMET
R813	NY504	D

4.3 Acid Insoluble Residue Modeling

Acid Insoluble Residue (AIR) is the portion of an aggregate sample not dissolved in hydrochloric acid. It is related to the carbonate and non-carbonate elemental microstructure of the aggregate; and as a result, the spectral patterns associated with given samples. It was expected that AIR would be an ideal property for model calibration.

While NYSDOT provided approximately 124 samples for scanning, the NYSDOT sample collection plans did not include provisions for the targeted collection of calibration samples that could be associated with test samples. The absence of a targeted NYSDOT sampling strategy limited the potential for highly accurate AIR model development. This is because regression models in general and multivariate PLSR aggregate models in particular, do not extrapolate and project values outside the range of the calibration space.[34] Despite this limitation the model results presented illustrate that with focused sample calibration planning AIR can be predicted by laser scanning. To make this case, the Research Team undertook a modeling strategy that involved a

[34] To supplement the sample population provided by NYSDOT, the Research Team independently collected samples from the R83 Quarry site, listed in Table 4.9. These samples provided the means to effectively calibrate a local limestone model.

stepwise approach which examined the progressive development of calibration models from a random calibration sample population to a more focused sample population in the following order:

- All Statewide Aggregates
- Carbonate Aggregates
- Limestone Aggregates
- Quarry (East Kingston) Aggregates

The underlying objective was to illustrate how more targeted and strategic sampling improves model efficacy. Partial Least Square Regression Models (PLSR) were respectively calibrated for each of the pre-selected sample populations. Calibration was undertaken in each of the four populations by randomly choosing approximately one-half the total samples from each population set chosen. The remaining half of the sample population was used as the validation or test set. All models were developed in pairs. The first model, referred to as Model 1, included the random selection of calibration samples from the sample population and the second model, referred to as Model 2, utilized samples in which the Model 1 calibration test and validation set samples were reversed. Employing such an approach provided a means to ensure that the model results were not overly biased by sample selection.

4.3.1 Modeling AIR with All Statewide Aggregates

The initial modeling effort utilized all 124 available samples to determine whether an AIR Super Model could be developed for all New York State samples, regardless of the source or lithology.[35]

Model 1 and Model 2 calibration models (see left side of figure) and the validation test results (see right side of figure) are graphically presented in Figure 4.1 and Figure 4.2, respectively. Each figure presents the relationship between the known (or observed) AIR value (abscissa) for each sample and the corresponding model-predicted value (ordinate). The figures also display a dashed line, which represents an ideal model, where the Observed and Predicted AIR values are equivalent; and a trend (least squares regression) line for the given results.

[35] A Super Model is a model where all samples, regardless of the type or source could effectively be introduced into the model. An effective Super Model would not require a targeted sampling strategy; but given the nature of AIR, this was not the case.

PLSR models are generally very effective in developing strong calibration models with calibration set samples. Both Model 1 and Model 2 calibrations show trend lines that highly correlate with the sample data. Predicted test set AIR sample results, as a group, also correlate well with actual AIR data; however, the residual errors associated with a large number of individual test samples were noticeably high. The residual error is defined as the difference between the predicted value and the dashed line in each of the figures.[36]

A tabulated list of the test results for Models 1 and 2 are respectively presented in Table 4.10 and Table 4.11. Samples exhibiting AIR residual errors less than 10% from the reported AIR values are highlighted in each table. While the Calibrated Super Models show relatively good correlation, the accuracy of the AIR test sample predictions, reflected by high residual errors, are poor for many samples. This can be seen by the large number of unshaded samples in Table 4.10 and Table 4.11.

The wide variety of aggregate types from different geologic, geographic, and lithological sources resulted in a poorly resolved spectral database, which translates into erratic model predictions for selected samples. Poor spectral resolution for selected samples occurs when an insufficient spectral database is available for those samples. The introduction of one or two random samples of aggregate with highly variable geochemical properties (see Table 4.1) adversely affects the model capacity to associate a spectral pattern with a particular AIR value. A much larger calibration set or more targeted model calibration for specific lithological categories would be required to resolve such a model. The distribution of samples provided by NYSDOT was not sufficiently robust to resolve the differences among these diverse populations.

[36] A perfect model would yield test set results that would fall along the dashed line shown.

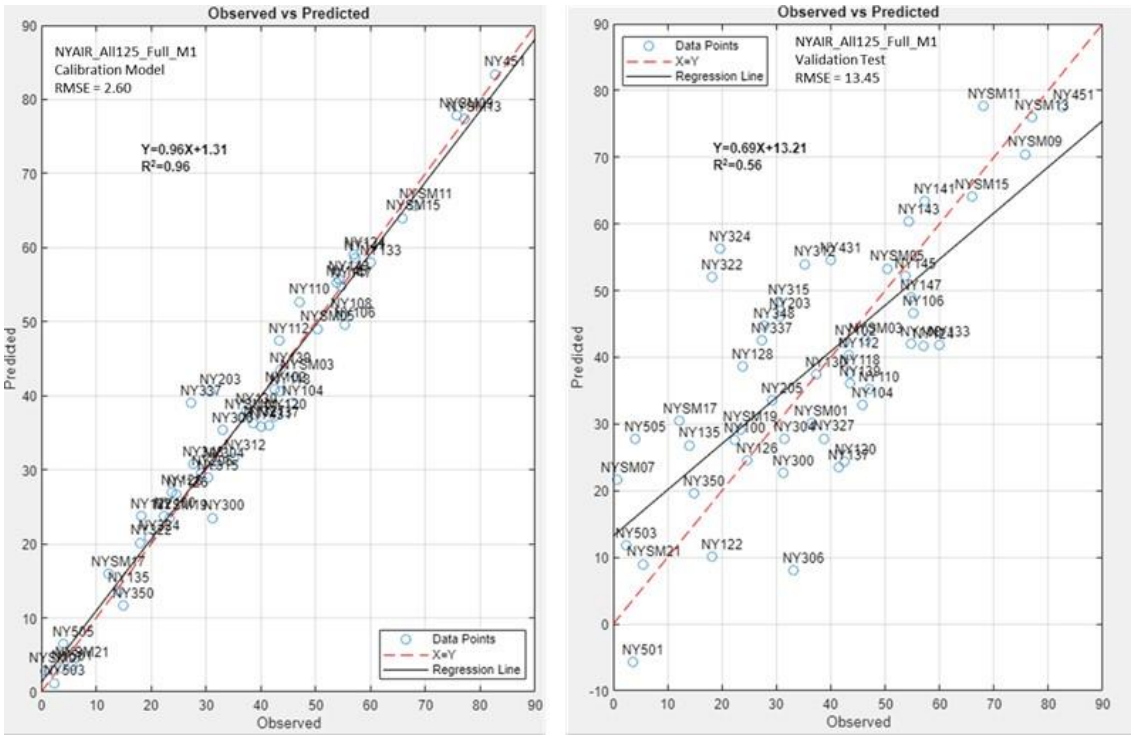

Figure 4.1: NYAIR Statewide Aggregate Model 1 (NYAIR_All125_Full_M1)

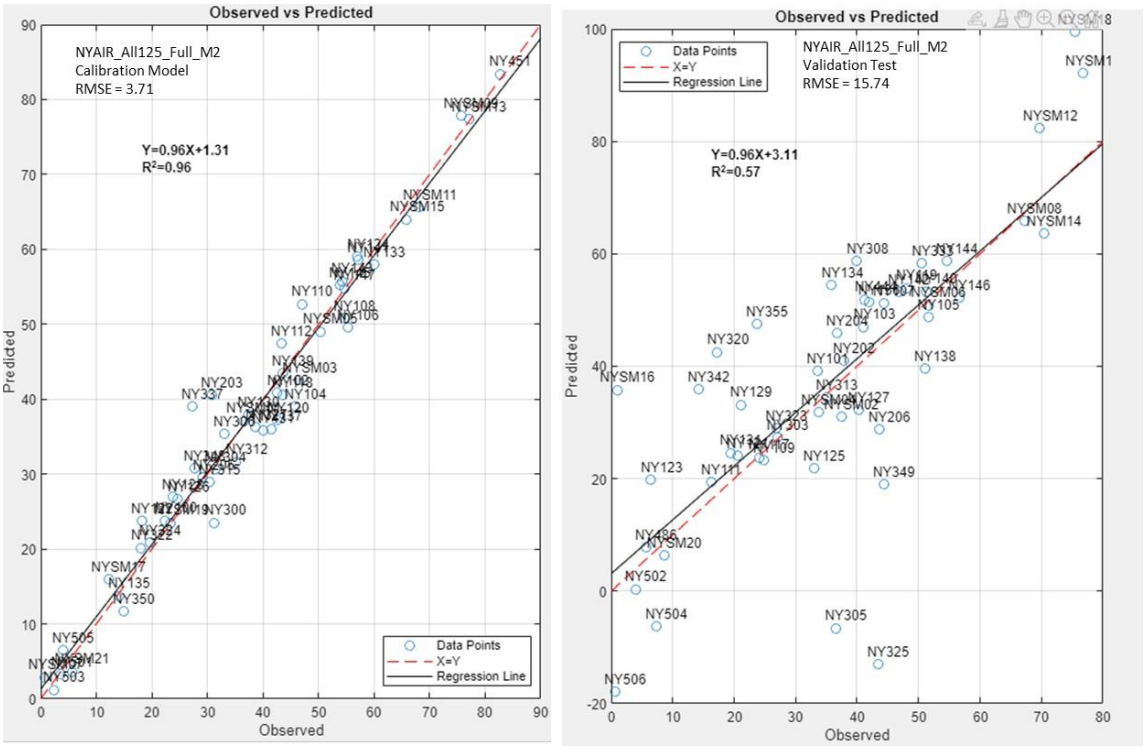

Figure 4.2: NYAIR Statewide Aggregate Model 2 (NYAIR_All125_Full_M2)

Table 4.10: Statewide Aggregate Model Results (NYAIR_All125_Full_M1)

Samples[37]	Predicted	Observed	Residual
NYSM07_M3.mat	21.6	0.8	-20.8
NY503_m3_737R_L_022020.mat	11.8	2.3	-9.5
NY501_m3_313R_L_022020.mat	-5.6	3.7	9.3
NY505_m3_948R_L_022020.mat	27.8	4.0	-23.8
NYSM21_M3.mat	9.0	5.6	-3.4
NYSM17_M3.mat	30.5	12.3	-18.2
NY135_m_5-7R.mat	26.8	14.1	-12.7
NY350_m2_44R_Dx_022020.mat	19.6	14.9	-4.7
NY322_m2_51R_Lx_022020.mat	52.0	18.1	-33.9
NY122_m_7_8RS1.mat	10.1	18.2	8.1
NY324_m3_29RS_L_022020.mat	56.3	19.6	-36.7
NY100_m_8_15RS_Becraft.mat	27.6	22.4	-5.2
NYSM19_M3.mat	29.2	23.5	-5.7
NY128_m_3_8RS.mat	38.6	23.8	-14.8
NY126_m_2_6RS1.mat	24.5	24.7	0.2
NY337_m3_817RS_L_022020.mat	42.5	27.3	-15.2
NY348_mn_3_8_RS_Dplus.mat	44.8	27.7	-17.1
NY205_m.mat	33.5	29.2	-4.3
NY315_m2_53R_17AR30_Lx_022020.mat	48.3	30.4	-17.9
NY203_m.mat	46.2	30.7	-15.5
NY300_m_1-26R_D.mat	22.6	31.3	8.7
NY304_mn_8_44R_Gr.mat	27.8	31.4	3.6
NY306_mn_8_5R_D.mat	8.1	33.1	25.0
NY312_m4_43RS_L_022020.mat	54.0	35.2	-18.8
NYSM01_M3.mat	30.1	36.5	6.4
NY130_mn_4-4RS.mat	37.4	37.3	-0.1
NY327_m4_39R1_LD_022020.mat	27.8	38.7	10.9
NY431_m3_57RS_L_022020.mat	54.5	40.0	-14.5
NY137_m_8-15RS.mat	23.6	41.4	17.9
NY102_m2_815RS_L_NS__022020.mat	42.2	42.6	0.4
NY120_m3_71RS_Dx_022020.mat	24.4	42.6	18.2
NY112_m_4_3RS.mat	40.3	43.4	3.1
NY118_m_8_15R.mat	37.7	43.6	5.9
NY139_m_8_15RS.mat	36.1	43.6	7.5
NY104_m3_815RS_L_022020.mat	32.9	45.8	12.9
NYSM03_M3.mat	42.5	46.5	4.0
NY110_m4_130R_L_022020.mat	35.3	47.1	11.8
NYSM05_M3.mat	53.3	50.4	-2.9
NY145_mn_8-15RS.mat	52.2	53.8	1.6
NY143_mn_8_15RS.mat	60.4	54.3	-6.1
NY108_m_8_17R.mat	42.0	54.7	12.7
NY147_mn_8_15RS.mat	48.9	54.7	5.8
NY106_m3_815RS_L_022020.mat	46.6	55.2	8.6
NY124_mn__1_23R.mat	41.7	57.0	15.3
NY141_mn_8-15RS.mat	63.4	57.2	-6.2
NY133_m_4_12RS.mat	41.9	60.0	18.1
NYSM15_M3.mat	64.1	65.9	1.8
NYSM11_M3.mat	77.7	68.2	-9.5
NYSM09_M3.mat	70.4	75.7	5.3
NYSM13_M3.mat	76.0	77.1	1.1
NY451_m3_86R_TR_022020.mat	77.5	82.7	5.2

[37] The extended sample names presented in the model output tables in this section are special names used by the Research Team to identify the sample source and location and whether sample scans were merged. The prefix of each name, prior to the first underscore in the name, identifies the actual sample. For example, NY118_m_8_15R.mat is sample NY118.

Table 4.11: Statewide Aggregate Model Results (NYAIR_All125_Full_M2)

Samples	Predicted	Observed	Residual
NY506_m3_1020RS_D_022020.mat	-17.9	0.7	18.6
NYSM16_M3.mat	35.8	1.0	-34.8
NY502_m3_734R_L_022020.mat	0.3	4.0	3.7
NY486_m3_876RS_M_022020.mat	7.8	5.6	-2.2
NY123_m_1_8R.mat	19.8	6.5	-13.4
NY504_m3_896R_D_022020.mat	-6.2	7.3	13.5
NYSM20_M3.mat	6.4	8.6	2.2
NY342_m4_152R_17AR62_DOL_022020.mat	35.9	14.3	-21.6
NY111_m_1_30RS.mat	19.5	16.3	-3.2
NY320_m3_410R_L_022020.mat	42.5	17.3	-25.2
NY131_m_4_11R.mat	24.6	19.4	-5.2
NY121_m_7_8R.mat	24.0	20.6	-3.4
NY129_mn_4-4R.mat	33.1	21.1	-12.0
NY355_m4_846R_M_022020.mat	47.5	23.7	-23.8
NY117_m_8_15RS.mat	23.8	24.1	0.3
NY109_m_8_17RS.mat	23.3	24.8	1.5
NY323_m3_57R_L_022020.mat	29.0	26.9	-2.1
NY303_m2_54R_DOL_022020.mat	27.3	27.1	-0.2
NY125_m_2_6R1.mat	21.9	33.0	11.1
NY101_m2_815RS_L_ALST__022020.mat	39.1	33.5	-5.6
NYSM04_M3.mat	31.9	33.8	1.9
NY313_m3_410RS_L_022020.mat	34.4	35.1	0.7
NY134_m_4_12RS.mat	54.4	35.9	-18.5
NY305_mn_9_6R_L.mat	-6.6	36.5	43.1
NY204_m.mat	45.9	36.8	-9.1
NYSM02_M3.mat	31.0	37.5	6.5
NY202_m.mat	41.0	37.9	-3.1
NY308_m2_910R_SS_022020.mat	58.8	40.0	-18.8
NY127_m_3_8R.mat	32.3	40.2	7.9
NY103_m2_815RS_L_PE__022020.mat	47.0	41.1	-5.9
NY444_m3_817R_L_022020.mat	51.9	41.3	-10.6
NY136_m_5-7RS.mat	51.4	42.0	-9.4
NY325_m2_29R_L_022020.mat	-13.0	43.5	56.5
NY206_m.mat	28.8	43.7	14.9
NY349_m3_44RS_D_022020.mat	19.0	44.3	25.3
NY107_m_8_15RS.mat	51.1	44.4	-6.7
NY142_mn_8_15RS.mat	53.1	46.7	-6.5
NY119_m3_815RS_L_022020.mat	53.9	48.1	-5.8
NY333_m4_35_022020.mat	58.3	50.6	-7.7
NY138_m_8-15RS.mat	39.6	51.1	11.5
NY140_m_8-15RS.mat	53.3	51.3	-2.0
NY105_m_8_15RS.mat	48.7	51.6	2.9
NYSM06_M3.mat	50.9	51.6	0.7
NY144_mn_8_15RS.mat	58.7	54.6	-4.1
NY146_mn.mat	52.2	56.7	4.5
NYSM08_M3.mat	65.9	67.3	1.4
NYSM12_M3.mat	82.3	69.8	-12.6
NYSM14_M3.mat	63.6	70.5	6.9
NYSM18_M3.mat	99.5	75.5	-24.0
NYSM10_M3.mat	92.1	76.7	-15.4

4.3.2 Modeling AIR with Statewide Carbonate Rock

A Statewide carbonate model, which included 79 total carbonate aggregate samples, was developed. This model included all limestones, dolomites, dolostones, dolomite-limestone mixtures, and marble. Model 1 and Model 2 calibration models and the validation test results are graphically presented in Figure 4.3 and Figure 4.4, respectively. The calibration model shows trend lines that exhibit high correlation with the calibration set sample data, and the test set data show relatively good correlation, but similar to the statewide all-sample results, individual AIR predictions exhibit higher than desirable residual errors. A tabulated list of the test results for Models 1 and 2 are respectively presented in Table 4.13 and Table 4.14. Samples exhibiting residual errors less than 10% from the reported AIR values are highlighted in each table.

The Calibrated Statewide Carbonate Model, similar to the State All-Aggregate Model, is not predictive for many samples. The wide variety of carbonate aggregate types (limestone, dolomite, dolostones, various mixtures, and marble) collected from different geologic and geographic sources resulted in a poorly resolved spectral database. The results of the Statewide Carbonate model, as gauged by the Root Mean Square Error (RMSE) of the test data, appear however, to be more effective than the All-Aggregate State Model. RMSE is a standard way to measure the overall error of a model in predicting quantitative data. The higher the RMSE the poorer the model. RMSE results for both models are tabulated in Table 4.12.

Table 4.12: RMSE Values for All-Aggregate and Carbonate Aggregate Models

Model	RMSE
Statewide All-Aggregate Model1	13.45
Statewide All-Aggregate Model2	15.74
Statewide Carbonate-Aggregate Model1	12.19
Statewide Carbonate-Aggregate Model2	12.17

A comparison of the RMSE data suggests that limiting statewide samples to just carbonate samples improved the effectiveness of the model, but the wide variety of carbonate geochemistry in the calibration set still limited the overall effectiveness of the model.

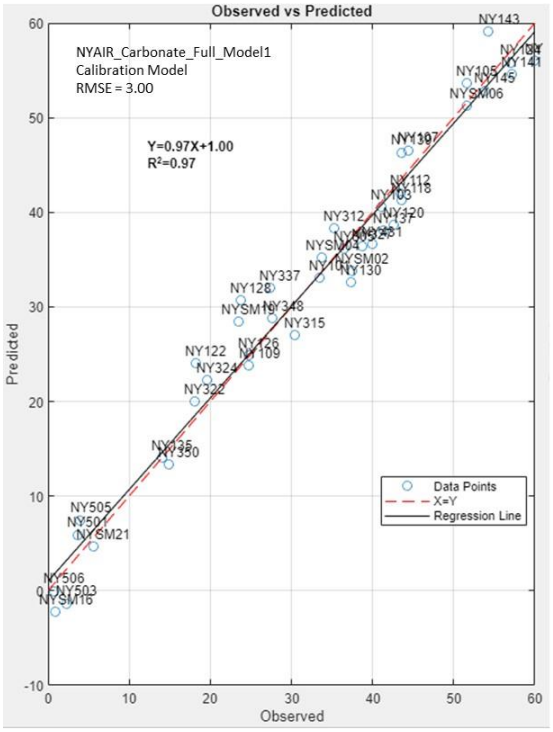

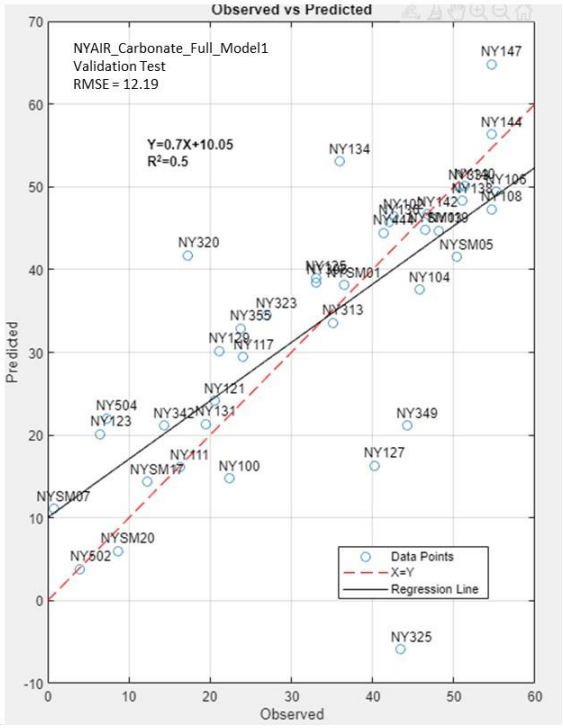

Figure 4.3: NYAIR Carbonate Model 1 (NYAIR_Carbonate_Full_Model1)

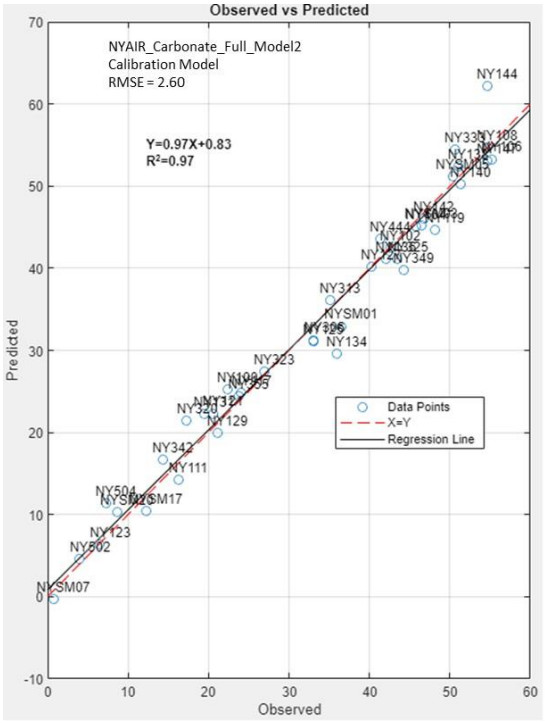

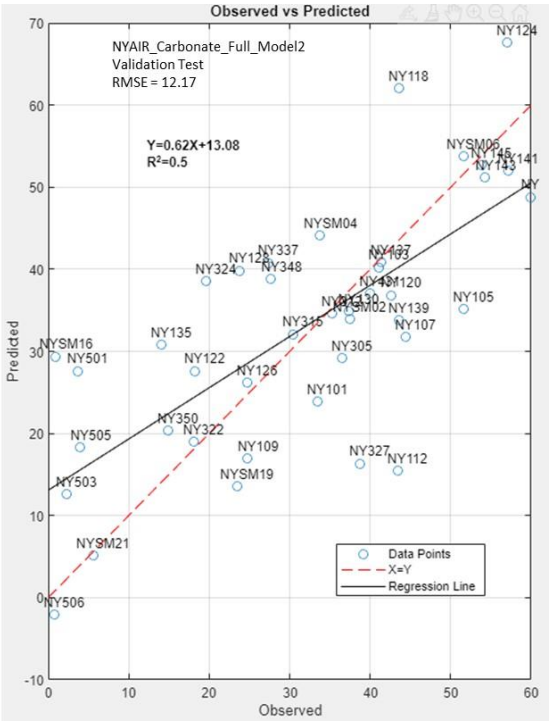

Figure 4.4: NYAIR Carbonate Model 2 (NYAIR_Carbonate_Full_Model2)

Table 4.13: NY Carbonate AIR Model 1 Results (NYAIR_Carbonate_Full_Model1)

Sample	Predicted	Observed	Residual
NYSM07_M3.mat	11.1	0.8	-10.3
NY502_m3_734R_L_022020.mat	3.8	4.0	0.2
NY123_m_1_8R.mat	20.1	6.5	-13.6
NY504_m3_896R_D_022020.mat	22.1	7.3	-14.8
NYSM20_M3.mat	6.0	8.6	2.6
NYSM17_M3.mat	14.4	12.3	-2.1
NY342_m4_152R_17AR62_DOL_022020.mat	21.1	14.3	-6.8
NY111_m_1_30RS.mat	16.1	16.3	0.2
NY320_m3_410R_L_022020.mat	41.7	17.3	-24.4
NY131_m_4_11R.mat	21.4	19.4	-2.0
NY121_m_7_8R.mat	24.1	20.6	-3.5
NY129_mn_4-4R.mat	30.2	21.1	-9.1
NY100_m_8_15RS_Becraft.mat	14.7	22.4	7.7
NY355_m4_846R_M_022020.mat	32.9	23.7	-9.2
NY117_m_8_15RS.mat	29.4	24.1	-5.3
NY323_m3_57R_L_022020.mat	34.4	26.9	-7.5
NY125_m_2_6R1.mat	39.0	33.0	-6.0
NY306_mn_8_5R_D.mat	38.5	33.1	-5.4
NY313_m3_410RS_L_022020.mat	33.6	35.1	1.5
NY134_m_4_12RS.mat	53.1	35.9	-17.2
NYSM01_M3.mat	38.2	36.5	-1.7
NY127_m_3_8R.mat	16.3	40.2	23.9
NY444_m3_817R_L_022020.mat	44.5	41.3	-3.2
NY136_m_5-7RS.mat	45.8	42.0	-3.8
NY102_m2_815RS_L_NS__022020.mat	46.4	42.6	-3.8
NY325_m2_29R_L_022020.mat	-5.8	43.5	49.3
NY349_m3_44RS_D_022020.mat	21.2	44.3	23.1
NY104_m3_815RS_L_022020.mat	37.6	45.8	8.2
NYSM03_M3.mat	44.8	46.5	1.7
NY142_mn_8_15RS.mat	46.7	46.7	0.0
NY119_m3_815RS_L_022020.mat	44.7	48.1	3.4
NYSM05_M3.mat	41.6	50.4	8.8
NY333_m4_35_022020.mat	49.9	50.6	0.7
NY138_m_8-15RS.mat	48.3	51.1	2.8
NY140_m_8-15RS.mat	50.1	51.3	1.2
NY144_mn_8_15RS.mat	56.4	54.6	-1.8
NY108_m_8_17R.mat	47.3	54.7	7.4
NY147_mn_8_15RS.mat	64.8	54.7	-10.1
NY106_m3_815RS_L_022020.mat	49.4	55.2	5.8

Table 4.14: NY Carbonate AIR Model 2 Results (NYAIR_Carbonate_Full_Model2)

Sample	Predicted	Observed	Residual
NY506_m3_1020RS_D_022020.mat	-2.0	0.7	2.7
NYSM16_M3.mat	29.4	1.0	-28.4
NY503_m3_737R_L_022020.mat	12.6	2.3	-10.3
NY501_m3_313R_L_022020.mat	27.6	3.7	-23.9
NY505_m3_948R_L_022020.mat	18.3	4.0	-14.3
NYSM21_M3.mat	5.1	5.6	0.5
NY135_m_5-7R.mat	30.8	14.1	-16.7
NY350_m2_44R_Dx_022020.mat	20.3	14.9	-5.4
NY322_m2_51R_Lx_022020.mat	19.0	18.1	-0.9
NY122_m_7_8RS1.mat	27.6	18.2	-9.4
NY324_m3_29RS_L_022020.mat	38.5	19.6	-19.0
NYSM19_M3.mat	13.5	23.5	9.9
NY128_m_3_8RS.mat	39.8	23.8	-16.1
NY126_m_2_6RS1.mat	26.2	24.7	-1.5
NY109_m_8_17RS.mat	17.0	24.8	7.8
NY337_m3_817RS_L_022020.mat	40.8	27.3	-13.5
NY348_mn_3_8_RS_Dplus.mat	38.8	27.7	-11.1
NY315_m2_53R_17AR30_Lx_022020.mat	32.1	30.4	-1.7
NY101_m2_815RS_L_ALST__022020.mat	23.8	33.5	9.7
NYSM04_M3.mat	44.1	33.8	-10.3
NY312_m4_43RS_L_022020.mat	34.6	35.2	0.6
NY305_mn_9_6R_L.mat	29.2	36.5	7.3
NY130_mn_4-4RS.mat	34.9	37.3	2.4
NYSM02_M3.mat	33.9	37.5	3.6
NY327_m4_39R1_LD_022020.mat	16.3	38.7	22.4
NY431_m3_57RS_L_022020.mat	37.1	40.0	2.9
NY103_m2_815RS_L_PE__022020.mat	40.2	41.1	0.9
NY137_m_8-15RS.mat	40.8	41.4	0.6
NY120_m3_71RS_Dx_022020.mat	36.9	42.6	5.7
NY112_m_4_3RS.mat	15.5	43.4	28.0
NY118_m_8_15R.mat	62.1	43.6	-18.5
NY139_m_8_15RS.mat	33.8	43.6	9.8
NY107_m_8_15RS.mat	31.7	44.4	12.7
NY105_m_8_15RS.mat	35.1	51.6	16.5
NYSM06_M3.mat	53.8	51.6	-2.2
NY145_mn_8-15RS.mat	52.7	53.8	1.1
NY143_mn_8_15RS.mat	51.2	54.3	3.1
NY124_mn__1_23R.mat	67.6	57.0	-10.6
NY141_mn_8-15RS.mat	52.0	57.2	5.2
NY133_m_4_12RS.mat	48.8	60.0	11.2

4.3.3 Modeling AIR with Statewide Limestones

Of the 79 suitable carbonate samples available, 53 were classified as limestones. The 53 limestone samples however were collected from 18 different quarries including the R83 quarry samples, which comprised 24 of the 53 total samples. The remaining 29 limestone samples came from 17 different quarry sites. Calibration samples (26 samples) were randomly selected from the 53 limestones samples collected statewide. The remaining 27 samples were used as the validation or test set samples. Similar to all previously described New York modeling efforts, two models were developed. The first (Model 1) as described above and the second (Model 2) in which the calibration and validation set samples were reversed from the those of the first model.

Model 1 and Model 2 calibration models and the validation test results are graphically presented in Figure 4.5 and Figure 4.6, respectively. The calibration models show trend lines that exhibit high correlation. A tabulated list of the test results for Models 1 and 2 are respectively presented in Table 4.16 and Table 4.17. Samples exhibiting residual errors less than 10% from the reported AIR values are highlighted in each table. The relative number of unshaded samples in the limestone model table are much less than the unshaded samples in the statewide and carbonate model tables previously presented.

RMSE results for the All-Aggregate, Statewide-Carbonate, and Statewide Limestone models are tabulated in Table 4.15. The lower RMSE values, shown in Table 4.15, for the Limestone Models reflect the improvement in model prediction efficiency. Nonetheless, due to the wide-ranging geochemical properties of the limestone samples provided by NYSDOT, a highly effective statewide Super Limestone Model could not be generated. More focused Source models, or an expanded calibration sample set are required.

Table 4.15: RMSE Values for All-Aggregate, Carbonate and Limestone Models

Model	RMSE
Statewide All-Aggregate Model1	13.45
Statewide All-Aggregate Model2	15.74
Statewide Carbonate-Aggregate Model1	12.19
Statewide Carbonate-Aggregate Model2	12.17
Statewide Limestone Aggregate Model 1	15.41*/10.11
Statewide Limestone Aggregate Model 2	10.18

This high 15.41 RMSE value was skewed by the NY325 sample, which exhibited a residual error of over 60 (see Table 4.16). With NY325, an apparent outlier removed, the RMSE was reduced to 10.11.

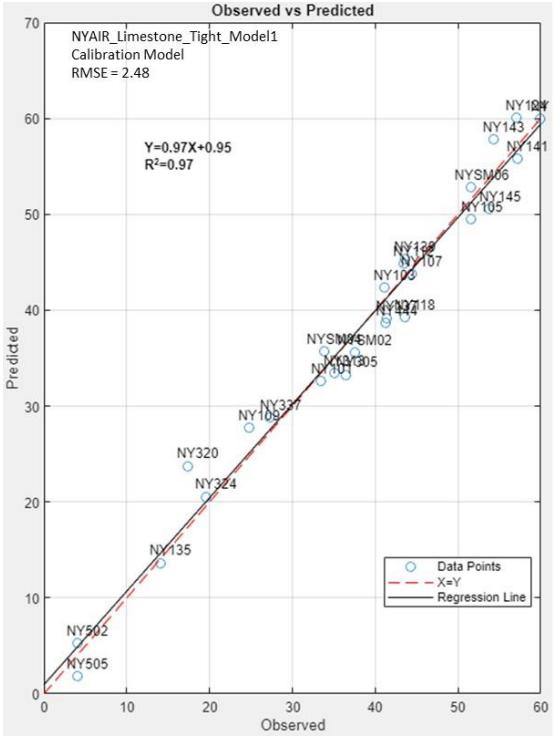

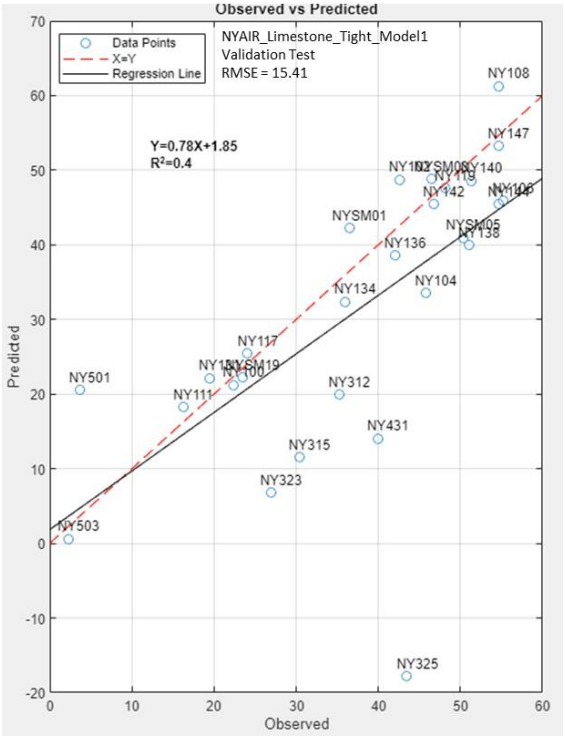

Figure 4.5: NY Limestone Sample Model 1 (NYAIR_Limestone_Model1_Tight)

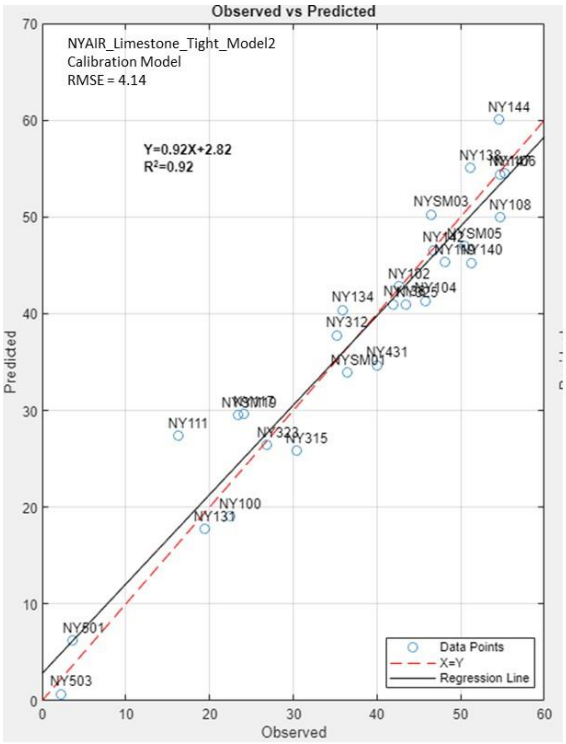

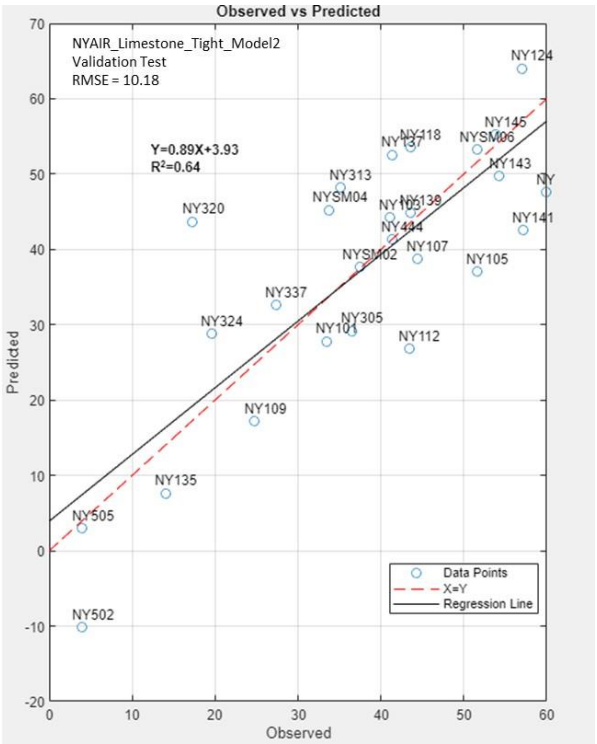

Figure 4.6: NY Limestone Sample Model 2 (NYAIR_Limestone_Model2_Tight)

Table 4.16: NY Limestone Aggregate Model 1 Results (NYAIR_Limestone_Model1_Tight)

Sample	Predicted	Observed	Residual
NY503_m3_737R_L_022020.mat	0.6	2.3	1.7
NY501_m3_313R_L_022020.mat	20.5	3.7	-16.8
NY111_m_1_30RS.mat	18.3	16.3	-2.0
NY131_m_4_11R.mat	22.2	19.4	-2.8
NY100_m_8_15RS_Becraft.mat	21.2	22.4	1.2
NYSM19_M3.mat	22.2	23.5	1.3
NY117_m_8_15RS.mat	25.4	24.1	-1.3
NY323_m3_57R_L_022020.mat	6.8	26.9	20.1
NY315_m2_53R_17AR30_Lx_022020.mat	11.5	30.4	18.9
NY312_m4_43RS_L_022020.mat	20.0	35.2	15.2
NY134_m_4_12RS.mat	32.4	35.9	3.5
NYSM01_M3.mat	42.2	36.5	-5.7
NY431_m3_57RS_L_022020.mat	14.1	40.0	25.9
NY136_m_5-7RS.mat	38.5	42.0	3.5
NY102_m2_815RS_L_NS__022020.mat	48.7	42.6	-6.1
NY325_m2_29R_L_022020.mat	-17.8	43.5	61.3
NY104_m3_815RS_L_022020.mat	33.5	45.8	12.3
NYSM03_M3.mat	48.8	46.5	-2.3
NY142_mn_8_15RS.mat	45.5	46.7	1.2
NY119_m3_815RS_L_022020.mat	47.6	48.1	0.5
NYSM05_M3.mat	40.9	50.4	9.5
NY138_m_8-15RS.mat	39.9	51.1	11.2
NY140_m_8-15RS.mat	48.6	51.3	2.7
NY144_mn_8_15RS.mat	45.4	54.6	9.2
NY108_m_8_17R.mat	61.3	54.7	-6.6
NY147_mn_8_15RS.mat	53.2	54.7	1.5
NY106_m3_815RS_L_022020.mat	45.9	55.2	9.3

Table 4.17: NY Limestone Aggregate Model 2 Results (NYAIR_Limestone_Model2_Tight)

Sample	Predicted	Observed	Residual
NY502_m3_734R_L_022020.mat	-10.2	4.0	14.2
NY505_m3_948R_L_022020.mat	3.0	4.0	1.0
NY135_m_5-7R.mat	7.6	14.1	6.5
NY320_m3_410R_L_022020.mat	43.7	17.3	-26.4
NY324_m3_29RS_L_022020.mat	28.8	19.6	-9.2
NY109_m_8_17RS.mat	17.1	24.8	7.7
NY337_m3_817RS_L_022020.mat	32.6	27.3	-5.3
NY101_m2_815RS_L_ALST__022020.mat	27.8	33.5	5.7
NYSM04_M3.mat	45.2	33.8	-11.4
NY313_m3_410RS_L_022020.mat	48.2	35.1	-13.1
NY305_mn_9_6R_L.mat	29.2	36.5	7.3
NYSM02_M3.mat	37.6	37.5	-0.1
NY103_m2_815RS_L_PE__022020.mat	44.3	41.1	-3.2
NY444_m3_817R_L_022020.mat	41.3	41.3	0.0
NY137_m_8-15RS.mat	52.6	41.4	-11.2
NY112_m_4_3RS.mat	26.8	43.4	16.6
NY118_m_8_15R.mat	53.5	43.6	-9.9
NY139_m_8_15RS.mat	44.9	43.6	-1.3
NY107_m_8_15RS.mat	38.8	44.4	5.6
NY105_m_8_15RS.mat	37.1	51.6	14.5
NYSM06_M3.mat	53.2	51.6	-1.6
NY145_mn_8-15RS.mat	55.3	53.8	-1.5
NY143_mn_8_15RS.mat	49.8	54.3	4.5
NY124_mn__1_23R.mat	64.0	57.0	-7.0
NY141_mn_8-15RS.mat	42.5	57.2	14.7
NY133_m_4_12RS.mat	47.6	60.0	12.4

4.3.4 Modeling AIR in R83 Quarry Limestones

To test the hypothesis that local Source models could generate an effective AIR model, the Research Team collected a total of 24 limestone samples from the R83 quarry for AIR model development.[38] Twelve samples were randomly selected for the calibration set and 12 for the validation set. Two R83 models were developed. The calibration and validation samples used for the first model (Model 1) were swapped for use in the second model (Model 2). Model 1 and Model 2 calibration models and the validation test results are graphically presented in Figure 4.3 and Figure 4.4, respectively. The calibration model shows trend lines that exhibit high correlation with the calibration set sample data. A tabulated list of the test results for Models 1 and 2 are respectively presented in Table 4.19 and Table 4.20. Only one sample, in Model 2, exceeded a 10% AIR residual error.

The Model 1 calibration, shown in Figure 4.7, has a noticeable gap between AIR value 25 and 43. The test samples predictions were very accurate, except for this range. Similarly, the Model 2 calibration, shown in Figure 4.8 has no data for AIR values less than 30. The test sample predictions were accurate, except for values less than 30. The Calibrated R83 Limestone Model is an accurate model. It is predictive within the range of values used in the respective calibration models. An increase in sample numbers and the range of AIR values that could be encountered at R83 would almost certainly improve the current spectral database. RMSE results for all New York models are tabulated in Table 4.12. The R83 models exhibit the lowest RMSE values; and the RMSE magnitudes values suggest an effective model.

Table 4.18: RMSE Values for All-Aggregate, Carbonate and Limestone Models

Model	RMSE
Statewide All-Aggregate Model1	13.45
Statewide All-Aggregate Model2	15.74
Statewide Carbonate-Aggregate Model1	12.19
Statewide Carbonate-Aggregate Model2	12.17
Statewide Limestone Aggregate Model 1	10.11
Statewide Limestone Aggregate Model 2	10.18
R83 Quarry Limestone Model 1	3.55
R83 Quarry Limestone Model 2	6.95

[38] Twenty-three samples were independently collected by the Research Team with the assistance of the quarry owner (Callanan). One E. Kingston sample was supplied by NYSDOT (NYSM05).

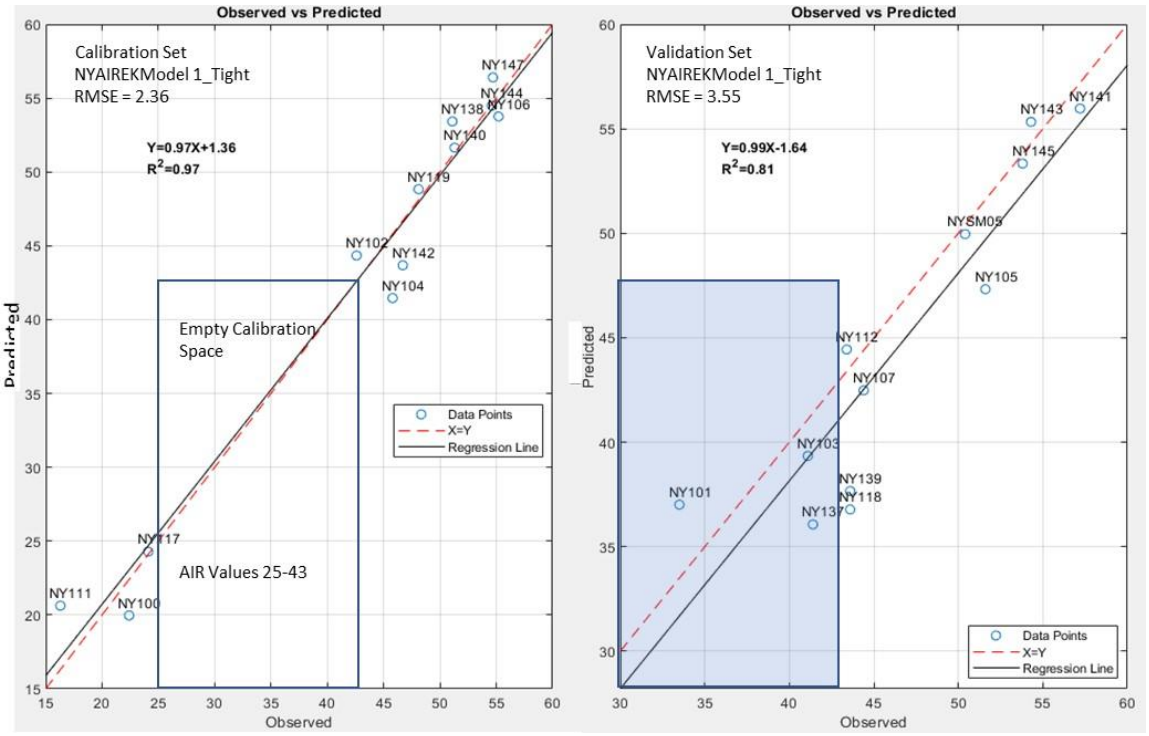

Figure 4.7: R83 Quarry Limestone AIR Model 1

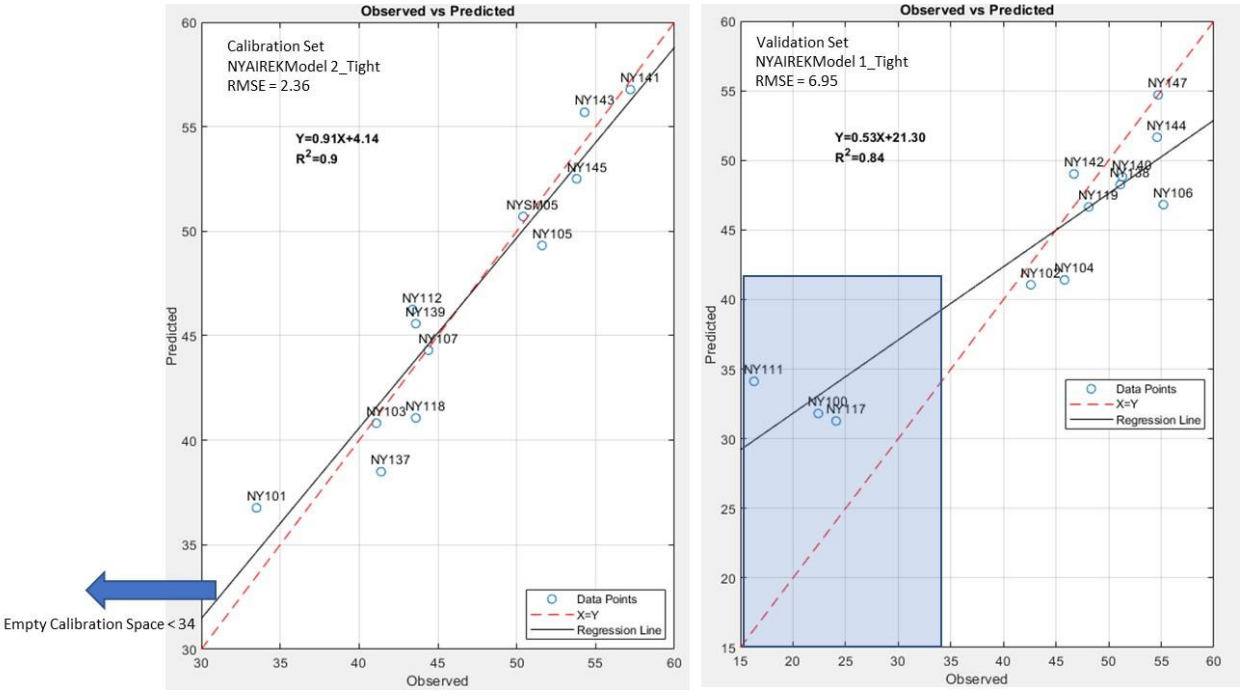

Figure 4.8: R83 Quarry Limestone AIR Model 2

Table 4.19: R83 Quarry Limestone Model 1 Results (NYAIREKModel 1_Tight)

Samples	Predicted	Observed	Residual
NY101_m2_815RS_L_ALST__022020.mat	37.0	33.5	-3.5
NY103_m2_815RS_L_PE__022020.mat	39.3	41.1	1.8
NY137_m_8-15RS.mat	36.1	41.4	5.3
NY112_m_4_3RS.mat	44.4	43.4	-1.0
NY118_m_8_15R.mat	36.8	43.6	6.8
NY139_m_8_15RS.mat	37.7	43.6	5.9
NY107_m_8_15RS.mat	42.5	44.4	1.9
NYSM05_M3.mat	50.0	50.4	0.4
NY105_m_8_15RS.mat	47.3	51.6	4.3
NY145_mn_8-15RS.mat	53.3	53.8	0.5
NY143_mn_8_15RS.mat	55.3	54.3	-1.0
NY141_mn_8-15RS.mat	56.0	57.2	1.2

Table 4.20: R83 Quarry Limestone Model 2 Results (NYAIREKModel 2_Tight)

Samples	Predicted	Observed	Residual
NY111_m_1_30RS.mat	34.1	16.3	-17.8
NY100_m_8_15RS_Becraft.mat	31.8	22.4	-9.4
NY117_m_8_15RS.mat	31.3	24.1	-7.2
NY102_m2_815RS_L_NS__022020.mat	41.1	42.6	1.5
NY104_m3_815RS_L_022020.mat	41.4	45.8	4.4
NY142_mn_8_15RS.mat	49.0	46.7	-2.3
NY119_m3_815RS_L_022020.mat	46.6	48.1	1.5
NY138_m_8-15RS.mat	48.3	51.1	2.8
NY140_m_8-15RS.mat	48.8	51.3	2.5
NY144_mn_8_15RS.mat	51.7	54.6	2.9
NY147_mn_8_15RS.mat	54.7	54.7	0.0
NY106_m3_815RS_L_022020.mat	46.8	55.2	8.4

4.3.5 Modeling New York State's SM Samples

NYSDOT independently collected and provided 21 unknown samples to the Research Team to be used as test samples. The list of 21 samples is shown in Table 4.21. This list includes nine Non-carbonate Rock sample mixtures, three Dolomites, two Marbles, and seven Limestones; all size fractionated and washed and collected from 18 different quarry sources.[39]

[39] SM samples provided by NYSDOT were all prewashed and size fractionated; however, no calibration samples previously provided by NYSDOT were prewashed or size fractionated.

Table 4.21: Unknown SM Sample Data

Test No.	SLT Code	Size	AIR or AIR Range (%)	AIR Median	Comments	Lithology
SM19033533	SM1	+1/8	36.5	36.5	washed	Limestone
SM19033537	SM2	+No.4	37.5	37.5	washed	Limestone
19GP0604	SM5	-3/4 +1/8 (12.5F2)	50.4	50.4	washed	Limestone
SM20002834	SM6	-3/4 +1/8 (9.5F2)	51.6	51.6	washed	Limestone
SM19068070	SM4	-3/4 +1/8 (9.5F2)	33.8	33.8	washed	Limestone
SM19069766	SM3	-3/8 +1/8 (6.3F2)	46.5	46.5	washed	Limestone
SM18013613	SM13	-3/8 +No.30	79.0 - 75.1	77.05	washed	Mix, Sandsone, Shales, Quartzite
SM18031031	SM14	-3/8 +No.30	65.6 - 75.3	70.45	washed	Mix, Sandsone, Shales, Quartzite
SM18031032	SM15	-3/8 +No.30	68.0 - 63.8	65.9	washed	Mix, Sandsone, Shales, Quartzite
SM18034601	SM16	-3/8 +No.30	0.9 - 1.0	0.95	washed	Marble Crushed
SM18044842	SM17	-3/8 +No.30	13.6 - 10.9	12.25	washed	Dolomite
SM18048069	SM18	-3/8 +No.30	77.0 - 74.0	75.5	washed	Mix, Sandsone, Shales, Quartzite
SM18052453	SM19	-3/8 +No.30	21.8 - 25.1	23.45	washed	Limestone
SM18053437	SM20	-3/8 +No.30	7.5 - 9.7	8.6	washed	Dolomite
SM18059183	SM21	-3/8 +No.30	4.8 - 6.4	5.6	washed	Dolomite
SM19012296	SM7	-3/8 +No.30	0.4 - 1.2	0.8	washed	Marble
SM19019480	SM8	-3/8 +No.30	66.7 - 67.7	67.3	washed	Mix Metamorphic
SM19031563	SM9	-3/8 +No.30	72.7 -78.7	75.7	washed	Mix Metamorphic
SM19044467	SM10	-3/8 +No.30	75.0 - 78.4	76.7	washed	Sandsone and Shales
SM19044933	SM11	-3/8 +No.30	67.5 - 68.8	68.15	washed	Mix Metamorphic
SM19063970	SM12	-3/8 +No.30	68.4 - 71.1	69.75	washed	Sandsone and Shales

No suitable calibration model was available to evaluate this diverse mix of samples. The Research Team unsuccessfully attempted to develop a model with these SM samples. The SM samples were not effectively included in any available calibration dataset.[40]

4.4 NYSDOT Findings and Conclusions

4.4.1 Findings

- AIR Super Models, using statewide samples generated models with very good overall correlation, but lacked accuracy for many samples that were not sufficiently represented by the calibration set data.
- Model accuracy and predictive efficiency were found to improve by selecting calibration samples with common lithology, common origins; and representative of the full range of AIR values encountered in test samples.
- An effective AIR Source Model for the R83 quarry was developed.

[40] The "random collection" of the SM samples by NYSDOT and the diverse lithology associated with the SM samples had no relationship to any previously collected calibration samples provided by NYSDOT.

4.4.2 Conclusions

- Laser scanning can effectively be used as a quality control tool to quantify AIR in NYS aggregate and has potential to compliment or replace current AIR lab testing procedures.
- AIR model development requires that close attention be given to sample selection during model calibration to ensure that the calibrated sample population will represent the test sample population.
- AIR Source Model (restricted lithological) development would be the simplest AIR modeling strategy; however, expanded Super Model development is feasible with focused sample calibration testing that account for the lithological categories of the calibration samples.

Chapter 5: Ohio Laser Scanning Analysis

5.1 Ohio Scanning Objectives

The Ohio Department of Transportation (ODOT) effort focused on determining whether laser scanning could be used to quantify the chert and shale content in ODOT aggregate sources. ODOT specifications limit the quantity of chert and shale, respectively, in selected applications. Percent chert content or shale content in Ohio is typically accomplished by petrographically analyzing an aggregate sample, segregating by hand, either the chert or shale particles, followed by weighing the recognizable chert or shale in the sample of a known size.

The ODOT laser scanning plan involved several tasks:

- Collecting aggregate samples known to contain deleterious materials (either chert or shale).
- Petrographically segregating the chert and shale in each sample from the parent source; and respectively quantifying the percent content of chert and shale present in each source.
- Shipping the chert (or shale) along with their respective parent sources to the laser laboratory for scanning to establish spectral patterns associated with the chert, shale, and all parent aggregates.
- Re-blending each chert and each shale with their respective parent sources in known blending ratios.
- Scanning the re-blended mixtures to determine whether models could be developed to predict the percent of either chert or shale present in samples with known blending ratios.

The goal was to develop a “Counting Model” that could be used to count the number of times during a laser scan of an unknown parent source, that the laser pulse would hit a chert or shale particle. The percentage of “positive hits” could be used to quantify the deleterious material content in the sample. Successful model development would be demonstrated if the model(s) were able to successfully predict the correct proportion of chert or shale in pre-prepared samples with known proportions.

5.2 Ohio Aggregate Samples and Sources

ODOT's Office of Materials Management was instrumental in the development of the aforementioned laser scanning plan and supplying samples that could be used to develop the "Counting Model." As part of this effort, ODOT supplied several aggregate samples to the Research Team, from selected source locations, that contained chert and/or shale. For each source location, ODOT provided one parent material sample, with an accompanying bag of chert or shale that was petrographically removed from each parent source. The Research Team selected several samples for scanning. The sample names (ID) and aggregate types (lithology) for the chert and shale samples used in the analysis are presented in Table 5.1. A total of 13 Ohio aggregate samples were included in the chert analysis and a total of 5 aggregate samples were included in the shale analysis. The chert parent aggregate samples included two limestones (OH21 and OH38), one dolostone (OH33), and 10 gravel samples. All of the shale parent aggregate samples were gravels.

Table 5.1: Parent Aggregate Samples

Parent Aggregate Samples for Chert		Parent Aggregate Samples for Shale	
Sample ID	**Type (Lithology)**	**Sample ID**	**Type (Lithology)**
OH21	Limestone	OH131	Gravel
OH33	Dolostone	OH136	Gravel
OH35	Gravel	OH138	Gravel
OH37	Gravel	OH141	Gravel
OH38	Limestone	OH146	Gravel
OH41	Gravel	--	--
OH42	Gravel	--	--
OH51	Gravel	--	--
OH53	Gravel	--	--
OH54	Gravel	--	--
OH56	Gravel	--	--
OH57	Gravel	--	--
OH61	Gravel	--	--

Photographs showing one parent gravel sample (OH56) and its corresponding chert sample, and one parent gravel sample (OH146) and its corresponding shale sample are respectively presented in Figure 5.1 and Figure 5.2.

Figure 5.1: OH56 Parent Gravel and Light Chert Sample

Figure 5.2: OH146 Parent Gravel and Shale Sample

Each of the 13 parent aggregate samples associated with the chert samples and similarly each of the five parent aggregate samples associated with the shale samples, listed in Table 5.1, were scanned. In addition, each of the chert and each of the shale samples were scanned.[41]

A photograph of the OH33 parent aggregate and its associated chert sample (OH33LC) are shown in Figure 5.3, in their respective scanning trays prior to laser scanning. The small quantity of chert is shown in the smaller tray.

[41] Sample scanning generated, for the chert analysis, 13 parent aggregate spectra and 13 light chert spectra; and 5 parent aggregate spectra and 5 shale spectra for the shale analysis.

Figure 5.3: OH33 Parent Aggregate and Light Chert in Laser Scanning Trays

The total number of scans and laser shots per scan for the chert and shale calibration set samples are listed in Table 5.2 and Table 5.3, respectively. Each sample listed in the table was scanned multiple times. Approximately 40 to 80% of the individual laser shots were used for each sample during the model calibration and testing process.[42]

Table 5.2: Chert Model Calibration Sets: Parent and Chert Scans

Parent Aggregate Sample				Chert Sample			
Sample ID	Number of Scans	Total Number of Shots	Total Shots Used	Sample ID	Number of Scans	Total Number of Shots	Total Shots Used
OH21	9	9843	3701	OH21LC	9	6491	4693
OH33	8	9514	3397	OH33LC	12	6030	4326
OH35	6	7279	3431	OH35LC	11	5465	4005
OH37	8	9057	3878	OH37LC	6	2415	1636
OH38	4	4950	2266	OH38LC	4	638	609
OH41	9	10728	4670	OH41LC	4	638	552
OH42	5	7329	3357	OH42LC	5	1681	1429
OH51	4	4590	2283	OH51LC	5	1623	1003
OH53	----------No Data ----------						
OH54	6	6634	2580	OH54LC	7	4287	3144
OH56	4	4479	2683	OH56LC	5	2019	1665
OH57	4	4910	2851	OH57LC	5	2259	1331
OH61	4	4943	3557	OH61LC	5	2284	1468

[42] This was due to the signal to noise ratio (SNR) filtering process (see Section 2.2)

Table 5.3: Shale Model Calibration Sets: Parent and Shale Scans

Parent Aggregate Sample				Shale Sample			
Sample ID	Number of Scans	Total Number of Shots	Total Shots Used	Sample ID	Number of Scans	Total Number of Shots	Total Shots Used
OH131	3	3751	1562	OH131S	2	1708	1206
OH136	3	3433	1086	OH136S	2	2087	1100
OH138	3	3607	1148	OH138S	2	2081	892
OH141	3	3920	1388	OH141S	2	2048	816
OH146	3	3820	1412	OH146S	2	2052	1066

5.3 Ohio Chert and Shale PLS Counting Models

5.3.1 OH Counting Model Calibration and Testing

Special Binary Partial Least Square Regression (PLSR) "Counting" Models were respectively calibrated for both the chert and shale analyses. A binary model, as previously described, is a model that predicts one of two outcomes (e.g., yes or no, pass or fail, or 1 or 0).[43]

In most PLSR models, the sample spectra used to develop and predict the model output is based on an average of many individual laser shots. In a "Counting Model" each laser shot, and the spectrum associated with that shot, is independently evaluated by the model. So, for example, if 1000 laser shots are taken at an aggregate sample, the model will count how many laser shots were a Yes and how many shots were a No; or how many shots scored a y-value of 1 and how many shots scored a y-value of 0. Each respective model type was calibrated by setting the y-values of all chert or shale particle spectra to 1 and the y-values of all parent aggregates to 0.[44]

In summary, the steps in the modeling process for chert were as follows:

- Scan chert samples, listed in Table 5.2, to define a chert spectrum associated with each parent.
- Scan all respective parent aggregates to define a parent aggregate spectrum associated with each of the chert samples.
- Re-blend each parent and chert sample in pre-selected proportions by weight.

[43] A more detailed description of PLSR Binary models is presented in Section 2.4.1.
[44] The y-value is the dependent variable of the PLSR model, which is the model output.

- Scan the blended samples and count the number of shots identified as chert and parent.
- Use the percentages of identified chert shots as a surrogate to the percent weight of chert in the sample.
- Establish the best calibration by selecting the VAD value that results in the maximum true positive tests and minimum false negative tests for each model.

The same steps were employed in the shale modeling development effort. In this case, the shale and corresponding parent aggregates used are listed in Table 5.3.

5.3.2 Spectral Data Filtration and Transformation

The ODOT modeling effort was the most challenging in the TPF Program. The primary objective was to develop spectral patterns that could be employed to "clearly" differentiate between parent and chert and/or shale particles for "each laser shot." No other modeling effort required shot-to-shot decision-making. All other modeling efforts made use of averaged spectral patterns derived from 1000–1500 shot scans. The spectrum of each individual laser shot is affected by both the heterogeneity of the underlying stone structure and the heterogeneity associated with the morphology of the laser-induced plasma. The result is a spectral pattern distribution with high individual shot variability. Since ODOT chert and shale maximum allowable levels are as low as 1 percent in certain applications, small errors in shot-to-shot decisions could easily result in mischaracterization of the chert and/or shale content of parent aggregate sample.

During the modeling effort several data processing techniques were investigated to magnify the differences between the parent aggregates and the chert and shale samples. The final methodology included the following:

- Signal to Noise Ratio Spectra Screening

  The Signal to Noise Ratio (SNR) screening process was previously described in Section 2.2. This SNR screen was used to remove poor laser spectra from the analysis.

- Line Model Selection

  Individual line models were developed, in lieu of full spectra to reduce the excess noise in the model. Line models are models in which the input spectra have been reduced from 14336 wavelengths to a pre-selected number of wavelengths, which by examination yield better results. Line models were previously described in Section 2.3.

- Spectral Scaling and Data Transformation

  Finally, spectral scaling and data transformation techniques were employed in an attempt to magnify the spectral differences between the Parent Material (P) and Deleterious Material (D) at each wavelength. The intent of spectral scaling and data transformation of the Ohio sample spectral data are conceptually illustrated in Figure 5.4.

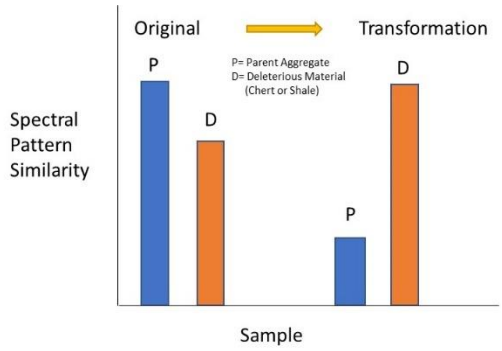

Figure 5.4: Spectral Data Transformation

Figure 5.4 depicts a histogram containing original spectral data for P aggregate and D aggregate on the left side of the graphic; and transformed data on the right side. The histogram height of each respective sample is intended as a measure of the similarity of the respective spectral patterns. The closer the heights of each sample, the more similar the respective spectra. Ideally, the less similar the P and D patterns, the easier it is to discriminate between the two materials. There is measurable difference between spectral patterns in the original (or raw) spectral data, shown on the left side of Figure 5.4; however, after transformation there is much greater difference, as shown on the right side of the figure. The transformed pattern data facilitates the differentiation process, which results in improved counting model accuracy.

The spectral data preprocessing techniques employed by the Research Team involved mean centering and standardization. This procedure transforms the spectral data from the raw intensity

values recorded by the spectrometer to standardized or normalized values. This transformation occurs by employing the equation below:[45]

$$Z = (x-\mu)/\sigma$$

Equation 5.1

Where:

Z = the final normalized value,

X = the value to be normalized,

μ = the arithmetic mean, or average of the distribution, and

σ = the standard deviation of the distribution.

In the Ohio aggregate scans, the mean of approximately 1500 laser shots were used to characterize the aggregate. This means that each wavelength (W) had a sample population of 1500 values from which to calculate the average intensity value (μ) and the standard deviation (σ) of the population. Since there are 14336 different wavelengths comprising each laser shot spectra, each wavelength will have its own sample population with a unique arithmetic mean (μ) and standard deviation (σ). It is common practice to organize spectral data in a matrix as shown in Table 5.4.[46]

Table 5.4: Tabular Laser Shot Intensity Array by Wavelength

	Wavelengths (W)					
Shot	**W_1**	**W_2**	**W_3**	**W_4**	**…**	**W_m**
S_1	X_{11}	X_{12}	X_{13}	X_{14}	…	X_{1m}
S_2	X_{21}	X_{22}	X_{23}	X_{24}	…	X_{2m}
S_3	X_{31}	X_{32}	X_{33}	X_{34}	…	X_{3m}
S_4	X_{41}	X_{42}	X_{43}	X_{44}	…	X_{4m}
…	...	...	...	...	…	…
S_n	X_{n1}	X_{n2}	X_{n3}	X_{n4}	…	X_{nm}
Average	μ_1	μ_2	μ_3	μ_4	…	μ_m
Standard Deviation	σ_1	σ_2	σ_3	σ_4	…	σ_m

[45] The Standardization procedure employs the Standardize function used in Microsoft Excel.

[46] The laser shot intensity for a given wavelength in Table 5.4 is represented by X_{nm}, where n represents the specific laser shot and m the measured wavelength. For the Ohio scans n goes from 1 to 1500 and m represents 14336 recorded wavelengths. Table 5.4 would have 1500 rows and 14336 columns. The average of all the shots for a particular wavelength is represented by μ_m and σ_m, respectively. For example, X_{43} represents the intensity associated with the fourth laser shot and wavelength W_3.

Mean centering and standardization are sometimes referred to as normalization or scaling.[47] Each intensity value is scaled using μ and σ associated with the intensity distribution defined by the specific wavelength. The procedure can be illustrated by focusing on the first laser shot (s_1), in the first row, and the first wavelength (W_1), in the first column. The intensity value x_{11} is scaled or normalized, yielding a scaled value Z_{11} by subtracting the intensity X_{11} by the average of all the W_1 intensities μ_1 and dividing this value by the standard deviation σ_1 of all W_1 laser shot intensities, or:

$$(Z_{11}) = (X_{11} - \mu_1) / (\sigma_1) \qquad \textbf{Equation 5.2}$$

The ratio of Z_{11} to the raw intensity value X_{11} is referred to as the Scaling Factor for this laser shot. Every intensity in the entire array (1500 x 14336) has a unique scaling factor. Standardization (or the development of Scaling Factors) requires a sample population from which both μ and σ can be calculated. Each Ohio analysis uniquely had two sample types and as a result two distinct sample populations. These include the Parent and Chert, and the Parent and Shale. A special data transformation step was employed in the Ohio analysis to magnify the differences between the Parent aggregates and the chert and shale aggregates. This involved the calculation of μ and σ at each wavelength using only the Parent Aggregate samples and applying these Parent Aggregate scaling factors to the corresponding intensities of both the Parent as well as the Chert and Shale samples at each respective wavelength. This procedure resulted in a magnification of the differences between the scaled Parent Aggregate intensities and the chert and shale intensities.[48]

5.3.3 Source Models and Super Models

The samples provided by ODOT presented the opportunity to develop two types of deleterious material counting models. The first is referred to as an Ohio Source Model. In a Source Model separate chert and shale counting models are independently calibrated for each local aggregate source. The second model type is referred to as an Ohio Super Model. In this model it

[47] Spectral scaling has the effect of giving all wavelengths equal weight in the analysis, thereby eliminating the bias that might be exhibited by one or more wavelengths in the spectrum

[48] Developing a scaling factor (SF) using the parent material is statistically appropriate because the parents are all part of the same sample population of parent material. Applying this Parent SF to the chert or shale samples is statistically questionable, since the chert and shale samples represent completely different sample population; nonetheless this procedure provides EMPIRICAL benefit since it helps to differentiate the two populations (parent and chert) in a PLS Binary analysis.

is assumed that one chert model and one shale counting model can be developed for all aggregate parent sources lumped together.[49]

A hypothetical multidimensional graphical representation of a Source Model clustering arrangement is presented in Figure 5.5, and a multidimensional graphical representation of a Super Model clustering arrangement is presented in Figure 5.6. In a Source Model, the cherts and/or shale are more closely related to the parent source than they are to other cherts or shale from other sources. In a Super Model, the cherts and/or shales cluster together in their own grouping that differ from the parent sources.

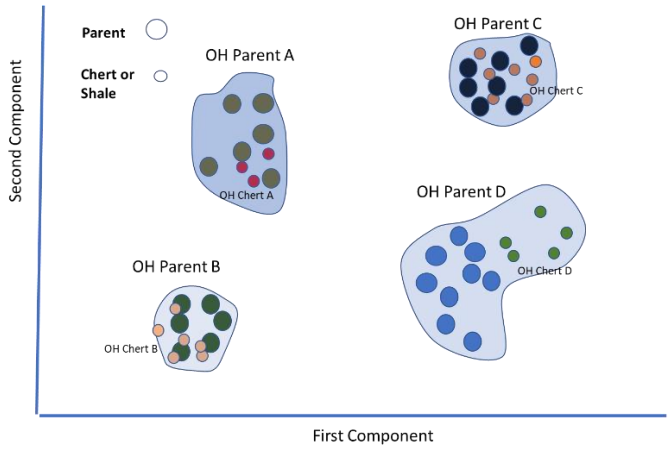

Figure 5.5: Graphical Representation of Parent and Chert Groupings in a Source Model

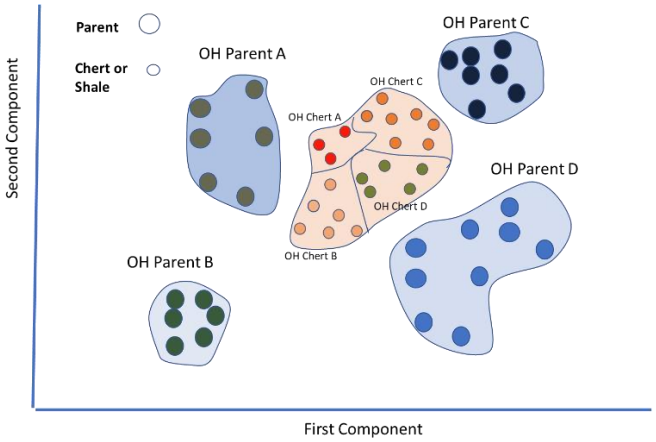

Figure 5.6: Graphical Representation of Parent and Chert Groupings in a Super Model

[49] Reference was previously made to Source and Super Models in Section 2.4.3 Sample Collection Requirements

It is noteworthy that the benefits of an effective Super Model far outweigh the benefits of a Source Model. With an effective Super Model any sample can be scanned, regardless of its source, and the quantity of chert or shale in the sample can be quantified. One model can cover the whole State of Ohio. A Source Model requires a separate model for each aggregate source. During the initial examination of the spectral data, it was believed that Source Models would be needed to accurately quantify chert or shale content. Subsequently it was discovered, after pre-processing the spectral data, that effective Super Models are possible. These findings are presented in the following sections.

5.4 Test Validation Approach and SLT Scanning

The efficacy of the calibrated counting models was tested by blending known percentages of chert or shale with each parent sample, scanning the blended sample and then comparing the predicted percentages (counts) to the known percentages. Shot counting validation testing is dependent on SLT scanning of an accurately blended sample that the laser can target. The SLT design is such that the laser only targets the surface layer of a given sample place in any sample tray. An OH146 shale sample with 1.25% shale in a sample tray is shown in Figure 5.7.

Figure 5.7: Blended Shale (1.25%) in OH146 Sample Tray

When shale is blended with a parent sample it is unlikely that the quantity of shale found in the top layer of the sample will comprise exactly 1.25% of the surface. This problem can be

remedied by scanning multiple samples during any analysis and remixing the new sample in the tray, prior to each replicate scan. As a result, a necessary requirement in SLT generated counts is that multiple samples be remixed and tested. The average count results when this approach is employed will converge on the true count value. It was unfortunate that during the chert and shale scanning program, which was initiated in early 2020, the desired number of mixed sample scans could not be undertaken.[50] Despite the low number of scans, which hampered the analysis, the Ohio chert and shale counting models that were developed were highly predictive.

5.5 Ohio Chert Counting Model Results

It was originally intended to prepare five different mixing concentrations of chert for each parent aggregate. It was also intended that each blend would be scanned somewhere between 5 and 10 times. Two factors interfered with this plan. The first was that in all cases sufficient chert was not available to prepare blends for each mix fraction; and the second that the COVID crisis impacted the ODOT chert testing schedule and forced a reduction in the planned scanning schedule. The quantity of chert blended into each parent sample is listed in Table 5.5. Blended chert quantities ranged from 0 to 10 percent. The number of scans associated with each sample are listed in the tables below.

Table 5.5: Ohio Chert Model Test: Sample Blends

Sample ID	Lithology	Percent Chert
OH21	Limestone	0, 1.25, 2.50, 5.0, 10.0
OH33	Dolostone	0, 2.50, 5.0, 10.0
OH35	Gravel	0, 1.25, 2.50, 5.0, 10.0
OH37	Gravel	0, 1.25, 2.50, 5.0, 10.0
OH38	Limestone	0, 5.0
OH41	Gravel	0, 1.25, 2.50
OH42	Gravel	0, 5.0, 10.0
OH51	Gravel	0, 2.50, 5.0, 10.0
OH53	Gravel	No samples run
OH54	Gravel	0, 1.25, 2.50, 5.0, 10.0
OH56	Gravel	0, 1.25, 2.50, 5.0, 10.0
OH57	Gravel	0, 1.25
OH61	Gravel	0, 5.0, 10.0

[50] This was due to a laser lab shut down that required a truncated program due to pandemic and other administrative issues.

5.5.1 Chert Count Source Model Results

Tabular and graphical results for each parent aggregate chert model are presented below. Each table provides for each aggregate source, the average count results, and the standard deviation of the results for the number of laser scans, for each blend scanned. Graphical results display the chert count model prediction. The standard deviation range and a dashed horizontal line representing the quantity (%) chert introduced into the scanned sample.[51]

Chert Source Model Sample: 0% Chert

Mean Parent aggregate counting model results, listed in Table 5.6 for 0% chert samples, were all 0.7% and below. The standard deviations around each mean value were all less than 0.32%. Graphical projections of the tabulated data presented in Figure 5.8 show all counting model predictions relative to the 0% target line. The model effectively predicted negligible chert levels for all sources.

Table 5.6: Tabular Model Prediction: 0% Chert

Sample	Average	Standard Deviation	Scans
OH21	0.0%	0.0%	3
OH33	0.0%	0.0%	3
OH35	0.70%	0.12%	3
OH37	0.23%	0.32%	3
OH41	0.0%	0.0%	3
OH42	0.05%	0.07%	2
OH51	0.0%	0.0%	2
OH54	0.0%	0.0%	3
OH56	0.0%	0.0%	2
OH61	0.0%	0.0%	2

[51] It is noteworthy that the Parent Sample tested was assumed to have no chert in it prior to mixing pre-defined amounts into the sample for Counting Model validation. The veracity of this assumption could not be verified; but if residual amounts of chert were present, it was assumed that the actual levels would to be very low (<1%).

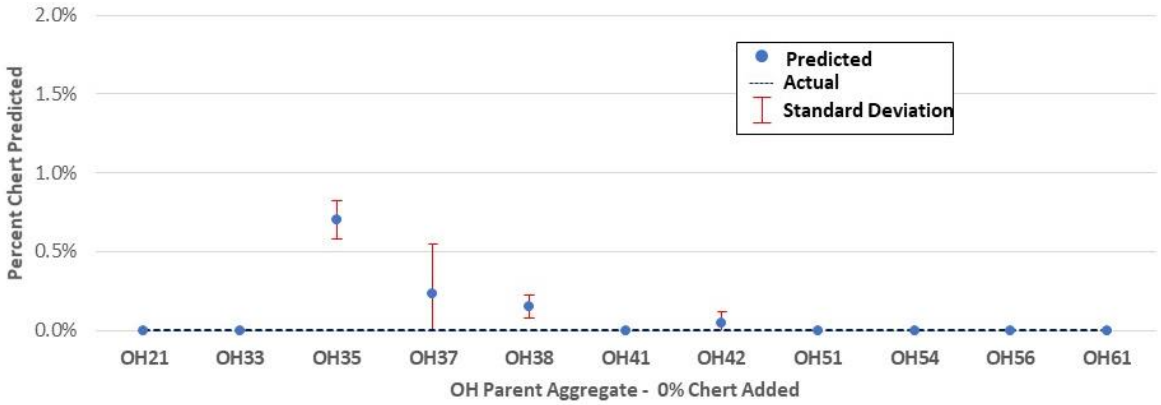

Figure 5.8: Graphical Source Model Predictions: 0% Chert

Chert Source Model Sample: 1.25% Chert

Mean Parent aggregate counting model results, listed in Table 5.7 for 1.25% chert samples, ranged from 0.1% to 1.6%. The standard deviations around each mean value were 0.42% or less. Graphical projections of the tabulated data presented in Figure 5.9 show the relationship of the counting model estimates to the 1.25% target line. All sample predictions were below 1.6%. Each sample was scanned only twice, well below an ideal number, nonetheless the model results were judged to be highly predictive.

Table 5.7: Tabular Model Prediction: 1.25% Chert

Sample	Average	Standard Deviation	Scans
OH21	0.30%	0.42%	2
OH35	0.20%	0.28%	2
OH37	1.6%	0.07%	2
OH54	0.20%	0.14%	2
OH56	1.5%	0.28%	2
OH57	0.10%	0.14%	2

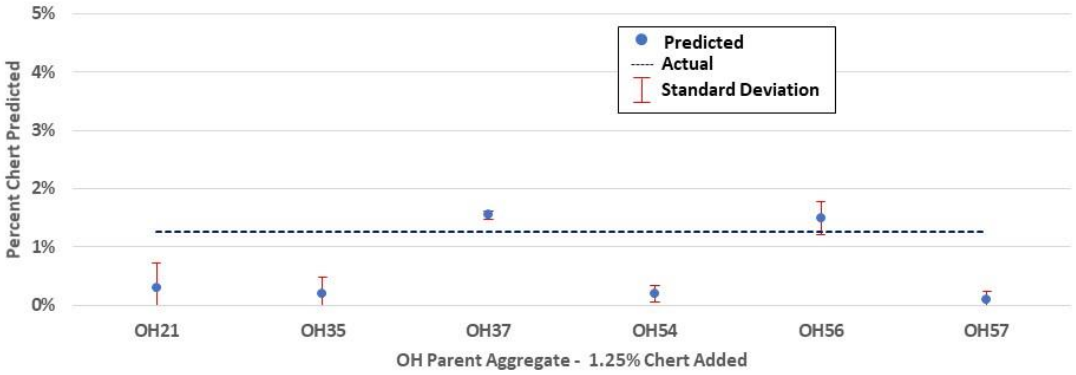

Figure 5.9: Graphical Source Model Predictions: 1.25% Chert

Chert Source Model Sample: 2.5% Chert

Mean Parent aggregate counting model results, listed in Table 5.8 for 2.5% chert samples ranged from 0.1% to 5.4%. The standard deviations around each mean value ranged from a low of 0.07% to a high of 4.4%. Graphical projections of the tabulated data presented in Figure 5.10 show that all counting model sample estimates were all close to the 2.5% target line.

Table 5.8: Tabular Source Model Predictions: 2.5% Chert

Sample	Average	Standard Deviation	Scans
OH21	0.13%	0.23%	3
OH33	2.8%	2.2%	3
OH35	1.7%	1.8%	3
OH37	4.4%	1.3%	3
OH51	0.55%	0.78%	2
OH54	0.45%	0.07%	2
OH56	5.4%	1.0%	2

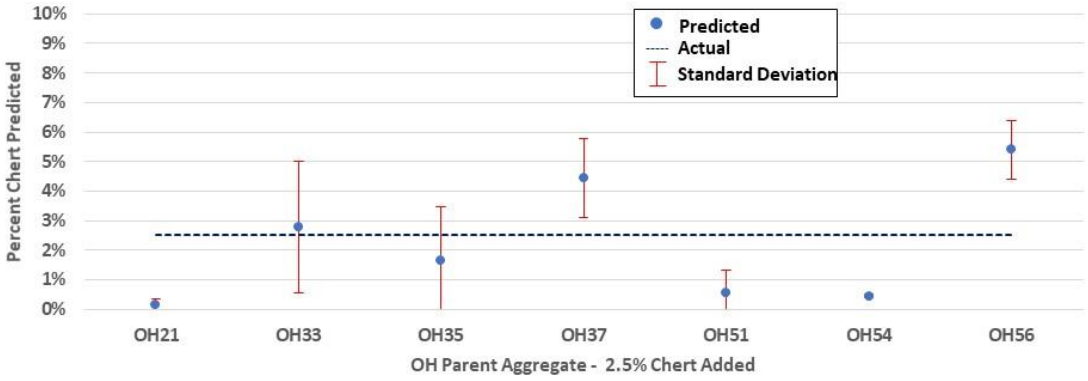

Figure 5.10: Graphical Source Model Predictions: 2.5% Chert

Chert Source Model Sample: 5% Chert

Mean Parent aggregate counting model results, listed in Table 5.9 for 5% chert samples ranged from 0.4 to 11.1%. The standard deviations around each mean value ranged from a low of 0.5% to a high of 8.8%. Graphical projections of the tabulated data presented in Figure 5.11 show all counting model sample estimates relative to the 5% target line. Some of the samples overpredicted the 5% target line. Each sample was scanned only three times, again well below a desirable number. Nonetheless these model results were also deemed predictive.

Table 5.9: Tabular Source Model Predictions: 5% Chert

Sample	Average	Standard Deviation	Scans	Sample
OH21	3.4%	2.8%	3	OH21
OH33	11.1%	8.8%	3	OH33
OH35	1.4%	1.2%	3	OH35
OH37	10.8%	2.5%	3	OH37
OH38	9.4%	8.4%	3	OH38
OH42	9.9%	7.9%	3	OH42
OH51	5.1%	3.7%	3	OH51
OH54	4.1%	0.56%	3	OH54
OH56	9.5%	3.8%	3	OH56
OH61	0.40%	0.40%	3	OH61

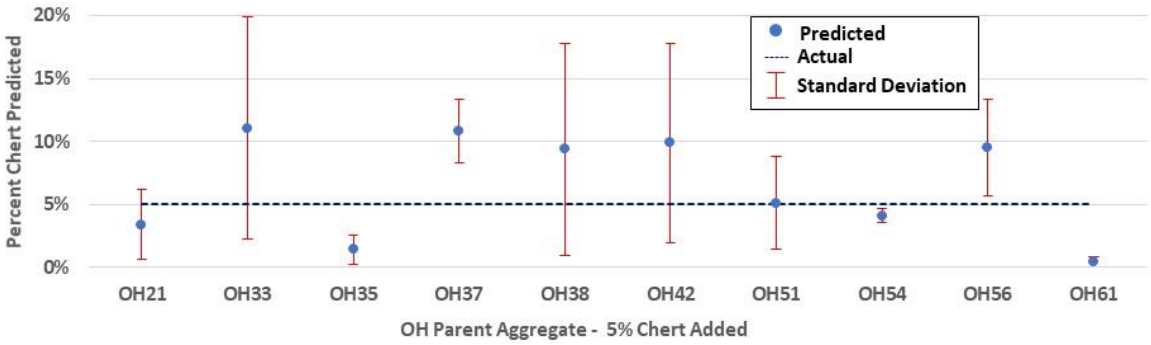

Figure 5.11: Graphical Source Model Predictions: 5% Chert

Chert Source Model Sample: 10% Chert

Mean Parent aggregate counting model results, listed in Table 5.10 for 10% chert samples ranged from 2.2% to 17.4%. The standard deviations around each mean value ranged from a low of 1.8% to a high of 9.2%. Graphical projections of the tabulated data presented in Figure 5.12 show all counting model sample estimates relative to the 10% target line. These model results were judged to be very effective.

Table 5.10: Tabular Source Model Predictions: 10% Chert

Sample	Average	Standard Deviation	Scans
OH21	6.9%	1.8%	3
OH33	10.6%	9.2%	3
OH35	9.0%	7.6%	3
OH37	11.8%	6.8%	3
OH42	13.5%	3.9%	3
OH51	15.3%	6.4%	3
OH54	3.1%	3.6%	3
OH56	17.4%	3.9%	3
OH61	2.2%	2.4%	3

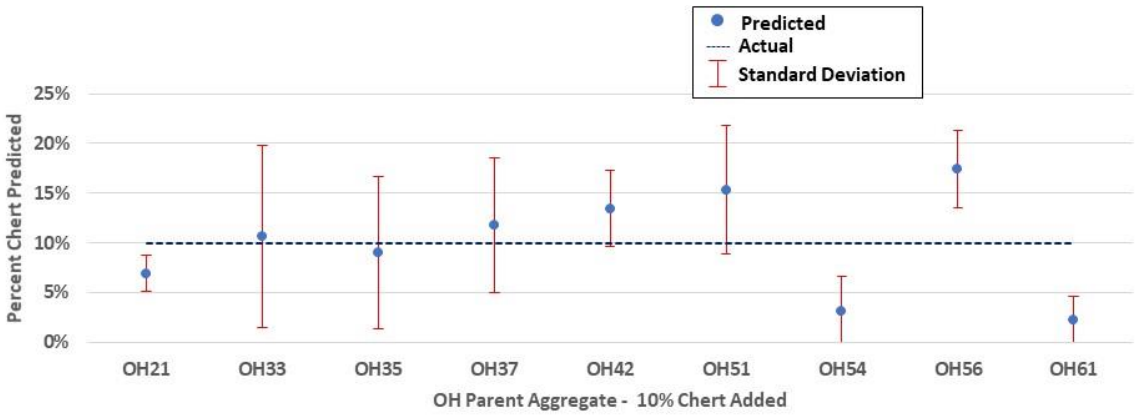

Figure 5.12: Graphical Source Model Predictions: 10% Chert

5.5.2 Chert Count Super Model Results

Chert Super Model Sample: 0% Chert

Mean Parent aggregate counting model results, listed in Table 5.11 for 0% Super Model chert samples ranged from 0.33% to 2.1%. The standard deviations around each mean value were less than 0.85%. Graphical projections of the tabulated data presented in Figure 5.13 show all counting model sample estimates relative to the 0% target line. Two results were greater than 1%. The remainder less than 1%. With just three scans for each sample, the results suggest that an effective chert Super Model is possible.

Table 5.11: Tabulated Super Model Predictions: 0% Chert

Sample	Predicted	Standard Deviation	Scans
OH21	0.67%	0.35%	3
OH33	0.33%	0.06%	3
OH35	0.40%	0.20%	3
OH37	1.3%	0.85%	3
OH42	0.13%	0.06%	3
OH51	0.30%	0.14%	2
OH54	0.27%	0.46%	3
OH56	0.65%	0.21%	2
OH61	2.1%	0.64%	2

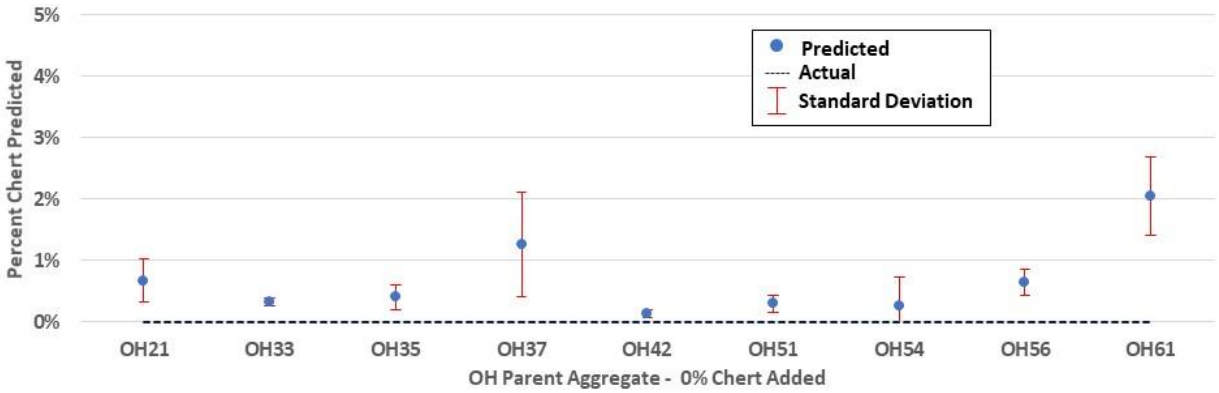

Figure 5.13: Graphical Super Model Predictions: 0% Chert

Chert Super Model Sample: 1.25% Chert

Mean Parent aggregate counting model results, listed in Table 5.12 for 1.25% Super Model chert samples ranged from 0.45% to 1.8%. The standard deviations around each mean value were all less than 0.57%. Graphical projections of the tabulated data presented in Figure 5.14 show all counting model sample estimates relative to the 1.25% target line. These model results were considered to be highly predictive.

Table 5.12: Tabulated Super Model Predictions: 1.25% Chert

Sample	Predicted	Standard Deviation	Scans
OH21	1.0%	0.49%	2
OH35	1.0%	0.57%	2
OH37	0.90%	0.14%	2
OH54	0.85%	0.35%	2
OH56	0.45%	0.21%	2
OH57	1.8%	0.28%	2

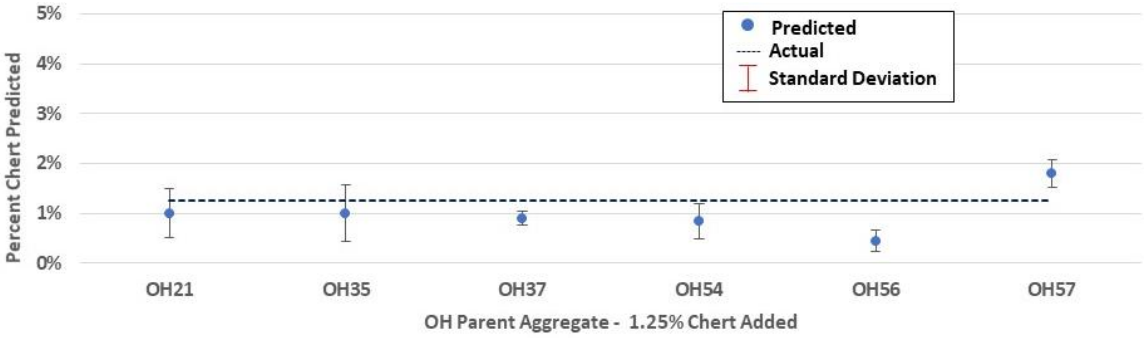

Figure 5.14: Graphical Super Model Predictions: 1.25% Chert

Chert Super Model Sample: 2.5% Chert

Mean Parent aggregate counting model results, listed in Table 5.13 for 2.5% Super Model chert samples ranged from 0.3% to 5.2%. The standard deviations around each mean value ranged from a low of 0.1% to a high of 2.1%. Graphical projections of the tabulated data presented in Figure 5.15 show all counting model sample estimates relative to the 2.5% target line. Again, these Super Model results were considered to be highly predictive.

Table 5.13: Tabulated Super Model Predictions: 2.5% Chert

Sample	Predicted	Standard Deviation	Scans
OH21	0.3%	0.10%	3
OH33	0.9%	0.40%	3
OH35	2.2%	2.00%	3
OH37	5.2%	1.10%	3
OH51	1.0%	0.50%	2
OH54	0.9%	0.60%	2
OH56	4.8%	0.50%	2

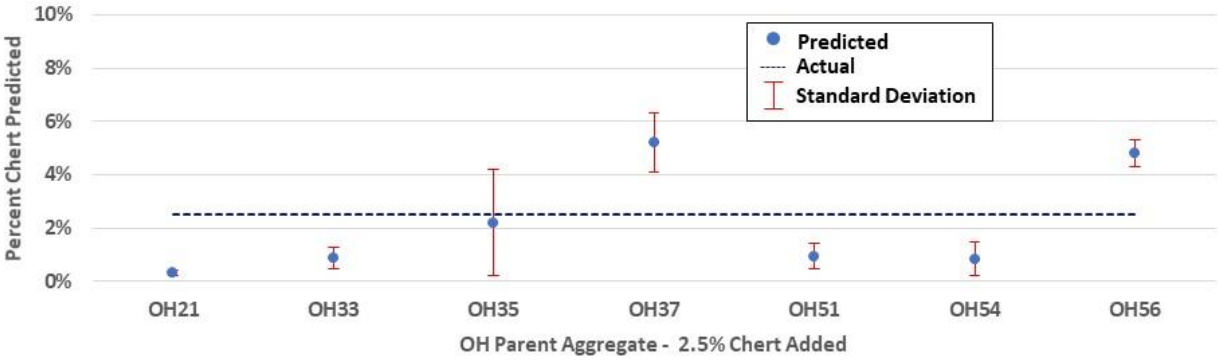

Figure 5.15: Graphical Super Model Predictions: 2.5% Chert

Chert Super Model Sample: 5% Chert

Mean Parent aggregate counting model results, listed in Table 5.14 for 5% Super Model chert samples ranged from 3.3% to 14.8%. The standard deviations around each mean value ranged from a low of 2.0% to a high of 12.4%. Graphical projections of the tabulated data presented in Figure 5.16 show all counting model sample estimates relative to the 5% target line. Most samples overpredicted the 5% target line.

Table 5.14: Tabulated Super Model Predictions: 5% Chert

Sample	Predicted	Standard Deviation	Scans
OH21	9.4%	5.1%	3
OH33	10.6%	7.3%	3
OH35	3.3%	2.5%	3
OH37	9.7%	2.0%	3
OH38	14.8%	12.4%	3
OH42	9.8%	7.5%	3
OH51	5.8%	4.0%	3
OH54	4.9%	0.60%	3
OH56	6.8%	3.4%	3
OH61	9.8%	3.1%	3

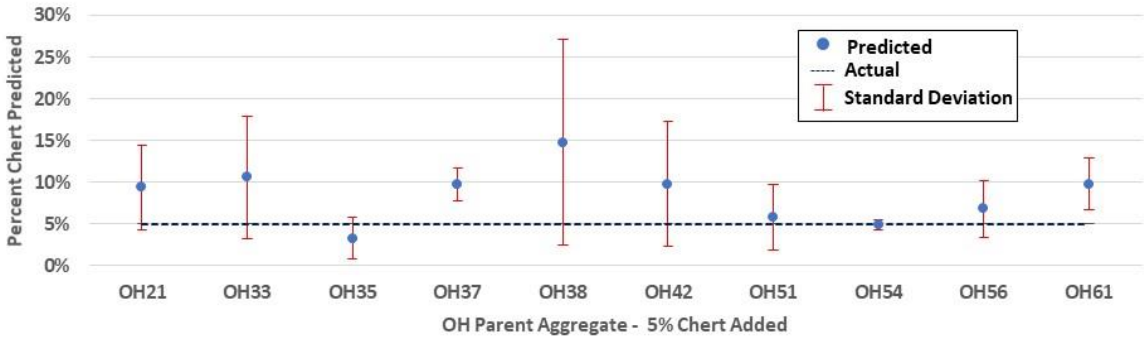

Figure 5.16: Graphical Super Model Predictions: 5% Chert

Chert Super Model Sample: 10% Chert

Mean Parent aggregate counting model results, listed in Table 5.15 for 10% Super Model chert samples ranged from 3.7% to 22.6%. The standard deviations around each mean value ranged from a low of 4% to a high of 11.4%. Graphical projections of the tabulated data presented in Figure 5.17 show all counting model sample estimates relative to the 10% target line. Most samples overpredicted the 10% target line.

Table 5.15: Tabulated Super Model Predictions: 10% Chert

Sample	Predicted	Standard Deviation	Scans
OH21	22.2%	9.8%	3
OH33	8.6%	4.6%	3
OH35	14.6%	11.4%	3
OH37	9.2%	5.1%	3
OH42	15.6%	5.4%	3
OH51	22.6%	8.9%	3
OH54	3.7%	4.0%	3
OH56	10.8%	5.1%	3
OH61	16.5%	6.5%	3

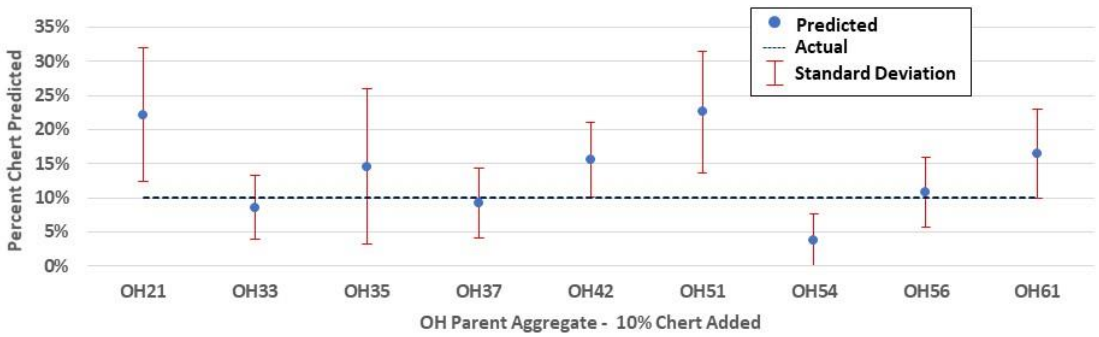

Figure 5.17: Graphical Super Model Predictions: 10% Chert

5.6 Ohio Shale Counting Model Results

The quantity of shale blended into each parent sample is listed in Table 5.16. Blended shale quantities ranged from 0 to 5.0 percent.

Table 5.16: Ohio Shale Model Test Sample Blends

Sample ID	Lithology	Percent Shale
OH131	Gravel	0, 1.25, 5.0
OH136	Gravel	0, 1.25, 5.0
OH138	Gravel	0, 1.25, 5.0
OH141	Gravel	0, 1.25, 5.0
OH146	Gravel	0, 1.25, 5.0

5.6.1 Shale Count Source Model Results

Shale Source Model Sample: 0% Shale

Mean Parent aggregate counting model results, listed in Table 5.17 for 0% shale target ranged from 0.73% to 1.3%. The standard deviations around each mean value were all less than 0.87%. Graphical projections of the tabulated data presented in Figure 5.18 show all counting model sample estimates relative to the 0% target line. The results show somewhat elevated shale levels above the 0% target line.

Table 5.17: Tabulated Source Model Predictions: 0% Shale

Sample	Predicted Average	Standard Deviation	Scans
OH131	0.83%	0.85%	3
OH136	0.73%	0.67%	3
OH138	1.3%	0.87%	3
OH141	0.73%	0.55%	3
OH146	0.90%	0.26%	3

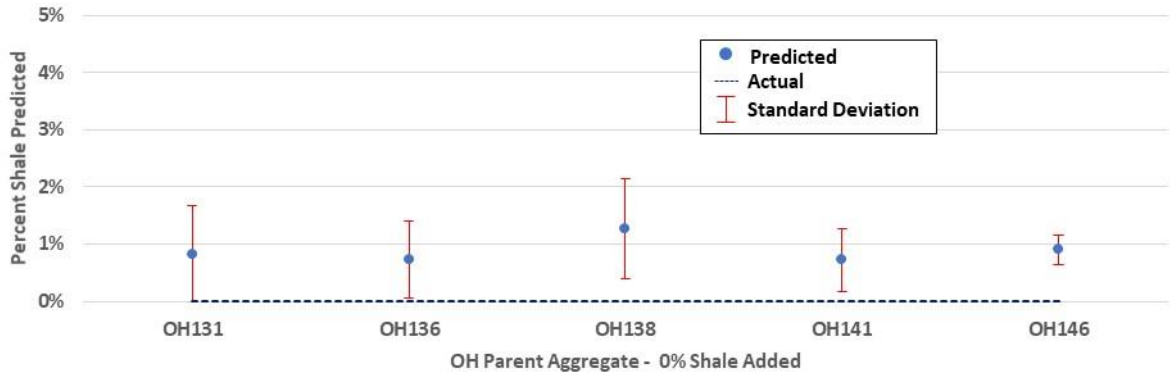

Figure 5.18: Graphical Source Model Predictions: 0% Shale

Shale Source Model Sample: 1.25% Shale

Mean Parent aggregate counting model results, listed in Table 5.18 for the 1.25% shale target ranged from 0.5% to 3.7%. The standard deviations around each mean value were less than 1.4%. Graphical projections of the tabulated data presented in Figure 5.19 show all counting model sample estimates relative to the 1.25% target line. The results show accurate model predictions.

Table 5.18: Tabulated Source Model Predictions: 1.25% Shale

Sample	Predicted Average	Standard Deviation	Scans
OH131	0.50%	0.0%	2
OH136	3.7%	1.4%	2
OH138	0.95%	0.21%	2
OH141	0.90%	0.71%	2
OH146	1.1%	0.42%	2

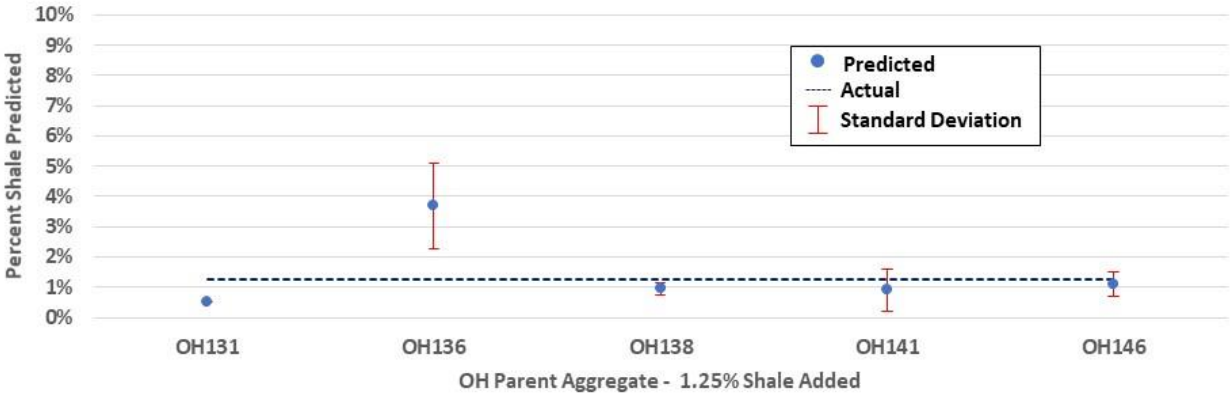

Figure 5.19: Graphical Source Model Predictions: 1.25% Shale

Shale Source Model Sample: 5% Shale

Mean Parent aggregate counting model results, listed in Table 5.19 for the 5% shale targets ranged from 0.43% to 7.6%. The standard deviations around each mean value ranged from a low of 0% to a high of 1.9%. Graphical projections of the tabulated data presented in Figure 5.20 show all counting model sample estimates relative to the 5% target line. The results show some very accurate counts and some high and low predictions, but all model predictions are in an expected range and additional scans would be expected to improve model accuracy.

Table 5.19: Tabulated Source Model Predictions: 5% Shale

Sample	Predicted Average	Standard Deviation	Scans
OH131	0.43%	0.40%	3
OH136	2.1%	0.0%	1
OH138	7.6%	0.21%	2
OH141	3.9%	2.4%	2
OH146	5.2%	1.9%	2

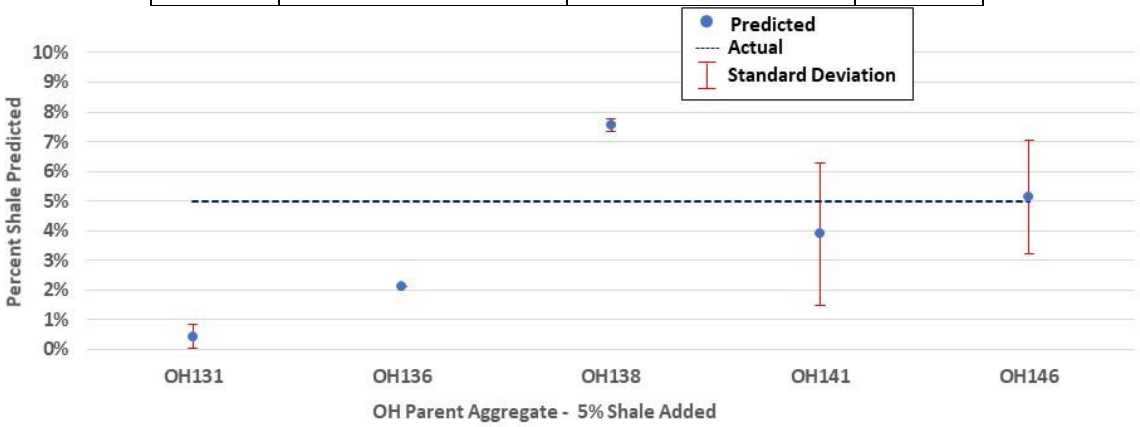

Figure 5.20: Graphical Source Model Predictions: 5% Shale

5.6.2 Shale Count Super Model Results

Shale Super Model Sample: 0% Shale

Mean Parent aggregate counting model results, listed in Table 5.20 for 0% Super Model shale samples ranged from 0% to 1.4%. The standard deviations around each mean value were all below 0.75%. Graphical projections of the tabulated data presented in Figure 5.21 show all counting model sample estimates relative to the 0% target line. The results show reasonably accurate model predictions.

Table 5.20: Tabulated Super Model Predictions: 0% Shale

Sample	Predicted	Standard Deviation	Scans
OH131	1.4%	0.60%	3
OH136	0%	0%	3
OH138	0.07%	0.12%	3
OH141	0.53%	0.61%	3
OH146	0.73%	0.75%	3

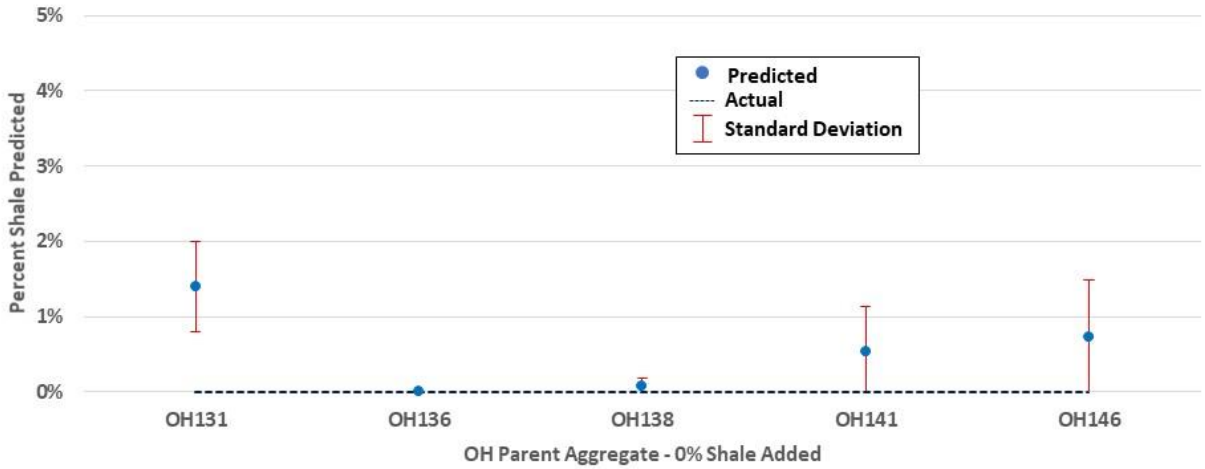

Figure 5.21: Graphical Super Model Predictions: 0% Shale

Shale Source Model Sample: 1.25% Shale

Mean Parent aggregate counting model results, listed in Table 5.21 for 1.25% Super Model shale samples ranged from 0.15% to 1.0%. The standard deviations around each mean value were less than 0.42%. Graphical projections of the tabulated data presented in Figure 5.22 show all counting model sample estimates relative to the 1.25% target line. The results show that the model slightly underpredicted the results, but within reasonable accuracy.

Table 5.21: Tabulated Super Model Predictions: 1.25% Shale

Sample	Predicted	Standard Deviation	Scans
OH131	1.00%	0.28%	2
OH136	0.40%	0.28%	2
OH138	0.15%	0.21%	2
OH141	0.70%	0.42%	2
OH146	0.65%	0.35%	2

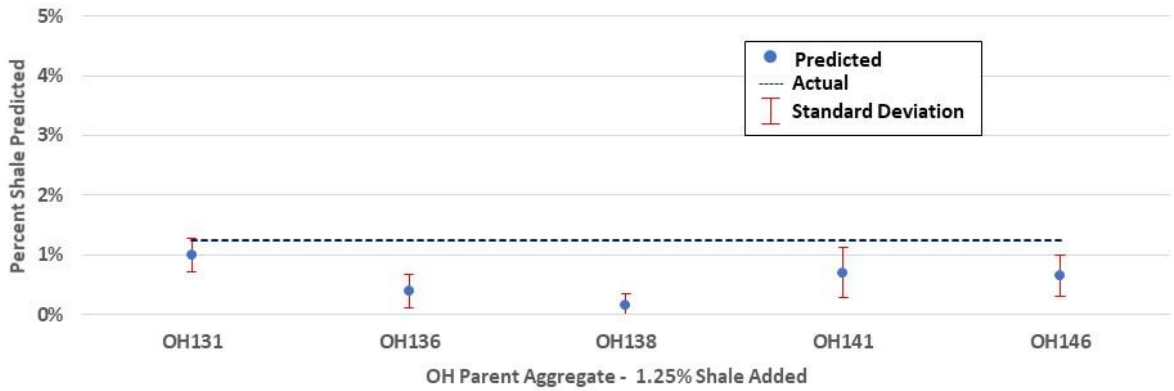

Figure 5.22: Graphical Super Model Predictions: 1.25% Shale

Shale Super Model Sample: 5% Shale

Mean Parent aggregate counting model results, listed in Table 5.22 for 5% Super Model shale samples ranged from 0% to 6.8%. The standard deviations around each mean value ranged from a low of 0% to a high of 4.9%. Graphical projections of the tabulated data presented in Figure 5.23 show all counting model sample estimates relative to the 5% target line. The results show effective predictions with the exception of OH136. Only one sample blend was scanned for this sample.

Table 5.22: Tabulated Super Model Predictions: 5% Shale

Sample	Predicted	Standard Deviation	Scans
OH131	3.9%	4.9%	3
OH136	0.0%	0.0%	1
OH138	2.6%	0.92%	2
OH141	3.0%	2.3%	2
OH146	6.8%	0.64%	2

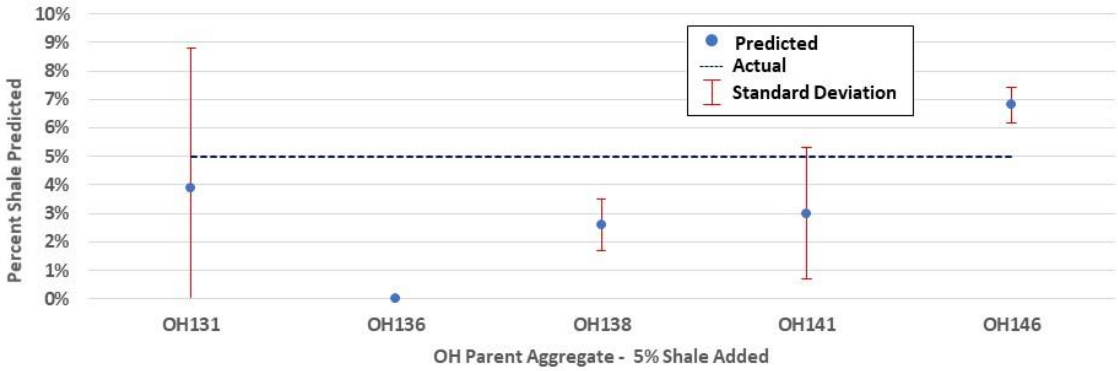

Figure 5.23: Graphical Super Model Predictions: 5% Shale

5.7 ODOT Findings and Conclusions

5.7.1 Findings

- Spectral fingerprints were identified that distinguished between chert and shale and their respective Parent Aggregate.
- Scaling and transforming the raw spectral data produced modified spectra that effectively magnified the difference between the parent aggregate and the chert and shale improving model accuracy.
- Using the modified spectra, predictive binary-line counting models were developed for both chert and shale.
- The transformed data resulted in the effective development of Super Models.
- These Super Models could detect chert and/or shale down to a level of one percent in the parent sample.
- Increasing the number of laser shots and scans included in the model increases the predictive accuracy of the models.

5.7.2 Conclusions

- Laser scanning can be used as a quality control tool to identify chert and/or shale in ODOT aggregate at specification limits defined by ODOT.
- One Statewide Chert and one Shale Super Model is sufficient to differentiate and predict chert or shale content. (It is unnecessary to develop a model for each aggregate source.)

Chapter 6: Maryland Laser Scanning Analysis

6.1 Maryland Scanning Objectives

The Maryland effort focused on two inquiries raised by MDSHA:

- Can laser scanning spectral data be used to identify the specific quarry from which an unknown aggregate sample was mined?
- Can laser scanning spectral data be correlated with British Pendulum Numbers (ASTM E303, 2018) and/or Dynamic Friction Values (DFV) (MSMT 416, 2016). Both test methods have been used by the Maryland State Highway Administration (MDSHA) to evaluate the friction properties of Maryland aggregate.

6.2 Maryland Aggregate Samples and Sources

MDSHA supplied a total of 42 aggregate samples that were collected from approved MDSHA quarry sources for scanning. These samples, which were collected in early 2018, comprised a data set that included at least 42 different quarries and at least 18 different lithological categories. A complete list of samples provided by MDSHA is presented in Table 6.1. Table 6.1 includes information on the lithology of each sample, the quarry source, categorization as a carbonate or noncarbonate rock, BPN number, and DFVs. In 2019, MDSHA supplied an additional five samples that were separately collected from one or more of the original 42 sources. These samples are referred to as MDA, MDB, MDC, MDD, MDE. No information was provided regarding the source or properties of these samples.

Table 6.1: Maryland Samples

Sample ID	Lithology	Quarry	Carb or Noncarb	BPN	DFV
MD1_mLS_Mill.mat	No Data	Millville	NC	24	ND
MD2_mBasal_Jeff.mat	Basalt	Jefferson County	NC	33	34
MD3_mSerp_York.mat	Serpentine	York	NC	31	44
MD4_mGran_Cecil.mat	Granite	Cecil Co.	NC	32	39
MD5_mND_ND.mat	Limestone	No quarry data	C	ND	ND
MD6_mLS_Alleg.mat	Limestone	Allegheny	C	30	26
MD7_mLS_Mineral.mat	Limestone	Mineral	C	28	31
MD8_mSS_LS_Wash.mat	Limestone	Washington	C	29	34
MD9_mGneiss_ND.mat	Gneiss	No quarry data	NC	34	42
MD10_mLS_Migmaite_Hartford.mat	Migmatite	Hartford	NC	28	35
MD11_mLS_Freder.mat	Limestone	Frederick	C	32	32
MD12_mBas_ND.mat	Basalt	No quarry data	NC	36	24
MD13_mSchist_Cecil.mat	Schist	Cecil	NC	33	43
MD14_mMarble_Balt.mat	Marble	Baltimore	C	33	44
MD15_mLS_Mineral.mat	Limestone	Mineral	C	ND	ND
MD16_mSand_Tucker.mat	Sand	Tucker	NC	ND	ND
MD17_mBasalt_Fair.mat	Basalt	Fairfax	NC	30	47
MD18_mSerp_York.mat	Serpentinite	York	NC	32	36
MD19_mDiabase_Berks.mat	Diabase	Berks	NC	32	43
MD20_mHornfells_Berks.mat	Hornfels	Berks	NC	33	47
MD21_mNoncarb_Somer.mat	Limestone	Somerset	C	38	40
MD22_mLS_Freder.mat	Limestone	Frederick	C	28	32
MD23_mDiabase_Laudon.mat	Diabase	Laudon	NC	31	43
MD24_mLS_Wash.mat	Frederick	Washington	C	26	22
MD25_mLS_Wash.mat	Limestone	Washington	C	27	17
MD26_mGneiss_Berks.mat	Gneiss	Berks	NC	31	ND
MD27_mSand_Franklin.mat	Sand	Franklin	NC	ND	ND
MD28_mLS_Franklin.mat	Limestone	Franklin	C	29	24
MD29_mCarb_Lancaster.mat	Carbonate	Lancaster	C	32	40
MD30_mCarb_Adams.mat	Carbonate	Adams	C	31	43
MD31_mCarb_Somer.mat	Carbonate	Somerset	C	39	53
MD32_mND_Adams.mat	No Data	Adams	NC	33	45
MD33_mCarb_Dauphin.mat	Carbonate	Dauphin	C	28	20
MD34_mLS_Lebanon.mat	Limestone	Lebanon	C	26	21
MD35_mGravel_Cumb.mat	Gravel	Cumberland	C	34	46
MD36_mCarb_Freder.mat	Carbonate	Frederick	C	33	29
MD37_mLS_York.mat	Limestone	York	C	26	29
MD38_mLS_York.mat	Limestone	York	C	28	25
MD39_mND_Fairfax.mat	No Data	Fairfax	NC	32	45
MD40_mNCarb_Harford.mat	Gabro- Diorite	Harford	NC	29	48
MD41_mDiabase_Berks.mat	Diabase	Berks	NC	ND	40
MD42_mBasalt_Fauquier.mat	Basalt	Fauquier	NC	31	52

6.3 MD Source Identification Modeling

As noted above, in 2019 MDSHA collected five samples, in addition to the 42 samples collected and provided to the Research Team in 2018. These samples were labelled MDA, MDB, MDC, MDD, and MDE. The only information available to the Research Team, regarding these samples, were that each sample was collected from one of the 42 quarries, each of which were respectively associated with one of the 42 samples collected in 2018 and listed in Table 6.1. The challenge to the Research Team, depicted in Figure 6.1, was to develop a model that could predict which source-sample each of the five unknown samples were associated with.[52]

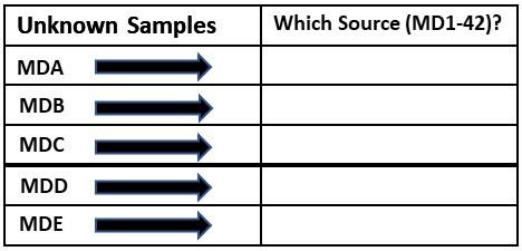

Figure 6.1: Aggregate Source Model Challenge

To characterize the spectral pattern associated with the MD samples, each of 42 samples (MD1-MD42) was scanned between seven and nine times; and each of the five unknown samples was scanned between five and seven times. Each scanning run comprised between 1000 and 1500 laser shots.

6.3.1 Source Identification Model Development

A Source Identification (SI) model is a model designed to match the spectral fingerprint of an unknown sample with spectral patterns known to be present in a known quarry source.

The hypothetical PC Score Plot, presented in Figure 6.2 provides a way to conceptually grasp the manner in which the SI model was constructed. Figure 6.2 provides a conceptual projection of spectral data and the clustered aggregate fields associated with eight MD aggregates.[53] The eight hypothetical aggregates (MD1, MD4, MD7, MD12, MD18, MD20, MD34, and MDB) form eight separate aggregate fields or groupings. Each group represents one MD

[52] It is important to note that MD1-MD42 and MDA-MDE samples were not from the same sample batch. They were collected from their respective quarry sources during different sampling years.
[53] This graphical depiction is generated using a Principal Components Analysis (PCA) Score Plot described in Section 2.4.1.

source or quarry. The dots shown within each respective grouping represent the individual samples making up the group. The individual samples are spectral patterns of the repeated scans recorded within that sample grouping. Their spatial distribution represents the degree of heterogeneity within that grouping. The grouping clusters that are closer together are more closely related. This means that the spectral fingerprints of the aggregates that make up these clusters are more similar than aggregates in groupings that are farther away. For example, examining Figure 6.2, the aggregates making up the MD1 grouping can be expected to exhibit greater geochemical similarity to aggregates in the MD34 grouping than aggregates in the MD18 grouping.

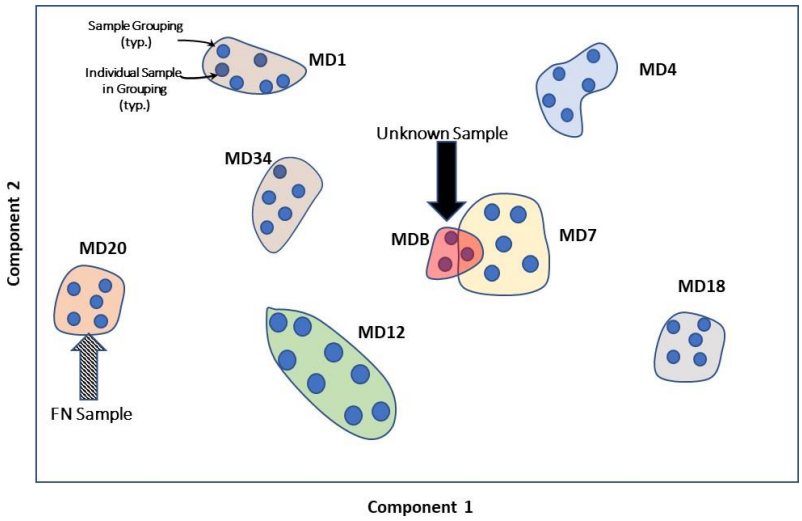

Figure 6.2: MD Sample Grouping Score Plot

When the Unknown Sample spectra (MDB), highlighted by the downward-pointing solid arrow in the figure, is included in the analysis, the identity of MDB can be projected based on the proximity of MDB to other clusters. In the example presented, it would be safe to assume that MDB comes from the same source as MD7. While the above description is theoretically correct, actual aggregate spectra in many cases will not segregate themselves into such neat groupings where "graphical" multivariate projections can easily differentiate between the groupings.[54]

[54] The lithology of the samples will, in most cases, determine the degree of grouping resolution. For example, limestones in one group and gravel in a second group and sand in a third group would generate three distinct groups. If all sources were from limestone quarries, then the groupings between the individual samples in each quarry sources might be less distinct.

To generate greater model resolution, a two-stage matching algorithmic process was employed.[55] The first stage is designed to select the grouping "least likely" to match the Unknown sample. In the hypothetical example depicted in Figure 6.2, this would be grouping MD20, highlighted by the upward-pointing slanted line arrow. MD20 is the grouping that is farthest from the Unknown sample (MDB). MD20 is labelled FN, which stands for Farthest Neighbor (FN) Grouping. This FN Grouping is then introduced into a PLS Binary Model to verify that the FN Grouping is not similar to MDB. If it is not similar, then this FN Grouping is removed from consideration as a potential candidate for the Unknown (MDB) source and the two-stage process is repeated. The primary objective of this process is to screen one grouping at a time, reducing the number of matching options available in each step, and determining which of the remaining groupings is most similar to the unknown sample. The second stage binary model, as noted above, double checks whether the "Farthest Neighbor" group is similar to the Unknown sample.

The SI binary model was calibrated by designating the FN Group with a y-value of 1 and all other known groupings with a y-value equal to 0. The model was then tested by introducing the Unknown sample (MDB), the test sample, into the model and calculating the y-values for all samples with a focus on the MDB grouping y-value.[56] If the model predicted an MDB y-value close to 1, this would mean that there was similarity between MDB and the FN Group. If closer to 0 then this would mean little similarity; and this FN Group would be eliminated from the data set and further consideration.

A new PCA score plot is generated with the remaining groupings and a second Farthest Neighbor grouping is selected. The binary PLS model once again checks the second Farthest Neighbor grouping and if the Unknown sample y-value output is not close to 1, this second grouping is eliminated, and the process moves on to the next step and continues to repeat itself until the model completes its analysis of all samples. The algorithmic process is separately comparing each Grouping to the Unknown Grouping and simultaneously weaning down the number of samples under consideration. This weaning process magnifies the differences in the

[55] The two-stage algorithmic model employs a PCA first stage model and a second stage PLS model

[56] The model output for each sample is a y value somewhere between approximately 0 and 1. An unknown sample exhibiting a y value close to 1.

remaining samples thereby providing greater model resolution. A flow diagram of the SI model algorithm is presented in Figure 6.3.[57]

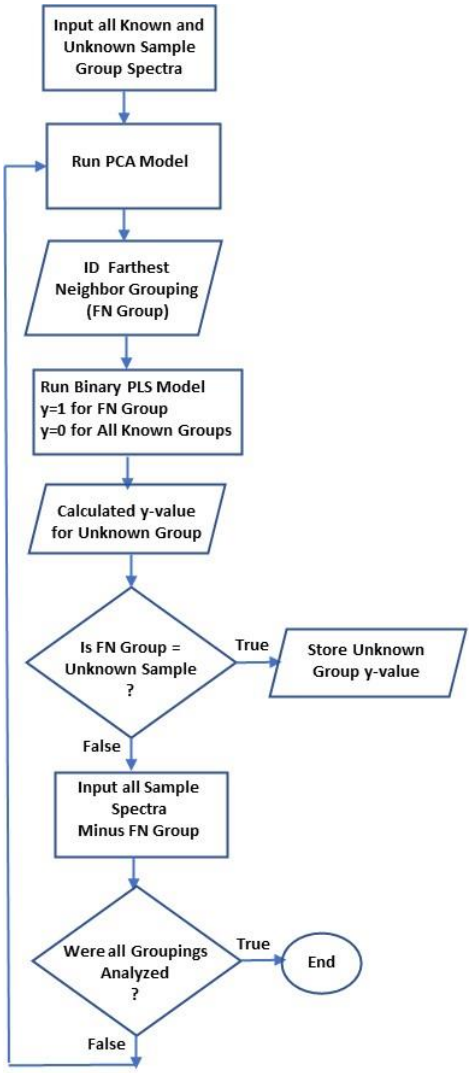

Figure 6.3: MD SI Model Algorithm

In summary, the MD Source Identification model outlined above, compares each group in turn to the other groups, removing a group once it has been identified. By comparing only one group to all the other beds, the unique characteristics of the group are better recognized by the model. Also, because groups are sequentially removed from the model, the model is able to

[57] The order of selection of each group in the algorithm is not random. It is based on an analysis of PCA models (score plots) to identify beds that are readily identifiable as Farthest Neighbor Groups. Those Groups that are most distinct are modeled first in the hierarchy. The remaining group spectra become more like each other as one proceeds through the modeling hierarchy by design.

recognize the small differences between groups later in the model sequence. When all groups are compared simultaneously, these small differences are insignificant and thus the groups are indistinguishable.

6.3.2 SI Model Calibration

SI model calibration involved several steps:

- Comparing the efficacy of individual line models versus full spectra models
- Screening spectra to remove poor shots with SNR screens

Five models were calibrated: one for each of the unknown samples (MDA, MDB, MDC, MDD, and MDE). Each model was tested by running trials using known samples as unknowns.[58] The models that were selected for MDA-MDE testing are listed in Table 6.2.

Table 6.2: MD SI Model Data Pre-processing

Unknown Sample	Spectra Selection	SNR Screen	Scaling/ Transforming Data	Model Name*
MDA	337 Lines	Yes	No	MDA_WHCTight with SNR_N1.mat
MDB	337 Lines	Yes	No	MDB_WHCTight with SNR_N1.mat
MDC	Full	Yes	No	MDC_Full_SNR.mat
MDD	Full	Yes	No	MDD_Full_SNR_NoScale.mat
MDE	739 Lines	Yes	No	MDE_ARNP_SNR_REMU_N1.mat

* The Model Names provided are shorthand codes used by the Research Team to keep track of the specific screening tools employed and have no other relevance.

6.3.3 SI Model Results

The source group predictions for each of the five models are presented in Table 6.3. On September 2, 2020, the Research Team submitted the MDA-MDE predictions to Maryland personnel and the MDSHA provided the results.

[58] This type of calibration is sometimes referred to as a cross validation. As an example, in these trials, the available spectra from a known sample (for example MD10) would be divided up whereby half of the MD spectra are used to represent the unknown sample ($MD10_u$) and the remaining half used to represent the known sample ($MD10_k$). The model would then be tested to see whether it predicts that $MD10_u = MD10_k$.

Table 6.3: Model Predictions and Results

Unknown Sample	Research Team Prediction	Actual Reported by MDSHA	MDSHA Comments	Lithology
MDA	MD7	MD6	MD6 & MD7 are very similar	Limestone
MDB	MD15	MD7	MD7 & MD15 are very similar	Limestone
MDC	MD13	MD13	Correct	Schist
MDD	MD23	MD23	Correct	Diabase
MDE	MD41	MD41	Correct	Diabase

The source of three (MDC, MDD, and MDE) of the five unknowns were accurately predicted. MDA and MDB sources were missed; but MDSHA reported that the model prediction were sources located in geographically close quarries and within the same formations as the actual source groups. The laser scanning model prediction results presented in Table 6.3 exceeded expectations. Predictions were made by:

- Collecting 42 samples, each weighing approximately 20 pounds, from 42 different source locations in 2018,
- Scanning each of the 42 samples,
- Collecting five samples, each weighing approximately 20 pounds, from five of the 42 original 2018 sample locations in 2019,
- Scanning each of the five samples, and
- Using the five 2019 sample scans, to match the forty-two 2018 sample scans.

The small sample sizes used to characterize each specific quarry source, the collection of the original 42 samples in 2018, and the five test samples collected a year later testified to the efficacy of the models developed during this analysis and the potential of laser scanning to target unknown aggregate sources, based on generated spectra.

6.4 Modeling British Pendulum Number and Dynamic Friction Value

Two test procedures that MDSHA has used to assess aggregate friction quality include:

- British Pendulum Number (BPN)

  ASTM E303 (2018), Standard Test Method for Measuring Surface Frictional Properties Using the British Pendulum Tester, and
- Dynamic Friction Value (DFV)

  Maryland State Highway Administration, Laboratory Method of Predicting Frictional Resistance of a Blend of Aggregates, MSMT 416 (2016).[59]

The purpose of the Maryland BPN/DFV analysis was to determine whether laser spectra could be used as a surrogate to predict either BPN or DFV numbers and potentially replace or reduce the need to conduct these tests on a regular basis. The 42 Carbonate and Noncarbonate samples, listed in Table 6.1, were used in the development of the BPN and DFV models.

6.4.1 BPN and DFV Correlation and Sensitivity

Both BPN and DFV are measures of pavement/aggregate friction. The higher each number or value, the greater the friction. As a result, BPN numbers and DFV values would be expected to correlate with each other. This means that for samples with both BPN and DFV data, the higher the BPN number the higher the DFV value and the lower the BPN number, the lower the DFV value. To examine if this was the case, the Research Team analyzed 18 carbonate samples and 17 noncarbonate samples, included in Table 6.1, for which BPN and DFV data were available.

The results of this analysis for carbonate samples are presented in Figure 6.4. An examination of Figure 6.4 reveals that BPN and DFV values for carbonate samples do correlate. From samples 1 to 18, BPN and DFV values move in tandem. Peaks and troughs occur together.

Sensitivity in modeling is a term used to describe how independent variables will impact a dependent variable; or in this case, how sensitive BPN numbers and DFV values are to a change in aggregate friction. An examination of Figure 6.4 reveals that DFV is more sensitive to changes in friction compared to BPN. For example, the MD sample labelled 11 has more than twice the DFV value than MD sample labelled 8. Sensitivity, in this case can be quantified by examining

[59] Based on, ASTM E660-90 (2015), Standard Practice for Accelerated Polishing of Aggregates or Pavement Surfaces Using a Small-Wheel, Circular Track Polishing Machine, ASTM International, West Conshohocken, PA, 2015.

the relationship between DFV and BPN values as shown in Figure 6.5, for carbonate samples. Figure 6.5 shows the positive correlation between DFV and BPN and also the slope of the trendline, which is approximately 2.

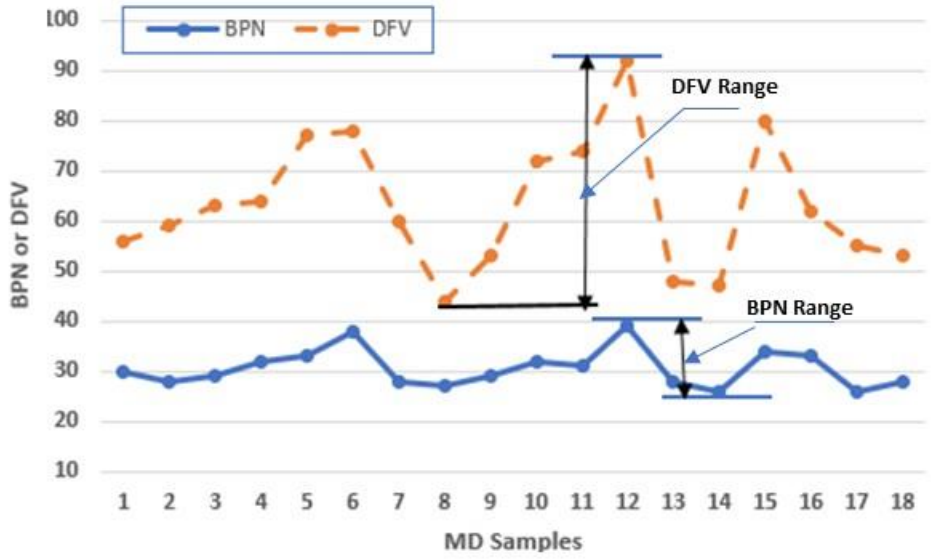

Figure 6.4: Carbonate BPN and DFV Correlation

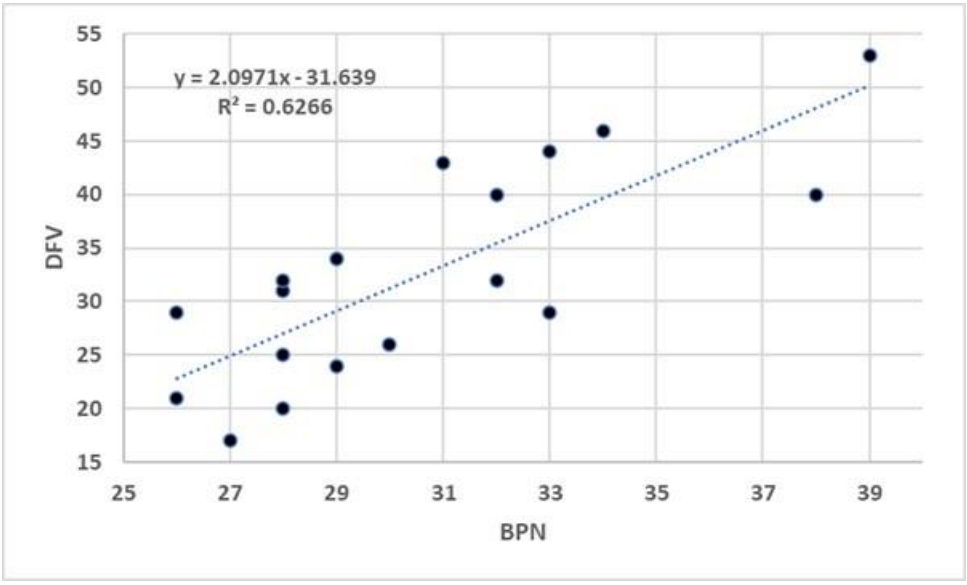

Figure 6.5: Carbonate Samples: DFV vs BPN Sensitivity and Correlation

The results of this analysis for noncarbonate samples are presented in Figure 6.6. An examination of Figure 6.6 reveals that BPN and DFV values for noncarbonate samples do not

correlate well. From samples 1 to 18, BPN and DFV values do not always move in tandem. Peaks and troughs do not necessarily occur together. The relationship between DFV and BPN for noncarbonate samples are shown in Figure 6.7. There is no correlation between DFV and BPN and the data suggest that DFV exhibits less sensitivity than BPN, as measured by the slope of the trendline.

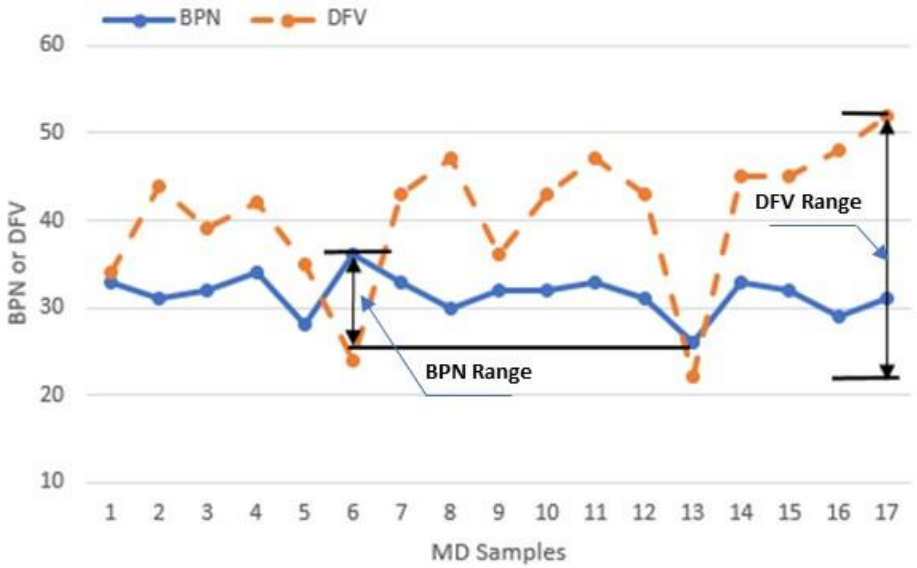

Figure 6.6: Noncarbonate BPN and DFV Correlation

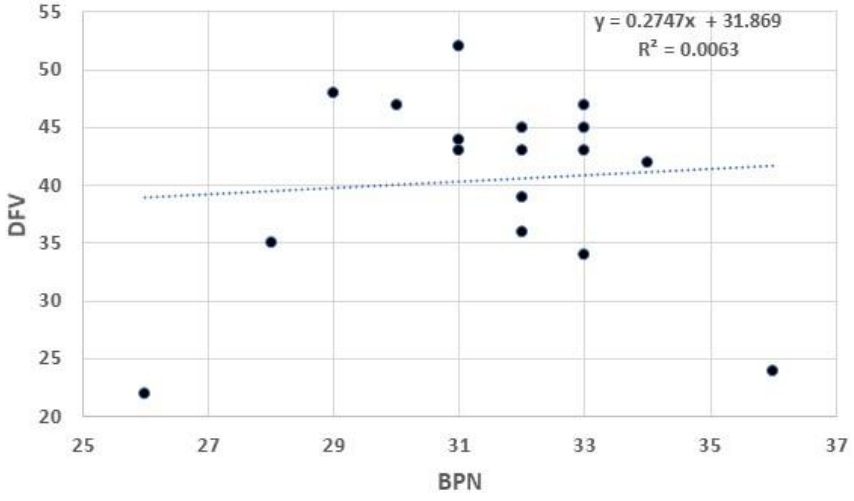

Figure 6.7: Noncarbonate Samples: DFV vs BPN Sensitivity and Correlation

6.4.2 MD BPN and DFV Model Development

This initial data evaluation, presented above, suggested that carbonate modeling would be more effective than noncarbonate modeling and that DFV modeling would be more effective than BPN modeling.

Nonetheless, Partial Least Square Regression (PLSR) models were developed for both BPN and DFV. Recall from Section 2.4.2, that a PLSR model is a multivariate model that is analogous to a familiar linear regression model, where a linear relationship between an independent x-value (or variable) and a dependent y-value (or variable) is established. Once this relationship is established it is then possible to predict the y-value in the linear model, given any x-value input. In the PLSR multivariate case, the X-value is the sample spectrum. PLSR models were developed to predict BPN and DFV values.

BPN and DFV models were calibrated and tested by initially using all samples together and subsequently dividing the available sample set into carbonate and non-carbonate categories, which were modeled independently. The 42 samples, listed in Table 6.1, were used in the analysis.

6.4.3 BPN and DFV Total Carbonate and Non-Carbonate Sample Modeling

Using all the carbonate and non-carbonate aggregate samples, listed in Table 6.1, models for BPN and DFV were calibrated and tested. This was undertaken by selecting one-half of the available samples for the calibration model and one-half of the available samples for the test model. The initial calibration set, and validation set samples comprised the first model calibrated. A second model was calibrated by reversing the calibration and validation sample sets.[60]

Results of the BPN calibration and test set model runs are presented in Figure 6.8 and Figure 6.9, for Model 1 and Model 2, respectively. The graphical results, shown on the left side of the figure, represents the BPN calibration model. The calibration models exhibited good correlation; however, the test set models themselves were not highly correlated. While the validation tests did not yield very good correlation, the residual errors in the BPN value predictions, embedded in tabular form in Figure 6.8 and Figure 6.9 were very low. These low

[60] BPN and DFV values were not available for all 42 Maryland samples. Thirty-seven samples had BPN data and 36 samples DFV data. Every other sample was randomly chosen for inclusion in either the calibration set or test set. The samples were then swapped to develop a second calibration and test set. This was done to verify that the sample selection process did not introduce bias into the analysis.

residual errors in the validation test suggest the spectral BPN models developed could have predictive potential, but further analysis would be required to verify this finding.

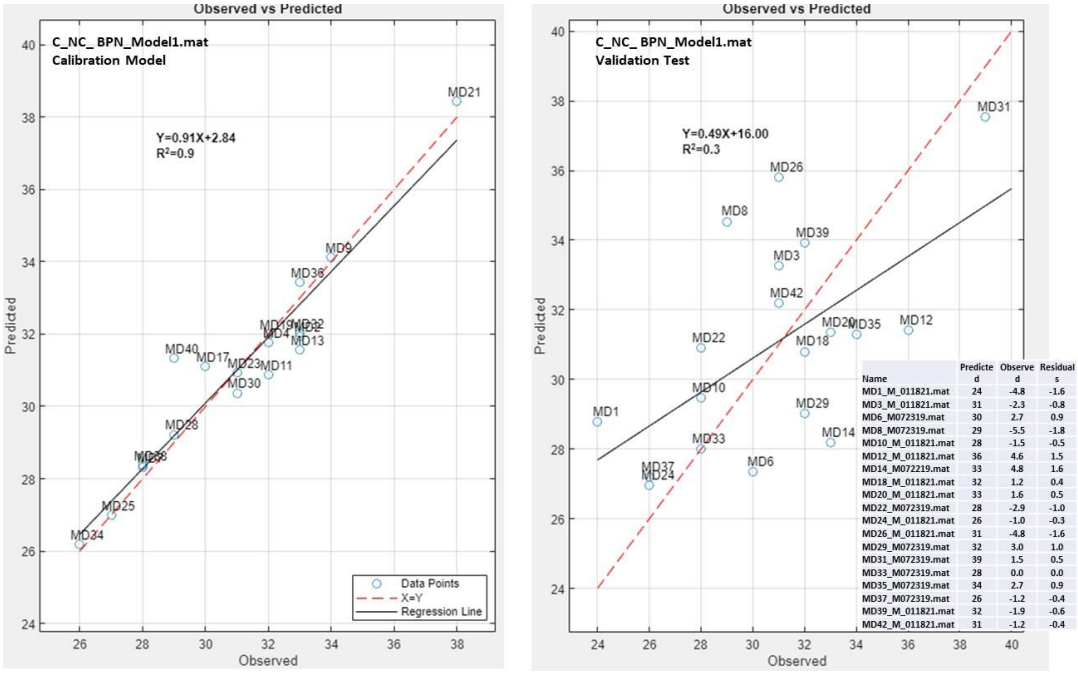

Name	Predicted	Observed	Residuals
MD1_M_011821.mat	24	-4.8	-1.6
MD3_M_011821.mat	31	-2.3	-0.8
MD6_M072319.mat	30	2.7	0.9
MD8_M072319.mat	29	-5.5	-1.8
MD10_M_011821.mat	28	-1.5	-0.5
MD12_M_011821.mat	36	4.6	1.5
MD14_M072219.mat	33	4.8	1.6
MD18_M_011821.mat	32	1.2	0.4
MD20_M_011821.mat	33	1.6	0.5
MD22_M072319.mat	28	-2.9	-1.0
MD24_M_011821.mat	26	-1.0	-0.3
MD26_M_011821.mat	31	-4.8	-1.6
MD29_M072319.mat	32	3.0	1.0
MD31_M072319.mat	39	1.5	0.5
MD33_M072319.mat	28	0.0	0.0
MD35_M072319.mat	34	2.7	0.9
MD37_M072319.mat	26	-1.2	-0.4
MD39_M_011821.mat	32	-1.9	-0.6
MD42_M_011821.mat	31	-1.2	-0.4

Figure 6.8: BPN Carbonate and Non-carbonate Model 1 Calibration and Test Results

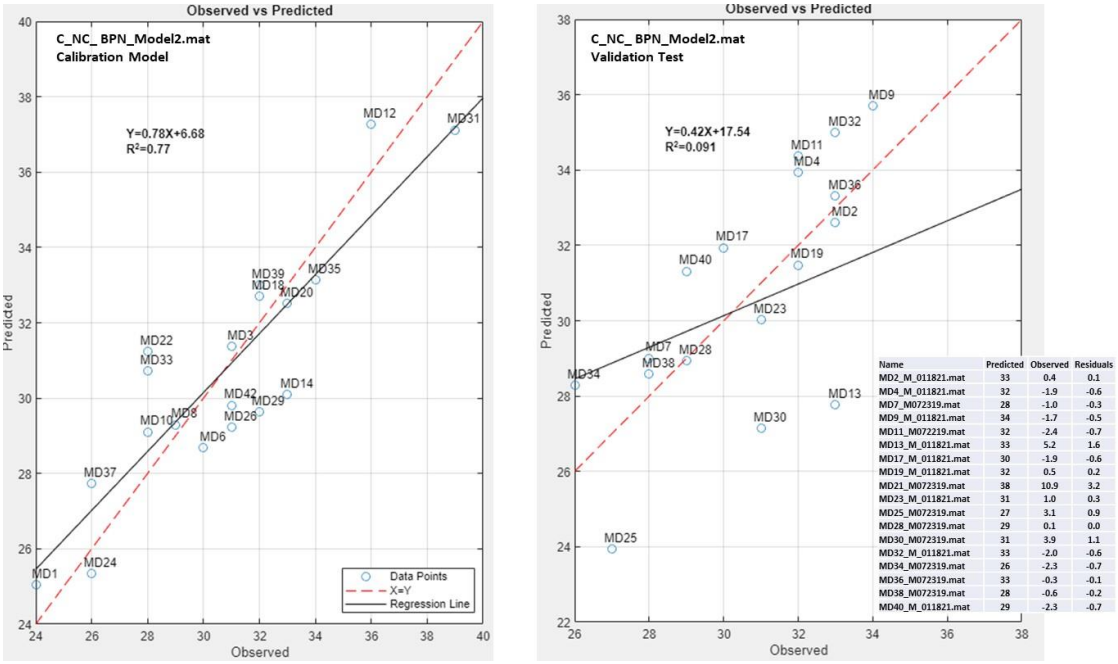

Name	Predicted	Observed	Residuals
MD2_M_011821.mat	33	0.4	0.1
MD4_M_011821.mat	32	-1.9	-0.6
MD7_M072319.mat	28	-1.0	-0.3
MD9_M_011821.mat	34	-1.7	-0.5
MD11_M072219.mat	32	-2.4	-0.7
MD13_M_011821.mat	33	5.2	1.6
MD17_M_011821.mat	30	-1.9	-0.6
MD19_M_011821.mat	32	0.5	0.2
MD21_M072319.mat	38	10.9	3.2
MD23_M_011821.mat	31	1.0	0.3
MD25_M072319.mat	27	3.1	0.9
MD28_M072319.mat	29	0.1	0.0
MD30_M072319.mat	31	3.9	1.1
MD32_M_011821.mat	33	-2.0	-0.6
MD34_M072319.mat	26	-2.3	-0.7
MD36_M072319.mat	33	-0.3	-0.1
MD38_M072319.mat	28	-0.6	-0.2
MD40_M_011821.mat	29	-2.3	-0.7

Figure 6.9: BPN Carbonate and Non-carbonate Model 2 Calibration and Test Results

DFV calibration and test set model run results are presented in Figure 6.10 and Figure 6.11, for Model 1 and Model 2, respectively. The calibration and model test results shown were similar to the BPN models.

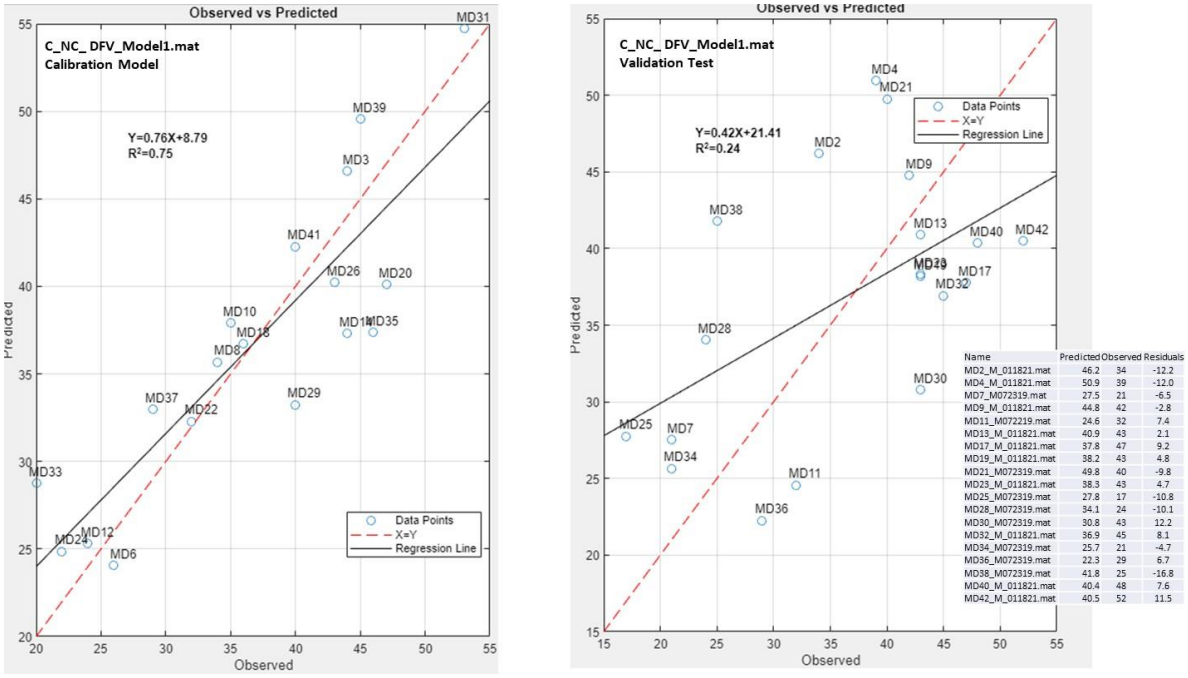

Figure 6.10: DFV Carbonate and Non-carbonate Model 1 Calibration and Test Results

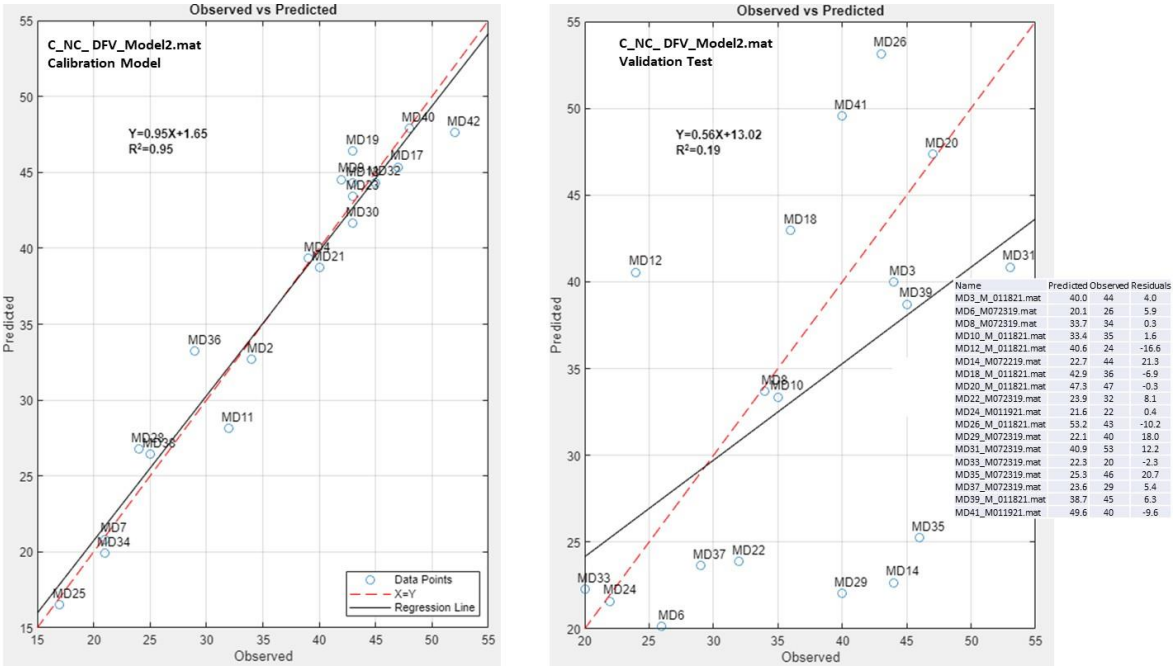

Figure 6.11: DFV Carbonate and Non-carbonate Model 2 Calibration and Test Results

6.4.4 BPN and DFV Carbonate Sample Modeling

Using all the carbonate aggregate samples, listed in Table 6.1, models for BPN and DFV were calibrated and tested. The results of the BPN Model 1 calibration model and validation test results are presented in Figure 6.12; and the BPN Model 2 calibration model and validation test results in Figure 6.13.[61] The carbonate calibration models exhibited improved test set predictions, and regression line coefficients compared to the combined carbonate and non-carbonate calibrations. While the validation tests did not yield very good correlation, the residual errors in the BPN value predictions, embedded in tabular form in Figure 6.12 and Figure 6.13 were very low. The low residual errors in the validation test suggest the spectral carbonate models developed have predictive potential.

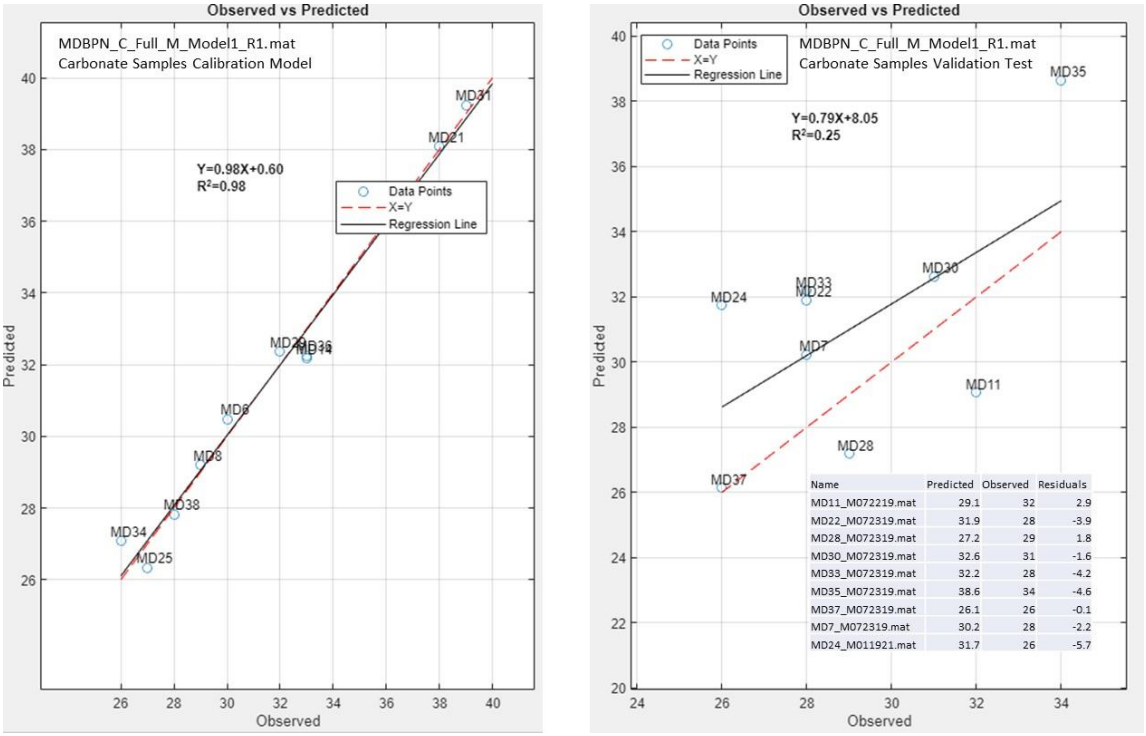

Figure 6.12: BPN Carbonate Model 1 Calibration and Test Results

[61] Two models were calibrated for each sample analysis. The first model was calibrated by randomly selecting one-half of the available samples for the calibration model and one-half of the available samples for the test model. A second model was calibrated by reversing the calibration and validation sample sets.

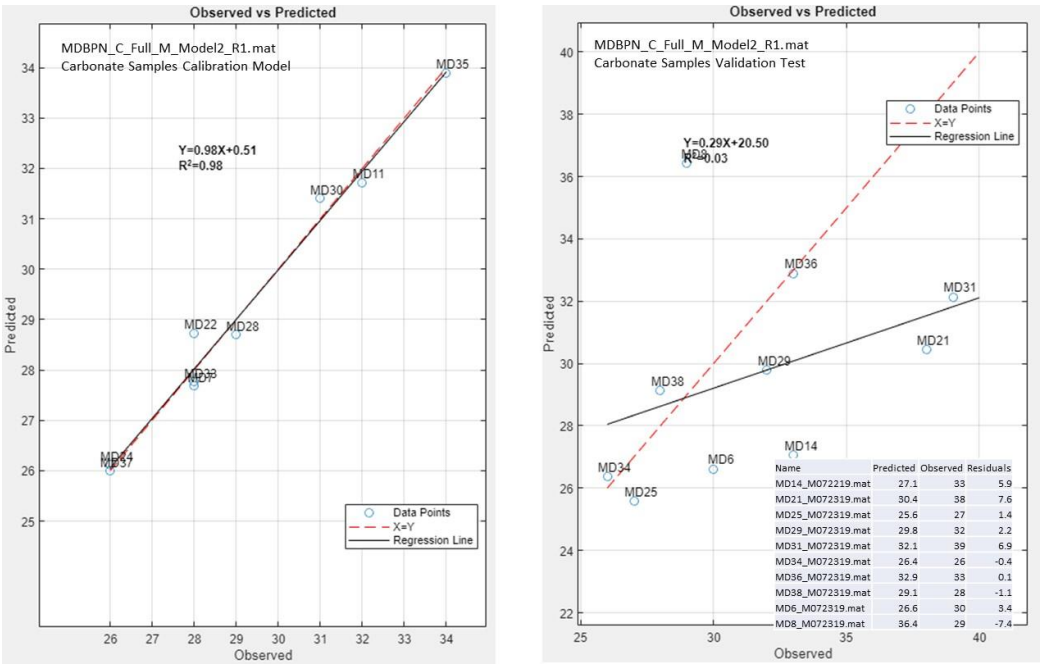

Figure 6.13: BPN Carbonate Model 2 Calibration and Test Results

The results of the DFV Model 1 calibration and validation test are presented in Figure 6.14, and the DFV Model 2 calibration and validation results in Figure 6.15. DFV test set data exhibited much better correlations than BPN models.

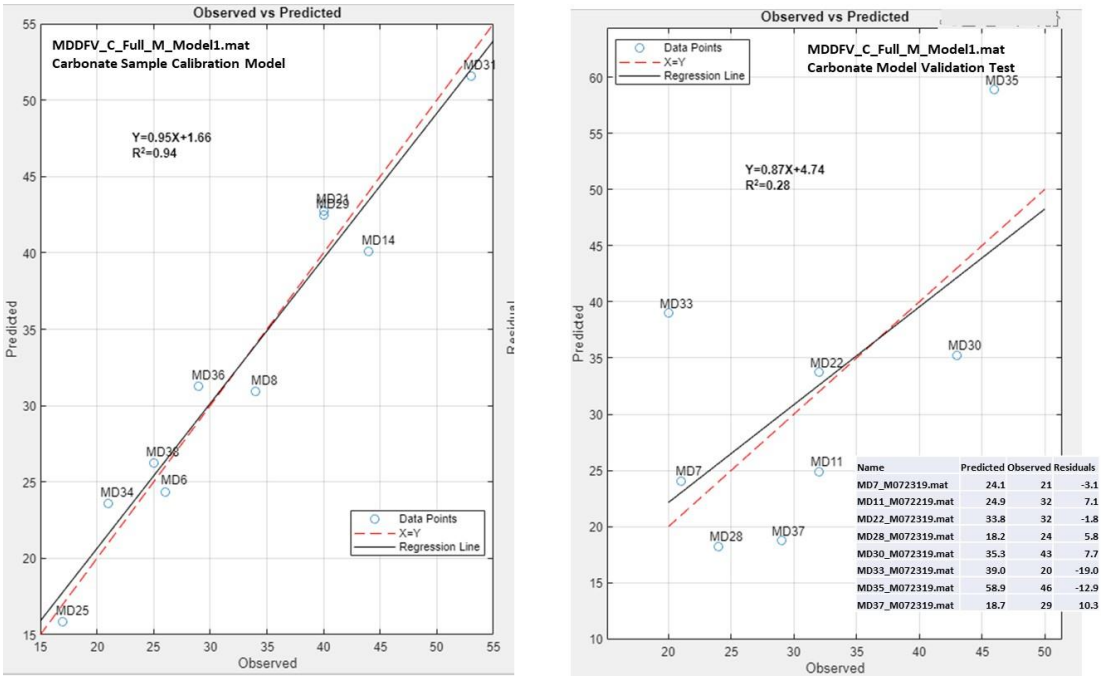

Figure 6.14: DFV Carbonate Model 1 Calibration and Test Results

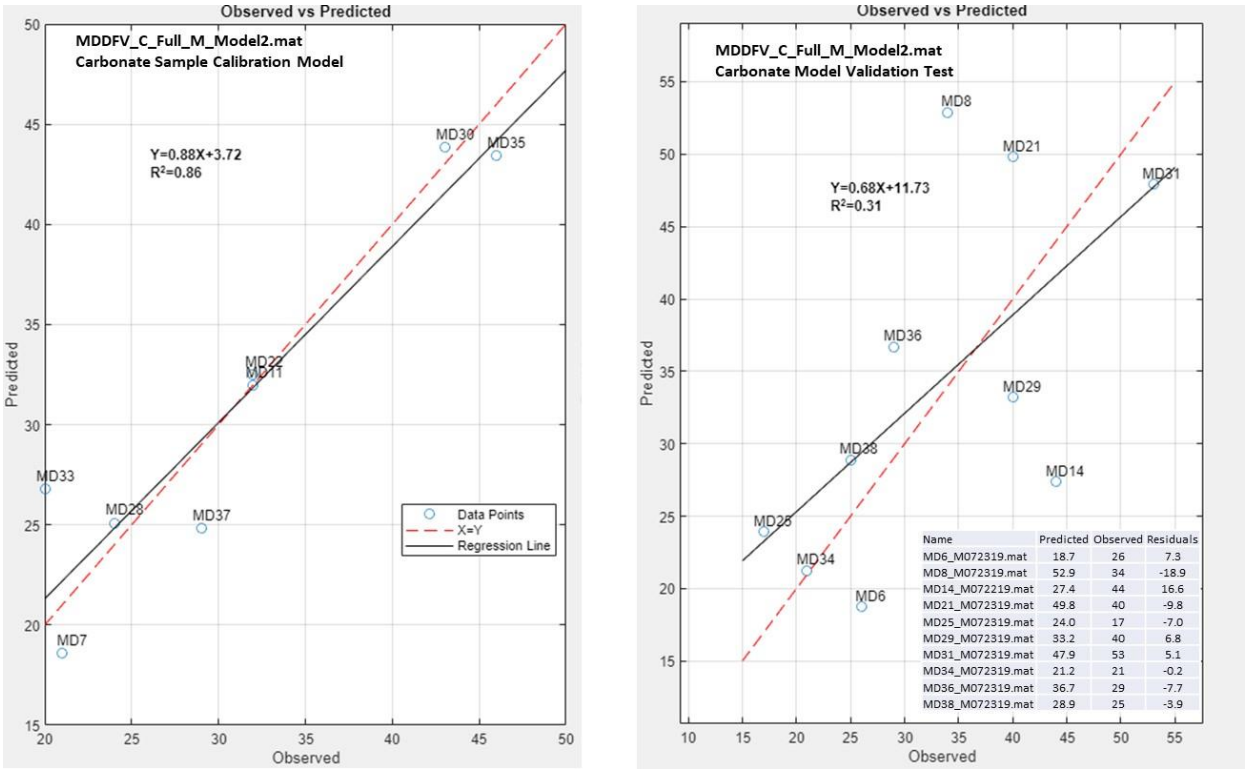

Figure 6.15: DFV Carbonate Model 2 Calibration and Test Results

6.4.5 BPN and DFV Non-Carbonate Sample Modeling

Using all the non-carbonate aggregate samples, listed in Table 6.1, models for BPN and DFV were calibrated and tested. BPN results for Model 1 and Model 2 are respectively presented in Figure 6.16 and Figure 6.17; and DFV results for Model 1 and Model 2 are respectively presented in Figure 6.18 and Figure 6.19. Neither BPN nor DFV non-carbonate models exhibited very effective predictive test set results.

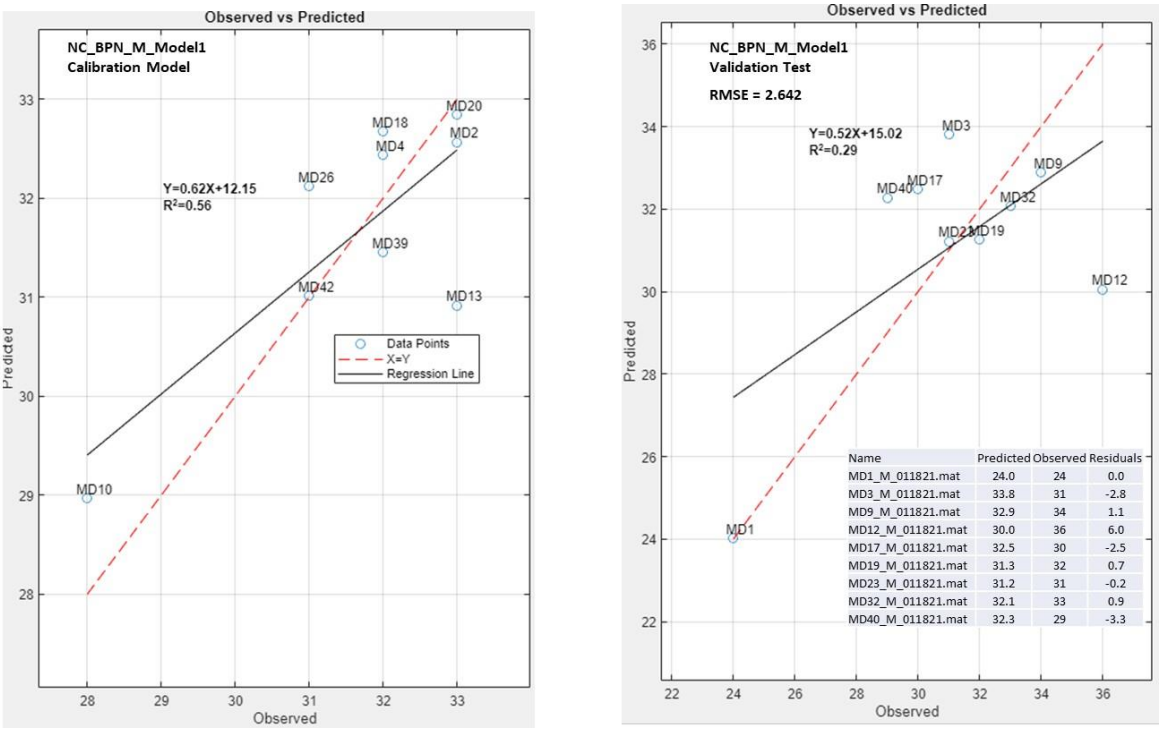

Figure 6.16: BPN Non-carbonate Model 1 Calibration and Test Results

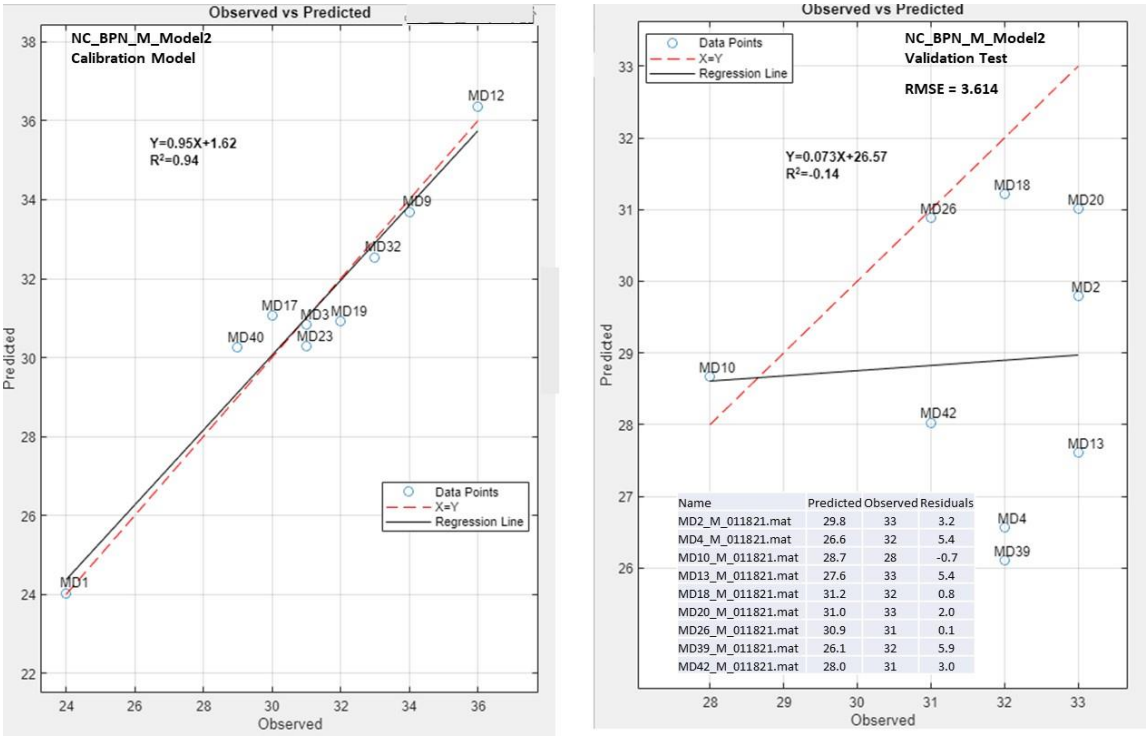

Figure 6.17: BPN Non-carbonate Model 2 Calibration and Test Results

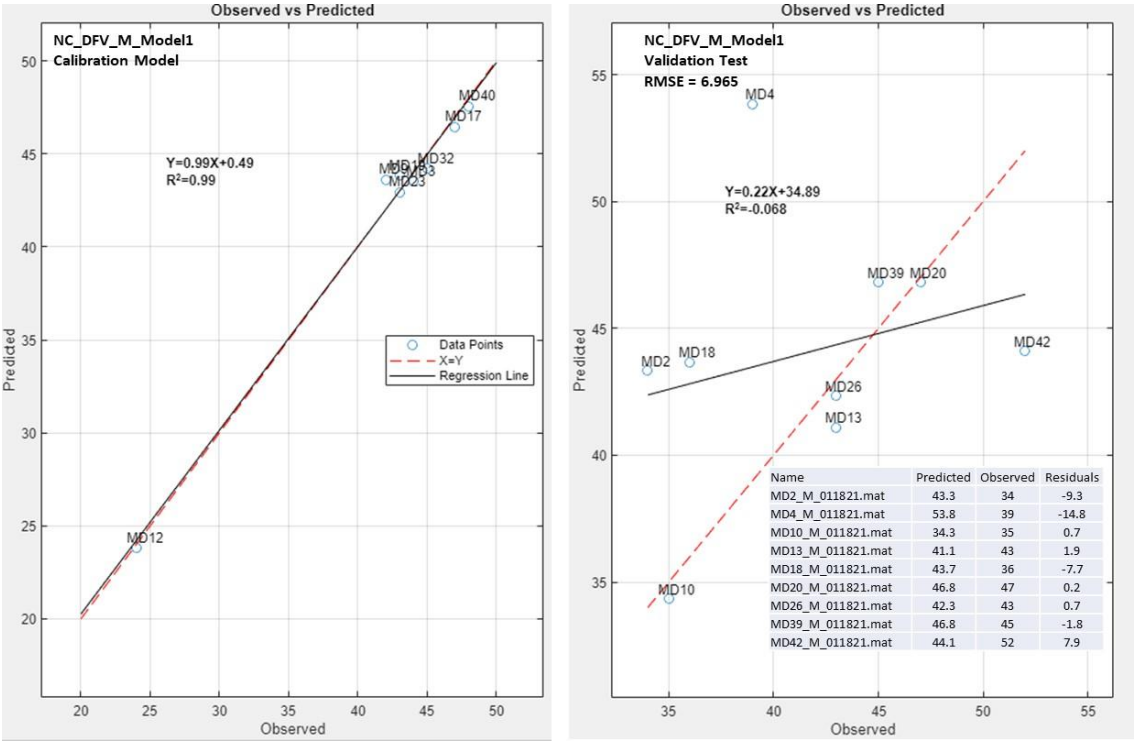

Figure 6.18: DFV Non-carbonate Model 1 Calibration and Test Results

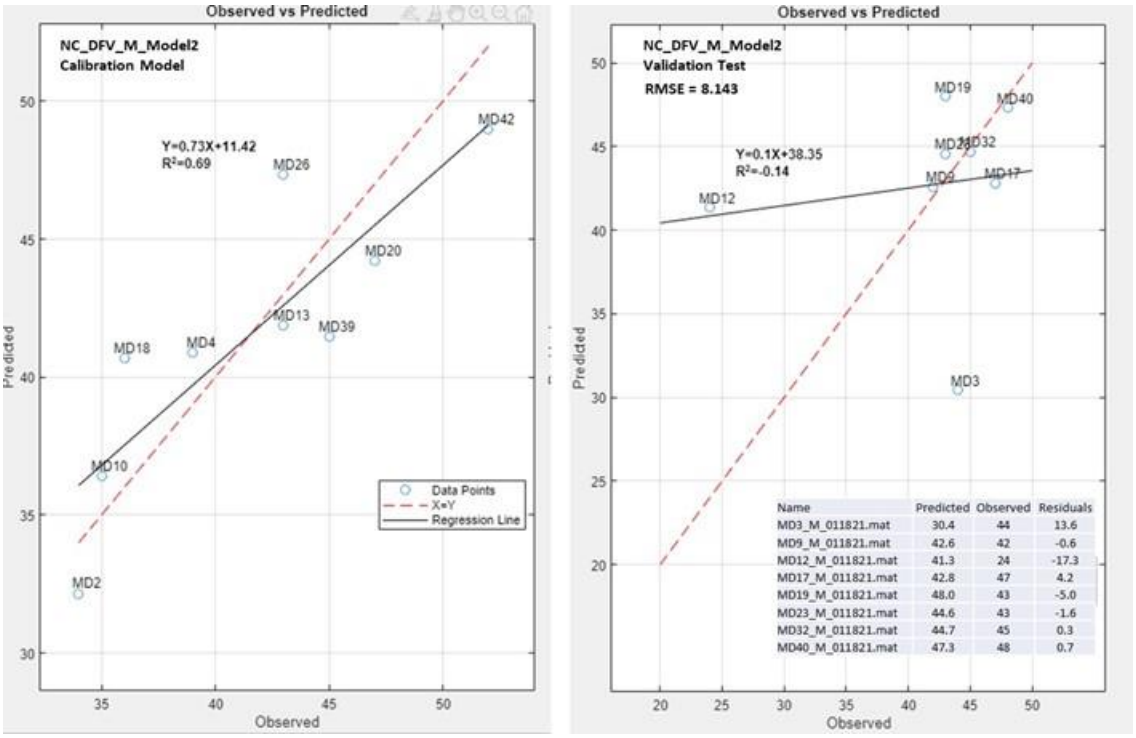

Figure 6.19: DFV Non-carbonate Model 2 Calibration and Test Results

6.4.6 DFV Carbonate Category Sample Modeling

MDSHA makes use of a DFV categorization system to classify the friction value, which determines the permissible applications in which the aggregate may be used (MSMT 416, 2016). This categorization system is divided into three broad groupings. They include High, Standard, and Low, designated as HDFV, SDFV, and LDFV categories. The categories are further subdivided by MDSHA into a series of categories and subcategories (Categories I-VI) presented below in Table 6.4. The measured aggregate DFV value determines which category the aggregate falls into. For example, a DFV value of 42 would designate the aggregate as a Category III aggregate.

The modeling strategy employed examined whether laser-generated spectra could be used to predict the appropriate DFV Grouping by comparing the model category prediction to the actual DFV sample value that MDSHA provided to the Research Team.

Table 6.4: Dynamic Friction Value Groupings and Categories

DFV Groupings	DFV Categories	DFV Value
HDFV	Category I	50
	Category II	45
	Category III	40
SDFV	Category IV	30
	Category V	25
LDFV	Category VI	20

Separate PLSR models were developed (calibrated and tested) to predict DFV values for carbonate and non-carbonate MDSHA aggregate samples.[62] In this DFV Category analysis, "individual sample spectra" were used in the model development process.[63] The carbonate and non-carbonate modeling results are respectively displayed in Figure 6.20 and Figure 6.21.[64] Each figure displays the following:

[62] Modeling carbonate and noncarbonate samples independently, rather than combining the carbonate and noncarbonate samples yielded better results.

[63] In previously presented analyses, all scanned samples were merged into one sample spectrum.

[64] Each figure contains two lines: one solid line and one dashed line. The solid line represents the linear regression line (line of best fit for the data) and the dashed line represents the ideal regression line where x = y.

- Rectangular boundaries defining the DFV Grouping limits, superimposed on a graph depicting the Observed (actual MD reported DFV values) versus the Model Predictions.
- Plots of the DFV results of each individual sample scan (e.g., each of 42 samples [MD1-MD42] were scanned between seven and nine times and the modeled results of each scan are shown independently; not averaged or combined).[65]
- The results of Model 1 and Model 2, respectively, shown in Figure 6.20 and Figure 6.21.[66]

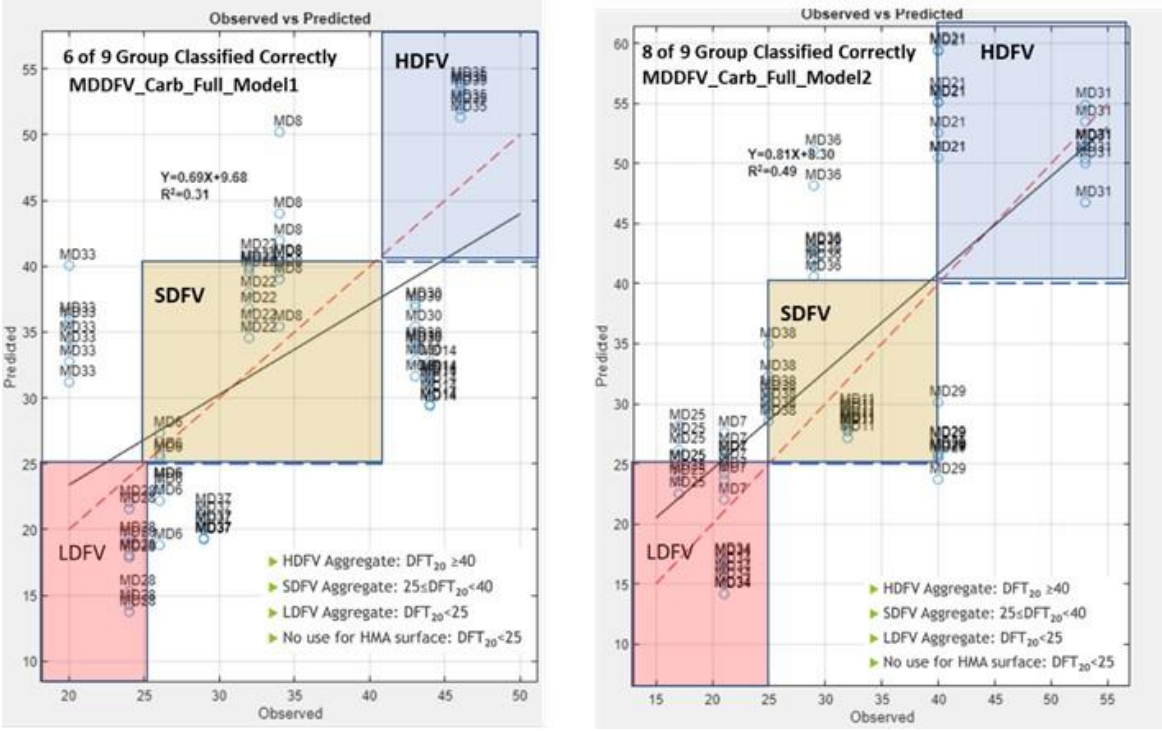

Figure 6.20: Carbonate Sample DFV Grouping and Category Results

[65] The projection of each sample independently as opposed to one merged sample, provided the means to incorporate the heterogeneity inherent in the samples and the model predictions.

[66] These are Models 1 and 2 previously described, where half of the samples were selected for the calibration set and the remaining samples were used to test the calibrated model; and the second model, where the calibration and tests set samples were reversed.

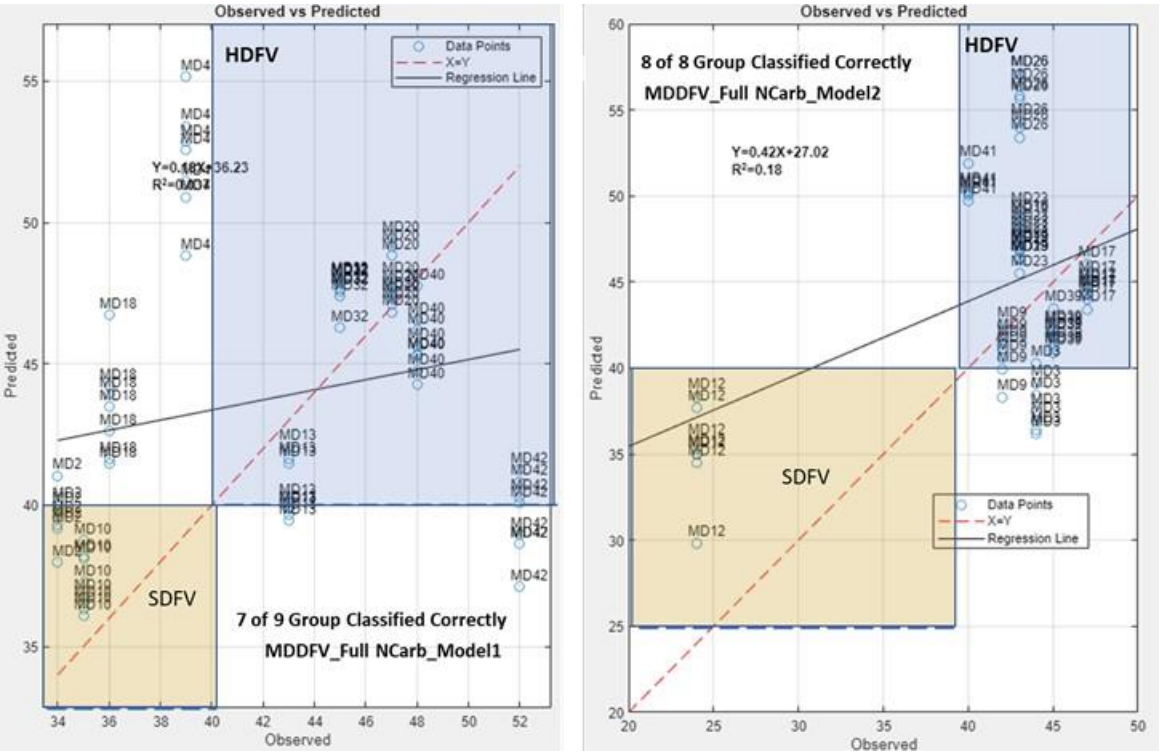

Figure 6.21: Non-Carbonate Sample DFV Grouping and Category Results

The efficacy of the models was determined by testing the Group and Categorization prediction success rate. These Grouping results, illustrated in Figure 6.20 and Figure 6.21, show 14 of 18 correct grouping predictions in the two Carbonate models combined; and 15 of 17 correct grouping predictions in the two Non-Carbonate models combined.[67] These results are extremely promising and suggest that laser scanning can effectively be used to identify DFV aggregate groupings. Additional sample scanning to supplement this initial database would almost certainly improve the very good success rates shown.

Individual scans were utilized in the analysis to generate a range of DFV values predicted by the individual scans for the same sample. These data reveal information about the spectral heterogeneity for each Sample ID. The DFV values can be seen to cluster in relatively tight ranges, shown in Figure 6.20 and Figure 6.21, but the model projections imply a measurable distribution to the scanned data. In this analysis, a Grouping Match was determined if one or more of the scans was projected into the one of the category ranges.

[67] A Grouping match was determined if one or more of the scans was predicted to be in the appropriate range.

6.5 MDSHA Findings and Conclusions

6.5.1 Findings

- MD Source Identification models effectively predicted the source of unknown aggregate materials from 42 possible quarry sites.
- MD models developed could not effectively predict BPN but could effectively predict DFV from carbonate aggregate models.
- MD DFV models have the potential to effectively predict LDFV, SDFV, and HDFV friction categories.

6.5.2 Conclusions

- Laser scanning models can be used to identify the quarry source of unknown aggregate materials.
- Limestones, most likely due to their similarity, were more difficult to differentiate than noncarbonate rock.
- Laser scanning models can be used to predict DFV values of carbonate aggregate and MDSHA friction categories of both carbonate and noncarbonate aggregate.

Chapter 7: Concluding Overview

Research and development activities over the past decade (described in Chapter 1) have demonstrated the laser scanning has the potential to provide a level of quality control that is not possible using existing materials testing methods. The Transportation Pooled Fund (TPF) study described herein presented a series of independent laser scanning studies to further examine the utility of this technology. The TPF effort was undertaken with the assistance four State agencies (Kansas, New York, Ohio, and Maryland). Each State effort, respectively, focused on specific State-related issues, and was designed to determine whether aggregate scanning could be beneficial compared to existing methodologies.

The Kansas Department of Transportation (KDOT) effort (see Chapter 3) provided test results that demonstrated that laser scanning could provide an alternative approach to the current KDOT D-cracking test method. D-cracking susceptibility could be determined by Laser scanning in one to two hours, compared to the multi-month testing protocols currently employed. The KDOT effort also demonstrated analytical procedures that could be employed to establish whether known aggregate sources are the source material for final production blends.

The New York State Department of Transportation (NYSDOT) effort (see Chapter 4) provided test results that show that laser scanning provides a means to determine whether aggregate sources meet NYSDOT AIR specifications within an hour or two without the need to conduct corrosive acid dissolution procedures that require special venting and concentrated acid management.

The Ohio Department of Transportation (ODOT) effort (see Chapter 5) provided test results that suggest that laser scanning could be used within hours to determine the level of shale and chert contamination in aggregate sources and whether such sources are suitable for use ODOT construction products (Portland cement concrete). Such a test procedure could replace ODOT's cumbersome petrographic particle counting or gravitational separation procedures, both of which exhibit questionable accuracy.

The Maryland State Highway Administration (MDSHA) effort (see Chapter 6) provided test results that demonstrated that laser scanning provides a potential method to predict the quarry

source of unknown aggregate materials. MDSHA does not have an alternative test method to make such a determination. In addition, laser scanning results have the potential to generate Dynamic Friction Value (DFV) models to effectively predict MDSHA LDFV, SDFV, and HDFV friction categories.

The emission spectra associated with laser scanning (described in Chapter 1) represent the data input to multivariate chemometric models (described in Chapter 2) that must be developed for each aggregate property evaluated. These models must be calibrated and validated as part of the technology development process. The results presented in each State chapter presented in this report, show that such models can be calibrated with a dedicated planning and laser scanning effort. Future work however will be required on the part of State Agencies to commit personnel resources for technology training and laser scanning QC/QA planning to oversee the development of the spectral database; and the acquisition of a laser scanning system to physically scan the State's aggregate.

Laser scanning technology is a new and unfamiliar approach to most transportation agencies. The lack of familiarity with laser scanning systems and spectral modeling will be a future barrier to its widespread deployment. However, the authors of this report believe that the technology, which is currently being employed on the Mars Rover to characterize Martian stone and soil, will be the future of geologic investigation here on earth. The speed of development of laser scanning technology in the transportation industry will be up to each State Agency.

In December 2020, the Kansas Department of Transportation (KDOT) became the first State Agency in the nation to install a scanning system in its State-run materials laboratory. By installing such a system in its own laboratory, KDOT presently has the means to expand the potential of the technology by characterizing its own aggregate resources, and to uniquely address the issues that are most pressing to KDOT.

References

ASTM E303-93R18. (2018). *Standard test method for measuring surface frictional properties using the British pendulum tester*. doi: 10.1520/E0303-93R18, www.astm.org

ASTM E1911-19. (2019). *Standard test method for measuring surface frictional properties using the dynamic friction tester*. doi: 10.1520/E1911-19, www.astm.org

Chesner, W. H., & McMillan, N. J. (2012). *Automatic laser spectrographic pattern matching for aggregate identification* (NCHRP IDEA Project 150). https://onlinepubs.trb.org/Onlinepubs/IDEA/FinalReports/Highway/NCHRP150_Final_Report.pdf

Chesner, W. H., & McMillan, N. J. (2015). *Prototype development: Automated and continuous aggregate sampling and laser targeting system* (NCHRP IDEA Project 168). https://onlinepubs.trb.org/onlinepubs/IDEA/FinalReports/Highway/NCHRP168_Final_Report.pdf

Chesner, W. H., & McMillan, N. J. (2016). *Real time laser scanning of aggregate materials in highway construction* (Report No. FHWA-KS-16-13). http://dmsweb.ksdot.org/AppNetProd/docpop/docpop.aspx?clienttype=html&docid=9750838

Clegg, S. M., Sklute, E., Dyar, M. D., Barefield, J. E., & Wiens, R. C. (2009). Multivariate analysis of remote laser-induced breakdown spectroscopy spectra using partial least squares, principal component analysis, and related techniques. *Spectrochimica Acta Part B: Atomic Spectroscopy*, *64*(1), 79–88.

Dunn, K. (2022). *Process improvement using data*. https://learnche.org/pid/contents

Geladi, P. (2003). Chemometrics in spectroscopy. Part 1. Classical chemometrics. *Spectrochimica Acta Part B: Atomic Spectroscopy*, *58*(5), 767–782. https://doi.org/10.1016/S0584-8547(03)00037-5

Geladi, P., & Kowalski, B. R. (1986). Partial least-squares regression: A tutorial. *Analytica Chimica Acta*, *185*, 1–17.

Geladi, P., Sethson, B., Nyström, J., Lillhonga, T., Lestander, T., & Burger, J. (2004). Chemometrics in spectroscopy: Part 2. Examples. *Spectrochimica Acta Part B: Atomic Spectroscopy*, *59*(9), 1347–1357.

Jaadi, Z. (2021). A step-by-step explanation of principal component analysis (PCA). https://builtin.com/data-science/step-step-explanation-principal-component-analysis

Kramer, R. (1998). *Chemometric techniques for quantitative analysis*. Boca Raton, FL: CRC Press.

KTMR-21 Kansas Test Method. (2012). *Soundness and modified soundness of aggregates by freezing and thawing*. Topeka, KS: Kansas Department of Transportation.

KTMR-22 Kansas Test Method. (2012). *Resistance of concrete to rapid freezing and thawing.* Topeka, KS: Kansas Department of Transportation.

MSMT 416. (2016). *Laboratory method of predicting frictional resistance of a blend of aggregates*. Baltimore, MD: Maryland Department of Transportation State Highway Administration.

NYSDOT Materials Method MM28. (2007). *Friction aggregate control and test procedures*. Albany, NY: New York State Department of Transportation.

Sartorius AG. (2020). *What is principal component analysis (PCA) and how it is used?* https://www.sartorius.com/en/knowledge/science-snippets/what-is-principal-component-analysis-pca-and-how-it-is-used-507186

AD ASTRA PER ASPERA

Kansas

Department of Transportation